

Dissertation

Dissection of CURT1 complex functions in thylakoid ultrastructure formation and photosynthesis



Wenteng Xu

03.07.2013



Dissection of CURT1 complex functions in thylakoid ultrastructure formation and photosynthesis

Dissertation

zur Erlangung des Doktorgrades der Fakultät für
Biologie der Ludwig-Maximilians-Universität
München

Wenteng Xu

München, 3.7.2013

Erstgutachter: Prof. Dr. Dario Leister

Zweitgutachter: PD Dr. Cordelia Bolle

Tag der Einreichung: 3.7.2013

Tag der mündlichen Prüfung: 09.08.2013

Summary

Grana, cylindrical structures of stacked thylakoid membranes, are ubiquitous in land plant chloroplasts. Their role in photosynthesis remains controversially discussed and little is known about the mechanism underlying their formation. In *Arabidopsis thaliana*, the CURT1 protein family, containing four members (CURT1A-D), is involved in the grana formation by facilitating membrane bending in the grana margins. This effect is CURT1 dosage-dependent, as overexpression of CURT1A (*oeCURT1A*) or loss of CURT1 proteins (*curt1abcd*) leads to opposite altered grana phenotypes. In this thesis, the photosynthetic performance and growth rate of *oeCURT1A* and *curt1abcd* lines were compared to WT under different light conditions. Both lines exhibited deficiency in photosynthesis and moderately retarded growth rate, suggesting that the grana formation is not essential, but beneficial for photosynthesis and growth.

Regarding the mechanism of membrane curvature, CURT1 proteins were shown to insert into the thylakoid membrane and to form oligomeric structures. Here, CURT1A was found to be the major component of the CURT1 protein complexes as (i) in the *oeCURT1A* line, overexpression of CURT1A induced shorter but higher grana stacking without simultaneously increased expression levels of CURT1B and C, and (ii) in *35S:CURT1A curt1abc*, CURT1A reconstituted grana stacking in the absence of CURT1B and C. Besides a dependence of the bending mechanism on CURT1 protein amounts, thylakoid phosphorylation was a suggested mechanism to regulate grana stacking. In this study, we showed that the effects of the CURT1 protein amounts dominated thylakoid phosphorylation in affecting grana formation, as *curt1abc tap38* mutants exhibited a similar grana phenotype as the *curt1abc* mutant line. Thus we propose that thylakoid phosphorylation rather functions on a regulatory level influencing grana plasticity. This regulation could be accomplished either by directly phosphorylating CURT1 proteins or a phosphorylation cascade. In this respect, the analysis of the assembly behavior of CURT1 proteins was initiated by investigating both PSE lines (lines complemented with CURT1 phospho-site exchange variants) and protein kinase/phosphatase mutant lines (PK/PP lines). Finally, based on an altered migration behavior of CURT1 proteins under HL conditions, a possible interplay between CURT1 protein phosphorylation and CURT1 complex formation is discussed with respect to the modulation of grana formation.

Zusammenfassung

Grana sind ubiquitär in den Chloroplasten von Landpflanzen vorzufindende zylindrische Strukturen von gestapelten Thylakoidmembranen. Ihre Funktion hinsichtlich der Photosynthese wird kontrovers diskutiert und über den zugrunde liegenden Mechanismus ist nur wenig bekannt. In *Arabidopsis thaliana* ist die CURT1 Proteinfamilie, bestehend aus CURT1A, B, C und D, bei der Ausbildung der Granastruktur involviert, indem sie die Membranbiegung in den Grana-Randbereichen (Grana margins) ermöglichen. Dieser Effekt ist von der CURT1-Menge abhängig, da eine Überexpression (*oeCURT1A*) und der Verlust (*curt1abcd*) der CURT1-Proteine zu gegensätzlichen Phänotypen führt. In dieser Arbeit werden die photosynthetische Leistung und die Wachstumsrate dieser Linien mit denen des Wildtyps unter unterschiedlichen Lichtbedingungen verglichen. Beide Linien zeigten eine Beeinträchtigung der Photosynthese und leicht reduzierte Wachstumsraten. Dies deutet darauf hin, dass die Granastruktur *per se* nicht essentiell für Photosynthese und Wachstum ist, aber einen adaptiven Vorteil bietet.

Über den Mechanismus der Membranbiegung ist bekannt, dass sich CURT1-Proteine in die Thylakoidmembran inserieren und Oligomere miteinander bilden. In dieser Arbeit wird gezeigt, dass CURT1A die Hauptkomponente des CURT1-Proteinkomplexes darstellt, da CURT1A (i) in der Überexpressorlinie (*oeCURT1A*) schlankere aber dafür höhere Granastapel verursacht ohne gleichzeitig die Expression von CURT1B und C zu erhöhen und (ii) in der *35S:CURT1A curt1abc* Linie (ohne das Vorhandensein von CURT1B und C) in der Lage ist den Phänotypen der Dreifachmutante zu komplementieren. Neben der Abhängigkeit der Membranbiegung von der CURT1-Proteinmenge wird auch die reversible Phosphorylierung der Thylakoide als regulatives Element der Granaausbildung angesehen. Hier konnte gezeigt werden, dass die Effekte der CURT1-Proteinmenge über die der Thylakoidphosphorylierung erhaben sind, da auch *curt1abc tap38* Mutanten einen ähnlichen Phänotypen wie die *curt1abc* Mutante in der Granastruktur zeigen. Daher stellen wir die Hypothese auf, dass die Thylakoidphosphorylierung eher einen regulatorischen Einfluss auf die Granaplastizität ausübt. Eine entsprechende Regulation könnte ebenfalls auf einer direkten Phosphorylierung von CURT1 beruhen. Dazu wurden Untersuchungen zum Assemblierungsverhalten von CURT1-Proteinen in PSE Linien (Austauschvarianten der Phosphorylierungsstellen) und in Mutanten von chloroplastidären Proteinkinasen und -phosphatasen (PK/PP Linien) initiiert. Anhand des veränderten Migrationsverhaltens von CURT1-Proteinen im Blau-Nativen Gelsystem nach Starklichtbehandlung wird schließlich ein mögliches Zusammenspiel von CURT1-Proteinphosphorylierung und CURT1-Komplexbildung im Zusammenhang mit Granastrukturveränderungen diskutiert.

Index

Summary	<i>i</i>
Zusammenfassung	<i>ii</i>
Index	<i>iii</i>
List of Figures and Tables	<i>v</i>
Abbreviations	<i>vii</i>
1. Introduction	<i>1</i>
1.1. Photosynthetic apparatus.....	<i>1</i>
1.2. Four major protein complexes in the thylakoid membrane	<i>1</i>
1.3. Linear electron transport (LEF) and cyclic electron transport (CEF)	<i>3</i>
1.4. Regulation of photosynthesis: short-term responses	<i>5</i>
1.5. Regulation of photosynthesis: long-term responses	<i>7</i>
1.6. Lateral heterogeneity—advantages of the organization	<i>8</i>
1.7. Multiple factors for membrane curvature	<i>9</i>
1.7.1. Phosphorylation status of thylakoid proteins.....	<i>9</i>
1.7.2. Lipid composition	<i>12</i>
1.7.3. Curvature-facilitating proteins.....	<i>12</i>
1.8. Curvature Thylakoid1 (CURT1) family	<i>13</i>
1.9. Aims of the thesis	<i>15</i>
2. Materials and Methods	<i>16</i>
2.1. Plant materials and growth conditions.....	<i>16</i>
2.2. Nucleic acid analysis.....	<i>16</i>
2.3. RNA isolation and cDNA synthesis	<i>18</i>
2.4. Agrobacterium binary vectors for complementation of <i>curt1a</i>, <i>curt1b</i>, and <i>curt1abc</i> mutant lines	<i>18</i>
2.4.1. <i>Agrobacterium</i> binary vectors for <i>curt1a</i> line	<i>18</i>
2.4.2. <i>Agrobacterium</i> binary vectors for <i>curt1b</i> line	<i>19</i>
2.4.3. <i>Agrobacterium</i> binary vectors for <i>curt1abc</i> line.....	<i>19</i>
2.5. Agrobacterium-mediated transformation	<i>20</i>
2.6. PAM measurements	<i>20</i>
2.7. Photoinhibition studies (D1 turnover assay).....	<i>21</i>
2.8. Isolation of chloroplasts and thylakoids	<i>22</i>
2.9. SDS-PAGE and Western blot analyses.....	<i>22</i>

2.10.	Blue-native (BN) and second dimension (2-D) PAGE.....	23
2.11.	Protein quantification	24
2.12.	Co-Immunoprecipitation (CoIP) assay	24
2.13.	Immunogold labeling	24
2.14.	Scanning electron microscopy (SEM) and transmission electron microscopy (TEM) analyses	25
3.	Results.....	32
3.1.	Characterization of <i>oeCURT1A</i> and <i>curt1abcd</i>.....	32
3.1.1.	CURT1A is mainly localized in the thylakoid margin in <i>oeCURT1A</i> line.....	32
3.1.2.	Growth of <i>oeCURT1A</i> and <i>curt1abcd</i> plants is retarded under various light conditions	32
3.1.3.	Differential CURT1A accumulation exerts pleiotropic effects on photosynthesis	34
3.1.4.	Overexpression of CURT1A has no effect on major thylakoid complex assembly and migration behavior	37
3.1.5.	The <i>oeCURT1A</i> line shows a more pronounced state 2 under GL conditions	38
3.1.6.	The overall CURT1 levels remain stable under dark, GL, and HL conditions	39
3.1.7.	D1 turnover is not affected in <i>oeCURT1A</i> , but slightly affected in <i>curt1abcd</i> , under short HL conditions.....	39
3.2.	Grana stacking is affected by (I) the amount of CURT1 and (II) thylakoid phosphorylation	42
3.2.1.	CURT1A levels are decreased in <i>stn7</i> and <i>stn7 8</i>	42
3.2.2.	Overall thylakoid phosphorylation is not altered in <i>oeCURT1A</i>	43
3.2.3.	The <i>curt1abc tap38</i> mutant shows grana stacking similar to the <i>curt1abc</i> mutant	45
3.3.	CURT1A represents the major constituent in formation of grana stacking	45
3.3.1.	Solely CURT1A amounts are increased in the <i>oeCURT1A</i> line	45
3.3.2.	CURT1A can induce grana formation in the <i>curt1abc</i> line.....	46
3.3.3.	CURT1A containing complexes are disassembled under HL exposure	47
3.4.	Effects of CURT1 phosphorylation: generation of phospho-site exchange (PSE) complementation lines.....	49
3.5.	Identification of putative interacting proteins of CURT1	52
3.5.1.	CURT1 oligomerization is STN8-independent under different light conditions.....	52
3.5.2.	Thylakoid rhodanese-like protein (TROL) is not a stable interaction partner of CURT1 complexes	53
3.6.	The CURT1 from <i>Synechocystis</i> (<i>synCURT1</i>) fails to induce grana formation in <i>A. thaliana curt1abc</i> line	54
4.	Discussion.....	56
4.1.	Is grana stacking essential for photosynthesis?.....	56
4.2.	How is grana formation induced by CURT1 proteins?	60
4.3.	How are grana structural dynamics regulated?.....	63
5.	Appendix	67

6. References	70
Acknowledgements	82
Curriculum vitae	83
Declaration / Ehrenwörtliche Versicherung	85

List of Figures and Tables

Fig. 1.1 Structures of the chloroplast and the thylakoid membrane	3
Fig. 1.2 Scheme on the plasticity of grana stacking under different light conditions and grana phenotypes of <i>oeCURT1A</i> and <i>curt1abcd</i>	11
Fig. 1.3 Mechanisms of membrane curvature	14
Table 2.1 T-DNA insertion lines in this work	27
Table 2.2 List of primers used for characterizing T-DNA insertion lines	28
Table 2.3 Primers used for the construction of the different complementation lines	29
Table 2.4 Complementation lines and lines including positional amino acid exchanges are categorized into three groups based on the mutant background	31
Fig. 3.1 Localization of CURT1A in <i>oeCURT1A</i> thylakoids by immunogold labeling	33
Fig. 3.2 Growth kinetics of <i>Ler</i>, <i>oeCURT1A</i>, and <i>curt1abcd</i> mutant plants under various light conditions	34
Table 3.1A PAM parameters of <i>Ler</i>, <i>oeCURT1A</i>, and <i>curt1abcd</i> plants under growth light	36
Table 3.1B PAM parameters of <i>Ler</i>, <i>oeCURT1A</i>, and <i>curt1abcd</i> under long day and short day	36
Table 3.1C PAM parameters of <i>Ler</i>, <i>oeCURT1A</i>, and <i>curt1abcd</i> under high light and low light	36
Fig. 3.3 CURT1 family members are not subunits of the known major thylakoid complexes	38
Fig. 3.4 Amounts of CURT1 family members remain stable regardless of the light conditions	39
Fig. 3.5 Photoinhibition and recovery analysis in WT (<i>Ler</i>), <i>oeCURT1A</i>, and <i>curt1abcd</i>	41
Fig. 3.6 CURT1A levels in thylakoid-protein kinase (PK) and phosphatase (PP) mutants, including <i>stn7</i>, <i>stn8</i>, <i>stn7 8</i>, <i>tap38</i>, and <i>pbcp</i>	43
Fig. 3.7 Thylakoid phosphorylation patterns of WT (<i>Ler</i>) and <i>oeCURT1A</i> under dark, GL and HL conditions	44
Fig. 3.8 TEM analysis of thylakoid ultrastructures of <i>curt1abc</i> and <i>curt1abc tap38</i>	45
Fig. 3.9 Quantification of CURT1 levels in <i>oeCURT1A</i>	46
Fig. 3.10 Effect of <i>curt1abc</i> complementation by single CURT1 member	47
Fig. 3.11 High molecular weight CURT1A complexes disassemble under HL conditions	49
Fig. 3.12 Complementation of <i>curt1a</i> and <i>curt1b</i> mutant plants with corresponding phospho-site exchange (PSE) variants	51
Fig. 3.13 CURT1B and CURT1A oligomerization behavior in Col-0, <i>stn8</i>, and <i>oeSTN8</i> under GL and HL conditions	53
Fig. 3.14 TROL is not a stable interaction partner of CURT1 complexes	54
Fig. 3.15 TEM analysis of <i>curt1abc</i> mutants complemented with the CURT1 of <i>Synechocystis</i> (<i>synCURT1</i>)	55

Fig. 4.1 Schematic model of CURT1 proteins promoting and regulating grana stacking under HL conditions	66
Fig. 5.1 PCR confirmation for <i>curt1abc tap38</i> line.....	67
Fig. 5.2 PCR confirmation for <i>curt1abcd backcross</i> line	67
Fig. 5.3 PCR confirmation for <i>curt1abcd pgr5</i> line.	68
Fig. 5.4 Analysis of CURT1 protein expression at different developmental stages	69

Abbreviations

1-qL	measure for the fraction of open PSII reaction centers
2-D	2-dimensional
<i>A. thaliana</i>	<i>Arabidopsis thaliana</i>
Ala	alanine
Asp	aspartic acid
β -DM	n-dodecyl β -D-maltoside
BN	blue-native
CaCl ₂	calcium chloride
cDNA	complementary DNA
CEF	cyclic electron flow
Cyt <i>b₆f</i>	the cytochrome <i>b₆f</i> complex
D	dark
DNA	deoxyribonucleic acid
EDTA	ethylene diamine tetraacetic acid
F _m	maximum fluorescence in the dark
F' _m	maximum fluorescence in the light
F ₀	fluorescence after dark adaptation
F _v	variable fluorescence
GFP	green fluorescent protein
GL	growth light
HEPES	4-(2-hydroxyethyl)-1-piperazineethanesulfonic acid
HL	high light
KCl	potassium chloride
KOH	potassium hydroxide
LEF	linear electron flow
LHCI/II	light harvesting complex I/II
LL	low light
LTR	long-term response
mRNA	messenger RNA
NaCl	sodium chloride

NADP ⁺	oxidized nicotinamide adenine dinucleotide phosphate
NADPH	reduced nicotinamide adenine dinucleotide phosphate
NaOH	sodium hydroxide
NDH	NAD(P)H dehydrogenase complex
NPQ	non-photochemical energy quenching
<i>oe</i>	overexpression
<i>oeCURT1A</i>	CURT1A overexpression line
<i>oeSTN8</i>	STN8 overexpression line
P ₆₈₀	PSII reaction center
P ₇₀₀	PSI reaction center
PAGE	polyacrylamide gel electrophoresis
PAM	pulse amplitude modulation
PCR	polymerase chain reaction
PK	protein kinase
pLHCII	phosphorylated light-harvesting complex of photosystem II
PP	protein phosphatase
PQ/ PQH ₂	plastoquinone (oxidized)/ plastoquinol (reduced)
PSE	phosphor-site exchange
PSI/II	Photosystem I/II
p-Thr	phosphothreonine
PVDF	polyvinylidene fluoride
qL	photochemical quenching
qT	fluorescence quenching because of state transition
RNA	ribonucleic acid
RT	room temperature
RT-PCR	reverse transcriptase-mediated PCR
SDS	sodium dodecyl sulphate
Ser	serine
Thr	threonine
Tris	tris (hydroxymethyl) aminomethane
WT	wild type
Y(II)	effective quantum yield of photosystem II

Units

°C	degree Celcius
g	gram
<i>g</i>	gravity
h	hour
k	kilo
kDa	kilodalton
l	litre
μ	micro
M	molar
m	metre
min	minutes
mL	millilitre
mM	millimolar
mol	molar
nm	nanometre
s	second
v	volume
w	weight

1. Introduction

1.1. Photosynthetic apparatus

Photosynthesis is a fundamental process on the earth, which assimilates solar light, produces sugar for energy storage, and converts CO₂ to O₂ to maintain the life cycle. Besides land plants, green algae and cyanobacteria also belong to the photosynthetic organisms, altogether designated photoautotrophs. Photosynthesis in eukaryotes (e.g. higher plant, green algae) takes place in the chloroplast, a specific organelle which evolved from cyanobacteria via an endosymbiosis event (Kutschera and Niklas, 2005). Chloroplasts of higher plants have double envelope membranes, the outer and inner envelopes surrounding a fluid, the stroma. The internal membrane system, known as thylakoid, is embedded within the stroma (shown in Fig. 1.1), and encloses a continuous internal space, the lumen. In general, there are two phases present in photosynthesis: the light reaction and the Calvin-cycle. Thylakoid membrane is the major place for light reactions, in which oxygen is produced during the water oxidization, and on the other hand, NADPH and ATP are generated for carbon fixation in Calvin-cycle (Taiz and Zeiger, 2010).

1.2. Four major protein complexes in the thylakoid membrane

The light reactions are carried out mainly by four complexes embedded vectorially in the thylakoid membrane, consisting of photosystem II (PSII), the cytochrome *b₆f* (Cyt *b₆f*) complex, photosystem I (PSI), and the ATP synthase (Fig 1.1).

As the first protein complex in photosynthesis, PSII can oxidize water to oxygen and release protons in the lumen. The PSII monomer in plants consists of 23 protein subunits, including 4 membrane-intrinsic proteins (PsbA-D), 3 membrane-extrinsic proteins (PsbO-Q), and 16 small proteins that span the membrane (Dekker and Boekema, 2005; Shi and Schroder, 2004). The dimeric PSII functions together with peripheral antennas, called light-harvesting complexes of PSII (LHCII). To date, six LHCII members (Lhcb1-6) have been described for PSII. With respect to their abundance, Lhcb1-3 are the major members that form a LHCII trimer, whereas

Lhcb4-6 are the minor ones existing as monomer. In brief, a typical PSII-LHCII supercomplex comprises of one PSII dimer, two tight- and two moderate-bound LHCII trimers, and two copies of Lhcb4-6 monomers (Dekker and Boekema, 2005)

The Cyt *b₆f* complex, providing the connection between PSII and PSI, is known as a 220 kDa, dimeric complex with each monomer composed of eight subunits (Baniulis *et al.*, 2008; Kurisu *et al.*, 2003). Among them, cytochrome *f* (Cyt *f*), cytochrome *b* (Cyt *b*), Rieske iron-sulfur protein (Rieske), and a 17 kDa subunit IV are the four major subunits associating with various cofactors. Heme is covalently attached to Cyt *f*, while a chemical equivalent of heme, protoheme, is noncovalently bound to Cyt *b*. In Rieske two iron atoms are bridged to the protein via two sulfur atoms. These cofactors are structurally and functionally important in delivering electrons and pumping protons from stroma into lumen for generation of proton motive force (Taiz and Zeiger, 2010).

In addition to PSII, the other photosystem is PSI, which accepts electrons from the Cyt *b₆f* complex and subsequently delivers them to NADP⁺ upon the absorbance of light energy. The PSI complex containing 15 subunits (PsaA-L, PsaN-P) mainly occurs as monomer (Jensen *et al.*, 2007), and is assembled to a PSI-LHCI supercomplex via interaction with four LHCI proteins (Lhca1-4).

The last complex, ATP synthase couples ATP production with the proton motive force of lumen (Allen, 2002). ATP synthase is a ~400 kDa enzyme complex that is comprised two parts: the membrane-embedded (CF₀) portion and the membrane-attached (CF₁) part anchored to the stromal side. In chloroplast, CF₀, consisting of four subunits with a stoichiometry of a, b, b', c₁₄, acts as the channel for the protons to pass through, while CF₁, the catalytic domain, contains five types of subunits with a stoichiometry of α₃, β₃, γ, δ, ε. The α₃β₃ hexamer generates a fan-like domain, which requires 14 protons for a full rotation, and in turn produces three ATP molecules (Allen, 2002; Taiz and Zeiger, 2010).

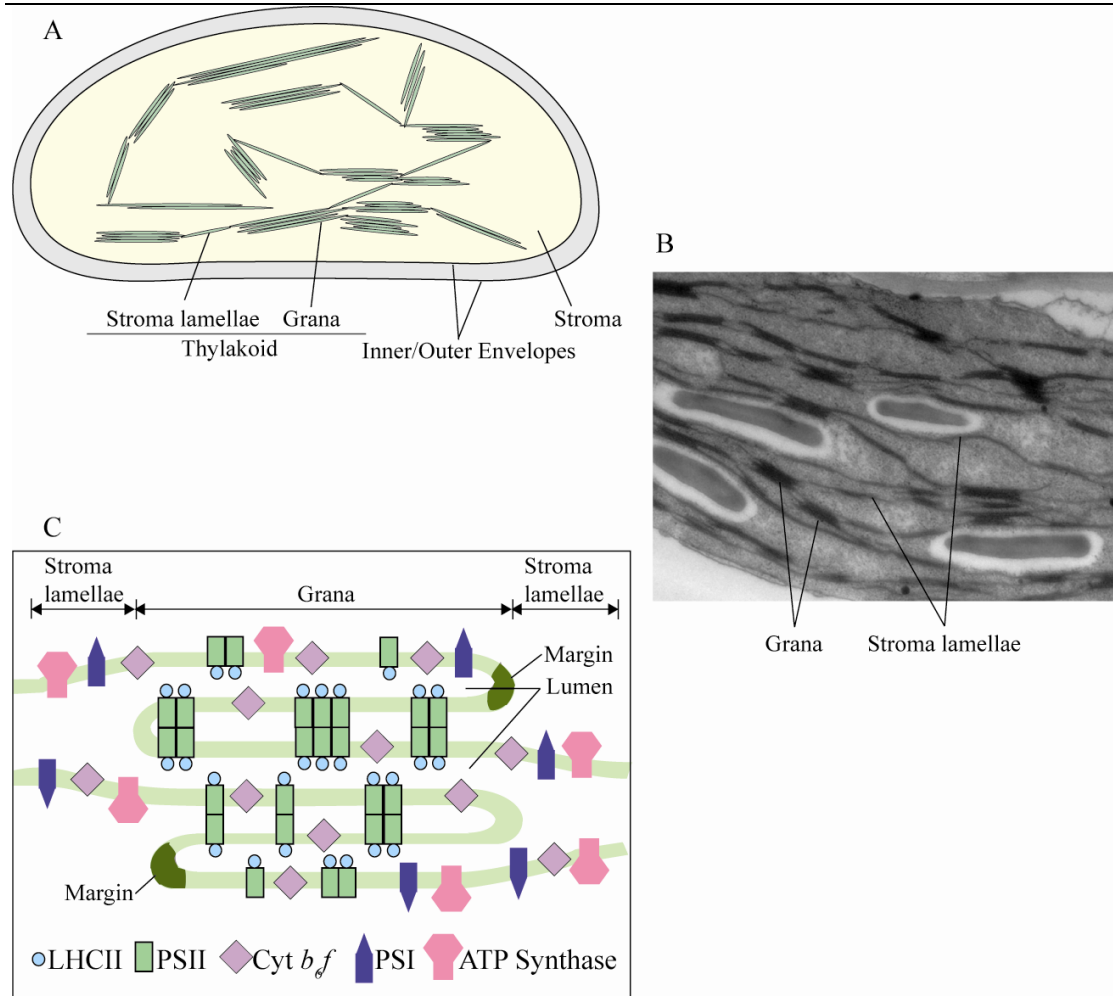


Fig. 1.1 Structures of the chloroplast and the thylakoid membrane. (A) The cartoon shows the structure of chloroplast. The outer and inner envelop membranes, the internal thylakoid membranes, and the stroma (aqueous phase surrounding thylakoid membranes) are indicated. (B) A transmission electron micrograph (TEM) of *A. thaliana* chloroplast obtained from the experimental data shows the structure of thylakoid. Grana and stroma lamellae are labeled. (C) The simplified model indicates the thylakoid structure. Grana are generated from curvature of a single thylakoid membrane and the lumen is a continuous part. Grana, stroma lamellae, margin, and lumen are indicated by lines. Cartoons are redrawn from Allen and Forsberg (2001).

1.3. Linear electron transport (LEF) and cyclic electron transport (CEF)

Linear electron transport (LEF) is referred to as electron transfer that starts from oxidation of water to reduction of NADP^+ and involves both PSII and PSI complexes. Instead, in the cyclic electron flow (CEF) electrons flow only through PSI system and consequently ATP is generated without accumulation of the reducing force, NADPH. It has been discovered that LEF and CEF orchestrate to adjust the ATP/NADPH ratio and meet the requirement of Calvin-cycle (Allen,

2002).

Although all components of LEF work simultaneously, while for convenience, here LEF is depicted stepwise following the electron flow from water to NADP^+ . First, the reaction center of PSII (P_{680}) is excited by light energy and transfers its energized electrons to a primary acceptor, pheophytin. After that, water is oxidized and split by the oxygen-evolving complex (OEC) of PSII, a process that extracts electrons to fill electron gaps in P_{680} and releases protons in the lumen and during which oxygen is produced as a by-product (Bricker *et al.*, 2012). Subsequently, pheophytin passes electrons to a plastoquinone, PQ_A , which is able to transfer the electrons to another plastoquinone, PQ_B . As it obtains two electrons from PQ_A and two protons from stroma, PQ_B is reduced to plastoquinol, PQ_BH_2 . Then PQ_BH_2 delivers two electrons to the Cyt *b₆f* complex, and simultaneously releases two protons into the lumen, and further returns to the oxidized form, PQ_B , which again retains the ability to accept electrons and protons. The reduced Cyt *f* donates electrons to plastocyanin, a small water-soluble protein localized in the lumen. Plastocyanin provides the electronic link between the Cyt *b₆f* complex and PSI. When PSI is excited by light, the reaction center (P_{700}) transfers the energized electrons to the primary acceptor, A_0 , followed by a chain of acceptors such as A_1 , and several iron-sulfur proteins including ferredoxin (Fd), which is the final acceptor of PSI. At last, the electrons of Fd are transferred to NADP^+ , which is catalyzed by ferredoxin- NADP^+ reductase (FNR). When protons pass through the channel (CF_0) of ATP synthase, the energy proton gradient drives ATP synthesis. In the LEF, the resulting NADPH and ATP are utilized for Calvin-cycle. Because the electron is energized twice in LEF, the process is also described as Z scheme (Allen, 2002; Evert and Eichhorn, 2013; Taiz and Zeiger, 2010).



In CEF, unlike the unidirectional electron flow in LEF, PSI behaves independently to drive a cyclic electron flow while PSII does not participate. At the beginning, the energized electrons from P_{700} follow the same way to Fd like LEF. However, electrons subsequently are delivered to plastoquinone pool rather than NADP^+ by several possible ways and then via Cyt *b₆f*, plastocyanin, finally return to the PSI reaction center. There are two principal pathways proposed for electron reinjection to the plastoquinone pool although the sources of the electron donor and acceptor remain elusive. One is mediated by the NADH dehydrogenase-like (NDH)

complex, which injects electrons from a yet unknown donor to the plastoquinone pool (Shikanai *et al.*, 1998). The other is the PGR5-dependent pathway (Proton Gradient Regulation 5), which is antimycin-sensitive (AA-sensitive) (Munekage *et al.*, 2002). PGRL1 (PGR5-Like), an essential component of the PGR5-dependent pathway, has been recently demonstrated to be the long-sought ferredoxin-plastoquinone reductase (FQR) that accepts electrons from Fd in a PGR5-dependent manner and reduces quinones in a AA-sensitive way (DalCorso *et al.*, 2008; Evert and Eichhorn, 2013; Hertle *et al.*, 2013). During the CEF process, a proton gradient for ATP synthesis is built up while no NADPH is generated. CEF is suggested to be involved in several physiological processes. For example, CEF is proposed to supplement ATP in addition to LEF since in Calvin-cycle carbon fixation requires a ATP/NADPH ratio of 3:2 rather than 9:7 as in LEF (Allen, 2002). Additionally, CEF contributes to the lumen acidification, which initiates non-photochemical quenching (NPQ), an essential regulation mechanism in plants to dissipate excess excitation energy (see section 1.4).

1.4. Regulation of photosynthesis: short-term responses

Since the photosystems have to cope with the light intensities in the environment, in respect of quality or quantity (e.g. excess light at noon, low light intensity under the canopy), it is challenging to perform a quick response (within seconds to minutes) to optimize the photosynthesis, which is defined as short-term response (Kulheim *et al.*, 2002; Wollman, 2001). When plants are exposed to excess light, toxic species such as superoxide, singlet oxygen, and peroxide, is produced. Due to the toxicity of these compounds, plants have evolved certain mechanisms of photoprotection acting on different levels including: nonphotochemical quenching (NPQ), the scavenging system, and the repair cycle (Asada, 1999; Li *et al.*, 2009). The first mechanism called NPQ aims to dissipate the excess light. During this process, excitation energy from the antenna system is dissipated as heat rather than utilized by photosystem (Baker, 2008; Krause and Weis, 1991). Several components probably coordinate to induce NPQ: (i) Xanthophyll cycle and (ii) PsbS-mediated pathway. The xanthophylls include three carotenoids: violaxanthin, antheraxanthin, and zeaxanthin (altogether short for VAZ). Under high light conditions, violaxanthin is converted to zeaxanthin via antheraxanthin

and bound to the antenna system, which changes the antenna conformation and further results in heat dissipation (Horton and Ruban, 2005). While it has been found that xanthophyll cycle itself is insufficient for initiation of NPQ, the binding of PsbS to the antenna system is also required (Li *et al.*, 2000; Muller *et al.*, 2001). Both of xanthophyll cycle and PsbS pathway are activated by the acidification of the lumen (ΔpH). The ΔpH dependent NPQ is designated qE, which is closely related to CEF since CEF deficient mutants (*pgr5*, *pgrl1*) can only generate reduced ΔpH in the lumen and therefore exhibit decreased NPQ values (DalCorso *et al.*, 2008; Johnson, 2005; Mullineaux, 2005; Munekage *et al.*, 2004). In addition to qE, NPQ includes qT (quenching due to state transitions) and qI (quenching due to photoinhibition), which will be described below. The second defense mechanism is the scavenging system, which relies on carotenoids, superoxide dismutase, and ascorbate. Toxic species mentioned above is generated when NPQ is incapable of dissipating all excess light. The scavenging system works to handle the toxic species and release the excess energy as heat. If the toxic species is still produced after the two above described mechanisms, it leads to the inactivation and damage of PSII (i.e. photoinhibition) (Long *et al.*, 1994). For this purpose, the third mechanism is responsible for the repair of PSII. Photoinhibition could be recovered in the early stage whereas prolonged damage requires the repair of photosystem. When the main target of photoinhibition, D1 subunit is destroyed, PSII is disassembled into monomers and migrates to the stroma lamellae. Then the damaged D1 is degraded and replaced with *de novo* D1 subunit synthesis. The D1 subunit interacts with the recycled undamaged PSII components, assembling the new functional PSII complex (Melis, 1999; Nixon *et al.*, 2010).

Besides excess light, plants often face the fluctuating light, which is variable in quality at different time points of day and specially preferred by PSI or PSII system. State transitions, are involved to deal with the imbalance of the energy distribution between the two photosystems (Allen and Forsberg, 2001; Finazzi, 2005). State transitions are based on the (de)phosphorylation of LHCII, which is ultimately controlled by the redox state of the plastoquinone pool. When the plastoquinone pool is reduced under certain conditions, for instance low white light or PSII-favoring light (red light), LHCII is phosphorylated by STN7 and associates with PSI to facilitate the light harvesting (State 2). In contrast, when darkness or PSI-favoring light (far-red light) induces an oxidation of plastoquinone pool, which leads to an

inactivation of STN7 and LHCII is gradually dephosphorylated by the recently discovered protein phosphatase, TAP38/PPH1, and finally re-associates with PSII (State 1) (Bellafiore *et al.*, 2005; Pribil *et al.*, 2010; Shapiguzov *et al.*, 2010). State transitions optimize the energy input between PSI and PSII to achieve the maximal efficiency of photosynthesis.

In addition, other short-term responses like water-water cycle also function to regulate photosynthesis (Kanervo *et al.*, 2005; Mehler, 1951; Miyake, 2010).

1.5. Regulation of photosynthesis: long-term responses

Imbalance of light excitation also leads to long-term response (LTR), which occurs in the time scale of hours and days, versus the short-term response taking place within minutes (Melis, 1991). According to different conditions, LTR alters relative gene transcription of the two photosystems and adjusts the stoichiometry of PSI and PSII, which can be monitored by measuring chlorophyll a/b ratio or F_s/F_m values (ratio of steady-state fluorescence to maximal fluorescence) (Fujita, 1997; Pfannschmidt *et al.*, 2001). Plants grown under PSI favoring light conditions usually exhibit decreased chlorophyll a/b ratio and increased F_s/F_m values. In contrast, plants display higher chlorophyll a/b ratio and lower F_s/F_m values under PSII favoring light conditions (Dietzel and Pfannschmidt, 2008). In *A. thaliana*, LTR is regulated by the redox state of the chloroplast and mediated by a two-component system, in which one kinase senses redox state of chloroplast and delivers the signals via phosphorylation of the second component, which therefore induces the following physiological responses (Stock *et al.*, 2000). A well characterized system in LTR is the CSK-SIG system, which is comprised of the chloroplast sensor kinase (CSK) and chloroplast sigma factor 1 (SIG1) (Baginsky *et al.*, 1999; Puthiyaveetil *et al.*, 2013; Puthiyaveetil *et al.*, 2010; Puthiyaveetil *et al.*, 2008; Shimizu *et al.*, 2010). Under PSI-favoring light conditions, SIG1 is phosphorylated (pSIG1) by CSK and then specifically represses the transcription of PSI genes, resulting in increase of stoichiometry of PSII relative to PSI (Fey *et al.*, 2005). While under PSII-favoring light, pSIG1 is gradually dephosphorylated as CSK is inactive. SIG1 shows no inhibition on gene transcriptions, PSI gene transcriptions are recovered under this light condition. In addition to the CSK-PTK system, STN7 is able to trigger the LTR in response to redox state, which possibly functions upstream

of the CSK because deletion of *stn7* results in no-response defects in LTR (Puthiyaveetil *et al.*, 2008). As the only known protein functioning in both state transitions (short-term) and LTR, STN7 might act as a redox-sensor and transducer that is essential for both responses (Bonardi *et al.*, 2005; Pesaresi *et al.*, 2010; Rochaix *et al.*, 2012; Tikkanen *et al.*, 2006).

1.6. Lateral heterogeneity—advantages of the organization

Thylakoids are comprised of grana and stroma lamella. A granum, consisting of several layers of thylakoid membrane, forms a column-shaped structure, which encapsulates the liquid matrix, the lumen. Within granum, thylakoid membrane displays strong bending in grana margin and thus leads to the stacking formation. Grana are interconnected by nonappressed layers, designated stroma lamellae (shown in Fig. 1.1) (Mustardy and Garab, 2003). In land plants, protein distribution differs between grana and stroma lamellae fractions (lateral heterogeneity): While Photosystem II (PSII) is mainly localized in grana and photosystem I (PSI) and ATP synthase are present in stroma lamellae, the Cyt *b₆f* complex shows a homogenous distribution all over thylakoid membrane (Dekker and Boekema, 2005). Grana structures are only found in higher plants and a recently evolved green algal group, indicating that grana might not be essential for photosynthesis (Anderson *et al.*, 2008). In addition, bundle sheath cells of chloroplasts of C₄ plant, where most thylakoid membranes are nonappressed, are quite distinct from those of C₃ plant or mesophyll cells of C₄ plant. So it is argued that heterogeneity is not essential for photosynthesis but an evolutionary solution to capture light under shade without disturbing quinone diffusion (Mullineaux, 2005).

Despite the controversy whether grana are indispensable for photosynthesis, the advantages of lateral heterogeneity are widely supported, such as prevention of excitation energy spillover, the organization of PSII-LHCII supercomplexes or even megacomplexes, switch between LEF and CEF to adjust ATP synthesis, regulation of light harvesting, regulation of PSII repair cycle *et al.*. (i) Prevention of excitation energy spillover. Because PSII is a rather ‘slow’ photosystem compared to PSI, excited chlorophyll can jump from PSII to PSI when they are closely localized. This situation is avoided by the development of grana, which has spatially segregated PSII from PSI (Trissl and Wilhelm, 1993). (ii) The organization of PSII-LHCII supercomplexes

or even megacomplexes (dimers of PSII supercomplex). In the grana, PSII-LHCII supercomplexes tend to form megacomplexes, which are more efficient in light harvesting, and thus far, three types of megacomplexes (type I, II, III) have been found in spinach. In *Arabidopsis* two types of megacomplexes (type III, IV) were identified whereas a type V was described for *Chlamydomonas reinhardtii* (Dekker and Boekema, 2005). (iii) Switch between LEF and CEF to adjust ATP synthesis: ATP synthesis of LEF is enhanced in grana, where the synthesis rate is two-fold higher than that of unstacked membranes. However, in some situations, enhancement of ATP synthesis by CEF is required. For example, when PSII is severely damaged during high light exposure, CEF needs to be stimulated for the supply of the ATP. Hence, the lateral heterogeneity ensures a fast switch between LEF and CEF for the optimal regulation (Chow, 1984; Joliot and Joliot, 2002). (iv) Regulation of light harvesting. State transitions occur for balance of energy flow between PSI and PSII (see section 1.4) and in state 2 the phosphorylated LHCII (pLHCII) is repelled from the grana and attached to PSI in the stroma lamellae (Chow *et al.*, 1981; Chow *et al.*, 2005). (v) Regulation of PSII repair cycles. Grana harbor photodamaged D1 subunits like a reservoir until the turnover takes place (Baena-Gonzalez *et al.*, 1999; Holt *et al.*, 2005; Rintamaki *et al.*, 1996).

1.7. Multiple factors for membrane curvature

1.7.1. Phosphorylation status of thylakoid proteins

The occurrence of grana in land plants raises an issue of how grana structures are formed and maintained in plant chloroplast. Based on previous work, there are several factors that can be envisioned to influence thylakoid membrane curvature, including the phosphorylation status of thylakoid proteins, membrane lipid composition, or curvature-facilitating proteins. These advances and their implications are discussed in the following.

Reversible phosphorylation regulates a wide range of cellular processes by affecting the activity or stability of target proteins (Cohen, 2000). By phosphoproteomic analyses in total 2597 unique phosphopeptides and 1346 phosphoproteins were identified from the whole cell lysates of *Arabidopsis* (Sugiyama *et al.*, 2008). Research on *Arabidopsis* seedlings resulted in identification of 3029 unique phosphopeptides and 1429 phosphoproteins, among which 174

are supposed to be chloroplast proteins (Reiland *et al.*, 2011). The protein phosphorylation reaction is catalyzed by protein kinases which transfer a phosphate groups from high energy molecules to specific substrate. There are ~1050 protein kinases known to be encoded by the nuclear genome in *Arabidopsis* (Martin *et al.*, 2009), 13 of these were confirmed to localize in the chloroplast, including STN7, STN8, cpCK2, TAK1, CIPK13, ABCK1, ABCK2, ABCK3, AtRP1, CSK, NDPK2, PPK, and At1g51170 (Bayer *et al.*, 2012). Among the extensively studied kinases, STN7 has been found to phosphorylate Lhcb1, Lhcb2, Lhcb4, Lhcb4, TSP9, and pTAC16 (Fristedt *et al.*, 2009a; Ingelsson and Vener, 2012; Rochaix, 2011) while STN8 predominantly catalyzes the phosphorylation of CP43, D1, D2, PSBH, Ca²⁺-sensing protein (CAS), and PGRL1 (Bonardi *et al.*, 2005; Vainonen *et al.*, 2005; Vainonen *et al.*, 2008). Two phosphatases TAP38/PPH1 and PBCP are recently reported to counteract STN7 and STN8, respectively. TAP38 and PBCP have some overlapping in substrates, i.e. TAP38/PPH1 is required for dephosphorylation of the Lhcb1, Lhcb2, D1, D2, and CAS, while PBCP mainly dephosphorylates D1, D1, and PSBH (Pesaresi *et al.*, 2011; Pribil *et al.*, 2010; Samol *et al.*, 2012; Schonberg and Baginsky, 2012; Shapiguzov *et al.*, 2010). It is well known that grana structures are changing to respond to light transitions, e.g. when plants are transferred from growth light (GL) to low light (LL) or shade, there are fewer grana per chloroplast, but more layers per grana stacking; When transferred from GL to high light (HL), the number of grana per chloroplast does not change, but each grana stacking contains more layers (Fig. 1.2A) (Anderson *et al.*, 1988; Anderson *et al.*, 2012). It has been widely supported that this short-term grana stacking plasticity is modulated by various (de)phosphorylation processes during light transitions (Fristedt and Vener, 2011; Fristedt *et al.*, 2009b; Tikkanen *et al.*, 2008). Additionally, the thylakoid ultrastructures of protein kinase (PK) or phosphatase (PP) mutants indicate that the deficiency in thylakoid (de)phosphorylation is closely linked to the alteration of grana formation and dynamics. For example, deletion of STN8 (*stn8*) not only led to aberrant grana stacking but also decreased the rate of D1 turnover under high light exposure (Fristedt *et al.*, 2009b). Furthermore, grana of *pbcp* and *tap38* mutants were also altered, although to a lesser extent (Samol *et al.*, 2012; Armbruster *et al.*, accepted). Despite no significant effect on grana stacking was observed for the *stn7* mutant, it is still a concentrated issue whether LHCI phosphorylation impacts on grana formation (Allen and Forsberg, 2001; Johnson *et al.*, 2011;

Kirchhoff *et al.*, 2011; Standfuss *et al.*, 2005).

Intriguingly, plants adapted to sun or high light contain more grana with fewer layers per chloroplast, while chloroplast of shade- and low-light acclimated plants harbors fewer grana with more stacked layers (Anderson *et al.*, 1988; Anderson *et al.*, 2012). The changes of grana stacking in the long-term seem to be also linked to phosphorylation processes (Bonardi *et al.*, 2005; Pesaresi *et al.*, 2010; Rochaix *et al.*, 2012; Tikkanen *et al.*, 2006).

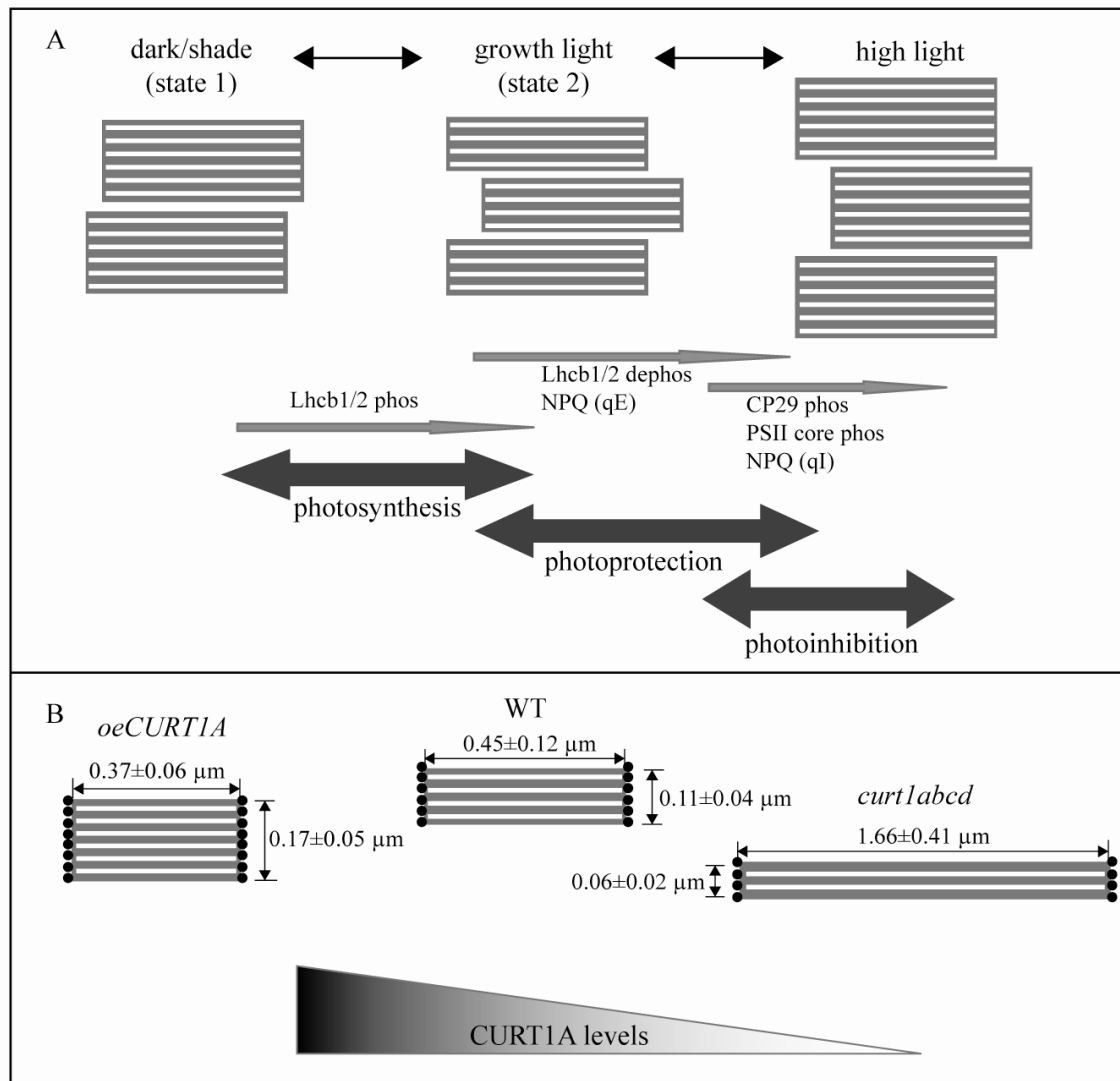


Fig. 1.2 Scheme on the plasticity of grana stacking under different light conditions (A) and grana phenotypes of *oeCURT1A* and *curt1abcd* (B). (A) Three light conditions were assessed—dark or shade (state 1), growth light (assumed as state 2) and high light. Associating with these light conditions, the respective formation of grana stacking and the biochemical reactions were shown. In accordance with these reactions, plants switched among efficient photosynthesis, photoprotection, and photoinhibition. (B) The average diameters and heights of grana stacking of *oeCURT1A*, WT, and *curt1abcd* are depicted. The CURT1A abundance is indicated by the arrow and its marginal localization is indicated by black cycles. Panel A is redrawn from Anderson *et al.* (2012); Panel B is based on results from Armbruster *et al.* (accepted).

1.7.2. Lipid composition

Membranes comprised of lipid bilayers with proteins embedded inside and this fluid mosaic model was first proposed in the 1970s (Singer and Nicolson, 1972). Lipids in biomembrane can be divided into three major types: phosphoglycerides, sphingolipids, and cholesterol. The observation that the lipid composition is variable among different cellular membranes suggests versatile roles for lipids regarding the physical properties of a membrane. Even within a lipid bilayer, lipid distribution can be asymmetrical between the two leaflets. Altogether, these findings indicate that the lipid composition and distribution play an important role in membrane curvature (Lodish *et al.*, 2013). Unlike most membrane systems, which are normally composed by over 50% of phosphoglycerides, the lipid composition of the thylakoid membrane shows a different composition with monogalactosyldiacylglycerol (MGDG) accounting for almost half of the lipid amount (Dorne *et al.*, 1990). However, MGDG displays no electrical charge and high degree of nonsaturation (containing six double bonds and a ring), such a high ratio of MGDG found in lipid was suggested to provide a more flexible membrane, facilitating movement of electron carriers or arrangement of large protein complexes (Gounaris and Barber, 1983).

1.7.3. Curvature-facilitating proteins

As a key component of biomembrane, proteins have inevitable effects on membrane curvature. So far, three mechanisms were proposed to play a role in generating membrane curvature. The first and second mechanisms represent so-called scaffold mechanisms in which the rigid protein scaffold is formed by either one large protein or oligomers of small proteins that bend membranes based on their intrinsic shape. The third mechanism represents a mechanism that is based on proteins containing amphipathic (AH) moieties. These proteins insert in only one layer of membrane, and by that provoke the monolayer deformation (Fig. 1.3) (Zimmerberg and Kozlov, 2006). Some proteins involved in membrane curvature have been functionally characterized in detail. For example, dynamin was firstly reported in fruit fly as a protein that forms a rigid scaffold structure, allowing for the constriction of membranes during endocytosis process (Chen *et al.*, 1991; Sweitzer and Hinshaw, 1998; van der Blik and Meyerowitz, 1991).

After that, epsin has been discovered in fruit fly, yeast, and mammalian cells and it facilitates curvature of clathrin-coated pits in endocytosis process. AH helix of epsin is the key motif for its function since mutations in this region abolished the curving ability (Ford *et al.*, 2002). Endophilin is another highly conserved cytoplasmic protein from nematode to human and involved in modulation of membrane dynamics. It can bend the membrane by insertion of its AH helix into bilayer and maintain the curvature by formation of a rigid crescent scaffold (Masuda *et al.*, 2006). Moreover, Pex11 is functionally conserved from yeast to human and is required to induce membrane curvature in peroxisome fission. The AH helix of Pex11 was suggested to be critical for membrane curvature as truncated peptides containing this region remained able to cause membrane tubulation (Opalinski *et al.*, 2011). Recent study on human α -synuclein and annexin B12 suggested that AH motif of protein is responsible for curvature sensing, while on the other hand binding of the curvature-facilitating protein to membranes is affected by other factors, e.g. charge density of membrane *et al.* (Borch Jensen *et al.*, 2011). In contrast to the progress of study in other organelles, the curvature-facilitating proteins in chloroplast are still poorly characterized. Grana-Deficient Chloroplast1 (GDC1) was recently reported to be essential for grana formation (Cui *et al.*, 2011). The deletion of *gdc1* completely abolished grana stacking formation in chloroplasts and consequently showed global defects in photosystem accumulation, causing seedling lethality. A more recently discovered protein family, the CURT1 protein family, is suggested to facilitate membrane curvature while their lack leads to only moderate defects on photosynthesis and growth rate (Armbruster *et al.*, accepted), which will be discussed in section 1.8.

1.8. Curvature Thylakoid1 (CURT1) family

The CURT1 family is a novel protein family in *Arabidopsis* involved in grana formation. Among the four family members, *CURT1A*, *B*, and *C* were identified as a regulon (a cluster of co-regulated genes under different conditions) based on transcriptomic analyses (Biehl *et al.*, 2005), while *CURT1D* was clustered with non-photosynthetic genes. CURT1 members are small nucleus-encoded proteins (*CURT1A*, 11.2 kDa; *CURT1B*, 13.9 kDa; *CURT1C*, 11.0 kDa; *CURT1D*, 15.7 kDa) containing amphipathic helix, form oligomers and are preferentially

localized in thylakoid margins. The single *curt1a* mutant contains flatter and longer grana with fewer layers. The double, triple and quadruple mutants exhibited even more severe effects on grana formation. In the contrast, grana stacking in *CURT1A* overexpression lines (*oeCURT1A*) were found to contain more layers, with a smaller diameter of grana (shown in Fig. 1.2B, lower panel). In addition to effects on grana stacking, these lines also showed pleiotropic effects on photosynthesis. For example, *curt1abcd* displayed lower Y(II) and higher 1-qL values, and additionally it was perturbed its state transitions and LEF process. Therefore, *curt1* mutants are the ideal objects to explore in detail the impact of altered grana structure on photosynthesis and the mechanism of grana formation (Armbruster *et al.*, accepted).

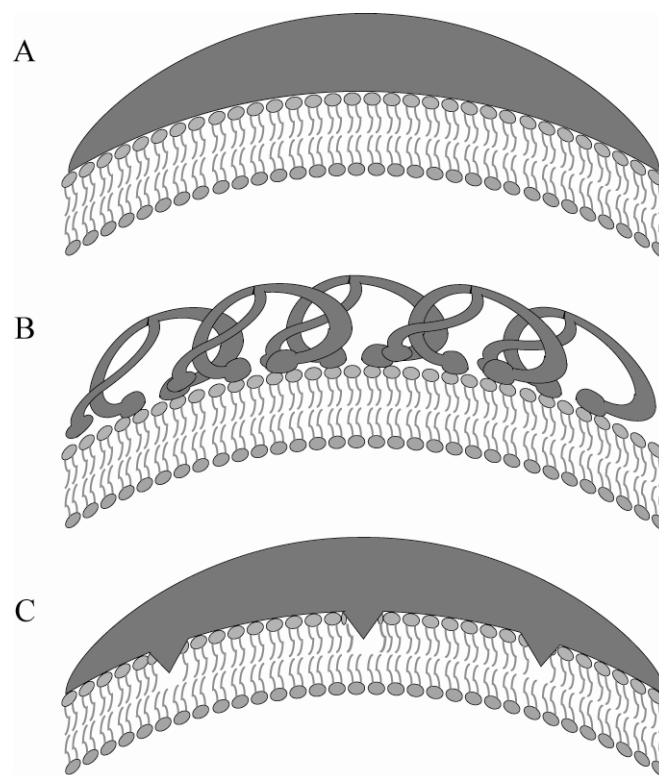


Fig. 1.3 Mechanisms of membrane curvature. (A) Scaffold mechanism. A rigid protein with an intrinsic curvature can bind and bend the membrane. (B) Polymerized proteins. Polymerized proteins form a rigid polymer exerting curvature stress on membrane. In this mechanism, the polymer sometimes links to membranes through adaptor proteins to stabilize the curvature (not shown). (C) Amphipathic helix insertion. By the insertion of amphipathic moieties of proteins into the lipid matrix, the membrane is deformed. Cartoons are redrawn from Zimmerberg *et al* (2006).

1.9. Aims of the thesis

The aims of this project were to study: (i) the effects of altered grana stacking on photosynthetic performance and growth rate, and (ii) to uncover the roles of CURT1 proteins and reversible phosphorylation in regulating grana formation in *Arabidopsis*, as well as the interplay between these two mechanisms.

To address the first part, *oeCURT1A* and *curt1abcd* mutants, which show distinct alternation in grana formation, were characterized in several aspects: (i) Photosynthetic performances and growth rates under various light conditions. (ii) D1 turnover kinetics under high light conditions. (iii) Distribution patterns of CURT1 and major thylakoid complexes under different light conditions.

The second part focuses on the effects of CURT1 amounts and reversible phosphorylation on grana formation.

Regarding the CURT1 proteins, the effects of CURT1 dosage and the functional redundancy were addressed. To this end, the expression levels of different CURT1 members were assessed in *oeCURT1A* line. Moreover, *curt1abc* mutants were complemented with CURT1 proteins from *Arabidopsis* or *Synechocystis* and thylakoid ultrastructure was analyzed by transmission electron microscopy (TEM).

In the light of phosphorylation, the goal was to check the role of phosphorylation on CURT1 proteins and grana stacking. The experimental approaches involved: (i) Assessment of CURT1 levels in PK/PP mutant lines, and (ii) Examination of the thylakoid ultrastructure of crossed mutants (*curt1abc/tap38*) and *curt1* mutants complemented with phospho-site exchange (PSE) proteins.

2. Materials and Methods

2.1. Plant materials and growth conditions

Arabidopsis thaliana (*A. thaliana*) seeds were sowed out on soil and left at 4 °C for 2 days in the dark to vernalize. Plants were grown in climate chambers under different light conditions. Chambers with growth light (GL, 120 $\mu\text{mol photons m}^{-2} \text{s}^{-1}$) have three light cycles, including long day (16 h light/8 h dark), intermediate day (12 h light/12 h dark), and short day (8 h light/16 h dark). High light (HL, 900 $\mu\text{mol photons m}^{-2} \text{s}^{-1}$, 12 h light/12 h dark) and low light (LL, 30 $\mu\text{mol photons m}^{-2} \text{s}^{-1}$, 12 h light/12 h dark) conditions were realized via a special Hg lamp (Osram Powerstar HQIBT-D/400 W) or phytotron (CLF Plant Climatics, Germany), respectively. Single (*curt1a*, *curt1b*, *curt1c*, *curt1d*) and the corresponding double, triple, and quadruple mutant lines, as well as *oeCURTIA* line, have been generated and screened before (Armbruster *et al.*, accepted). The *curt1a-1* and *curt1a-2* mutant lines (independent T-DNA insertions) were in Landsberg *erecta* (*Ler*) background, *curt1b* mutant line in Nossen (No-0) background, the *curt1c* and *curt1d* mutant lines in Col-0 background. The quadruple (*curt1abcd*) mutant was backcrossed twice to Columbia (Col-0) to reduce the other genetic backgrounds. All lines used in this work are summarized in Table 2.1 and new lines were generated on the basis of the existing lines.

To compare the growth rates of wild type (WT) and the different mutants under various light conditions, pictures of plants were taken once per week since two weeks after sowing out. The ImageJ software was used to calculate leaf areas (Abramoff *et al.*, 2004) and the obtained data were plotted into growth curves afterwards.

2.2. Nucleic acid analysis

Genomic DNA isolation was performed as previously reported with minor modifications (Liu *et al.*, 1995). In short, one *Arabidopsis* leaf was subjected to liquid nitrogen and broken to powder by metal beads, then incubated at 37 °C with 400 μL isolation buffer (200 mM Tris/HCl pH 7.5, 250 mM NaCl, 25 mM EDTA, 0.5% SDS) for 10 min. Subsequently,

samples were centrifuged at 16000 g at room temperature (RT) for 15 min. 350 µl supernatant was picked and mixed with the same volume of isopropanol for precipitation. After centrifugation at 16000 g at RT for 20 min, the pellet of genomic DNA was washed with 70% ethanol and resuspended in water.

PCR was performed by using specific DNA templates and Taq polymerase (Qiagen), and the following program were applied: initial denaturation at 94 °C for 3 min, followed by 33 cycles of 20 s denaturation at 94 °C, 30 s annealing at 55 °C and 1 min 30 s elongation at 72 °C. After the final elongation step of 5 min at 72 °C, the PCR products were analyzed by agarose gel electrophoresis. Two pairs of primer combination were used to determine whether a genetic locus is homozygous: one pair for detection of the T-DNA insertion, the other for amplification of the endogenous gene region. Primer combinations for respective T-DNA insertions are as follows: *CURTIA* (410as and Ds3-1); *CURTIB* (222s and Ds3-2); *CURTIC* (20s and LBB1); *CURTID* (1125as and LB1); *STN8* (exon1R and LBB1); *TAP38* (tap-as and LB1). Primer combinations for gene regions are: *CURTIA* (154s and 995as); *CURTIB* (222s and 521as); *CURTIC* (20s and 817as); *CURTID* (10s and 1125as); *STN8* (promF and exon1R); *TAP38* (tap-s and tap-as). The *oeCURTIA* line was generated in the *curt1a-2* mutant background and primers (411s and 916as) were designed to check for the insertion. All relevant primers in this work are listed in Table 2.2.

Genomic DNA of *Synechocystis* sp. PCC6803 (*Synechocystis*) was obtained from Stefania Viola (AG Leister). In detail, 1 ml logarithmic-phase cell culture was collected in the tube by centrifuge at 6000 g for 15 min and resuspended in 50 µl TER buffer (10 mM Tris/HCl pH 7.4, 1 mM EDTA pH 8.0, 100 µg/µl RNase A). Then 750 µl of XS buffer (1% Potassium ethyl xanthogenate, 100 mM Tris/HCl pH 7.4, 20 mM EDTA pH 8.0, 1% SDS, 800 mM NH₄OAc) was added and mixed by inverting the tube and the mixture was incubated at 70 °C for 2-3 h. The suspension was subjected to vortex for 10 s and left on ice for 30 min, subsequently centrifuged at 13000 g for 10 min. Supernatant was mixed with 750 µl isopropanol and incubated at RT for 10 min, followed by centrifuge at 12000 g for 10 min. Pellet was washed by 70% ethanol and dried for 10 min, then resuspended in 100 µl TE buffer (10 mM Tris/HCl pH 7.4, 1 mM EDTA pH 8.0).

2.3. RNA isolation and cDNA synthesis

Total RNA was extracted from fresh leaf materials using the TRIzol reagent (Invitrogen, Karlsruhe, Germany). First-strand cDNA was obtained by reverse transcriptase-mediated PCR (RT-PCR) following the protocol of iScript[™] cDNA Synthesis Kit (Bio-Rad). In brief, 500 ng RNA was mixed with 1 μ l iScript and 0.25 μ l transcriptase. DEPC-water was supplemented to final 5 μ l volume. Reaction was performed with the following program: initial step at 25 $^{\circ}$ C for 5 min, elongation step at 42 $^{\circ}$ C for 40 min and deactivation step at 85 $^{\circ}$ C for 5 min. The cDNA was diluted 1:20 with water for further experiments.

2.4. *Agrobacterium* binary vectors for complementation of *curt1a*, *curt1b*, and *curt1abc* mutant lines

2.4.1. *Agrobacterium* binary vectors for *curt1a* line

The cDNA (see section 2.3) was used as template to amplify *CURTIA* and *CURTIB* sequences. The genomic DNA of *Synechocystis* was used for amplification of the *CURT1* from *Synechocystis* (*synCURT1*). Since GATEWAY Technology (Invitrogen) was applied for vector construction, attB flanking sites were included in the primer sequences. For *CURTIA*, primers *CURTIA* Gate F and *CURTIA* Gate R were employed to amplify the native coding sequence (underlined sequence indicating the attB sequence, the rest coding for gene-specific region, see Table 2.3). To obtain single amino acid substitutions at position 64, 65 or 68, primers with altered nucleotide sequences (as indicated by lowercase alphabets in S64A F, S64SA R, S65A F, S65A R, S68A F, S68A R) were designed. These primers were combined with *CURTIA* Gate F or *CURTIA* Gate R (e.g. S64A F with Gate R, S64A R with Gate F) respectively to generate two fragments, containing an overlap because primers S64A F and S64A R are complementary. These two fragments were used as templates, combined with primers *CURTIA* Gate F and *CURTIA* Gate R to obtain the gene sequence with the altered nucleotide sequence at position 64. The same strategy was followed by inducing substitutions at position 65 and 68. To simultaneously substitute three amino acids at positions 64, 65, and 68, the primers tripleA F, tripleA R, tripleD F, and tripleD R (altered nucleotides are labeled

by lowercase letters, see Table 2.3) were designed and used for the same amplification strategy as described before. For better annealing, the *CURT1A* sequence containing a single mutation was used as a template. Finally, 6 gene sequences (NATIVE, S64A, S65A, T68A, STT-AAA, and STT-DDD) were obtained for vector constructions (see Table 2.4). For all vector construction steps, Phusion ® HF DNA polymerase (BioLabs) was applied in PCR. If not otherwise stated, the PCR program was as follows: initial denaturation at 98 °C for 5 min, followed by 10 cycles of 15 s denaturation at 98 °C, 30 s annealing at 75 °C (decreased by 1 °C per cycle) and 30 s elongation at 72 °C, then followed by 20 cycles of 15 s denaturation at 98 °C, 30 s annealing at 65 °C and 30 s elongation at 72 °C. After a final elongation step for 10 min at 72 °C, the PCR products were analyzed by agarose gel electrophoresis and purified by using gel purification kit (Qiagen).

Generation of *Agrobacterium* binary vectors was completed by applying the GATEWAY Technology according to manufacturer's instruction. In detail, the PCR fragments with attB sites were cloned into an entry vector (pDONR201) by BP reaction and then via LR reaction into a binary vector (pB7YGW2), which contains a GFP tag at the C-terminus (here a stop code was included to obtain protein without GFP tag). Heat-shock transformations were performed to introduce constructs into *Escherichia coli* DH5 α (*E. coli*) (Bethesda Res. Lab., 1986) and electroporation was used for transformation of constructs into *Agrobacterium tumefaciens* GV3101 (*A. tumefaciens*) (pMP90RK) (Koncz *et al.*, 1990).

2.4.2. *Agrobacterium* binary vectors for *curt1b* line

For *CURT1B*, the procedure was similar to that of *CURT1A*, the only difference was that only two amino acid residues were targeted for mutations. 5 gene sequences (NATIVE, T65A, T66A, TT-AA, and TT-DD) were finally cloned into the vectors (see Table 2.4).

2.4.3. *Agrobacterium* binary vectors for *curt1abc* line

Native *CURT1A*, *CURT1B*, *CURT1C*, *CURT1D*, and syn*CURT1* were employed to complement *curt1abc*. Generation of native *CURT1A* and *CURT1B* constructs was described in sections 2.4.1 and 2.4.2. For *CURT1C* and *CURT1D*, primers (*CURT1C* Gate F and *CURT1C* Gate R, *CURT1D* Gate F, and *CURT1D* Gate R) were designed to obtain the native

gene sequences. For *synCURTI*, chloroplast transit peptide (cTP) was added at its N-terminus to allow for the correct import into chloroplast. First, the cDNA of *A. thaliana* was used as a template to amplify the cTP sequence of the small subunit of the RuBisCO (*synCURTI* Gate F and *synCURTI* Fusion R). On the other hand, *synCURTI* gene sequence was amplified from *Synechocystis* genomic DNA (*synCURTI* Gate R and *synCURTI* Fusion F). The two fragments have overlapping sequence because S64A F and S64A R are complementary, which were fused by PCR with primers *synCURTI* Gate F and *synCURTI* Gate R.

2.5. *Agrobacterium*-mediated transformation

Arabidopsis plants (*curt1a*, *curt1b*, and *curt1abc*) were transformed with respective constructs using the floral-dipping method as previously described (Clough and Bent, 1998). Plants were dipped for 30 s in an *Agrobacterium* suspension solution containing 5% sucrose and 0.02% Silwet L-77. Afterwards, plants were sealed with plastic bags overnight to maintain a humid environment. Transformed plants were grown in the greenhouse until seeds (T1 material) were collected.

After selection by resistance to herbicide, positively transformed T1 plants were further tested for the presence of the respective coding sequences by PCR and protein accumulation by Western blot analysis. T2 seeds were harvested from positive T1 plants and used for further experiments if not otherwise stated.

2.6. PAM measurements

The Dual-PAM 100 system was applied to monitor PSII parameters (Walz, Germany). The Pulse Amplitude Modulation 101/103 system was used to measure *in vivo* chlorophyll a fluorescence as described before (Varotto *et al.*, 2000). Four to five plants of each genotype were analyzed, and F_v/F_m , Y(II), NPQ, and 1-qL were determined. The procedures were as follows, plants were dark-adapted for 15 min and minimal fluorescence (F_0) was measured. Then the maximum fluorescence (F_m) was determined by applying a saturation pulse (5000 $\mu\text{mol photons m}^{-2} \text{s}^{-1}$, 0.8 s). Subsequently, leaves were exposed to actinic light (37 $\mu\text{mol photons m}^{-2} \text{s}^{-1}$) for 10 min to drive electron transport between PSII and PSI in order to

determine the steady-state fluorescence (F_s) and the maximal fluorescence of light adapted plants (F'_m). In the end, the minimal fluorescence of light adapted plants (F'_0) was recorded after switching off the actinic red light. The four parameters were calculated as: $F_v/F_m = (F_m - F_0)/F_m$ (maximum quantum yield of PSII), $Y(II) = (F'_m - F_s)/F'_m$ (effective quantum yield of PSII), $1 - qL = 1 - (F'_0/F_s)(F'_m - F_s)/(F'_m - F'_0)$, and $NPQ = (F_m - F'_m)/F'_m$ (non-photochemical quenching) (Kramer *et al.*, 2004).

Quenching of chlorophyll fluorescence due to state transitions (qT) was measured according to (Pribil *et al.*, 2010). In brief, dark-adapted leaves were illuminated for 15 min with red light ($35 \mu\text{mol m}^{-2} \text{s}^{-1}$) and the maximum fluorescence in state 2 (F_{m2}) was measured. Afterwards, state 1 was induced by exposure to far-red light (level 20 in the Dual-PAM setting) for 15 min and F_{m1} was recorded. qT was calculated according to the following equation. $qT = (F_{m1} - F_{m2})/F_{m2}$.

The transient NPQ was determined to confirm the homozygosity of *pgr5* mutants. To this end, plants were previously dark-adapted for 16 h and then exposed to actinic light ($72 \mu\text{mol photons m}^{-2} \text{s}^{-1}$) for 2 min. In between saturation pulses ($5000 \mu\text{mol photons m}^{-2} \text{s}^{-1}$, 0.8 s) were applied every 10 s. The NPQ was calculated according to the same equation, as the $[NPQ = (F_m - F'_m)/F'_m]$, but represents transient NPQ due to transient acidification of thylakoid lumen (Munekage *et al.*, 2002).

2.7. Photoinhibition studies (D1 turnover assay)

To estimate D1 turnover rates in *Ler*, *oeCURTIA*, and *curt1abcd* plants, PSII functionality (F_v/F_m) were measured after HL exposure. Water and lincomycin (an inhibitor of plastid-encoded protein translation) treatments were applied according to methods described by Fristedt *et al.* (2009b) with some modifications. In detail, detached leaves with petioles were submersed into water or 1 mM lincomycin solution in darkness at 4 °C for 16 h. The leaves were placed on wet filter paper to prevent them from drying out, and then illuminated under HL exposure for 3 h followed by 3 h dark recovery. In between, *in vivo* chlorophyll a fluorescence was recorded by using the Walz Imaging PAM system. Different HL intensities, either 900 (HL) or $1300 \mu\text{mol photons m}^{-2} \text{s}^{-1}$ (Intense high light, IHL), were tested. Saturating light flashes ($5000 \mu\text{mol photons m}^{-2} \text{s}^{-1}$) were applied every half an hour or one hour to

determine F_v/F_m after 15 min of dark incubation.

2.8. Isolation of chloroplasts and thylakoids

Leaves of 4 to 5 week-old plants were homogenized in homogenization buffer (HB buffer: 450 mM sorbitol, 20 mM HEPES/KOH pH 8.4, 10 mM EDTA, 10mM NaHCO₃, 0.1% BSA) and filtrated through two layers of Miracloth (Calbiochem). Chloroplasts were collected by centrifugation at 4 °C, and 600 g for 4 min, followed by slow deceleration. The pellet was carefully resuspended with cut-tip in homogenization buffer and loaded on a 40/80 Percoll gradient (Aronsson and Jarvis, 2002). Intact chloroplasts migrated at the interface between the two Percoll phases after centrifugation at 6500 g for 20 min with slow acceleration and no brake. Chloroplasts were resuspended and washed with resuspension buffer (RB buffer, 300 mM sorbitol, 20 mM HEPES/KOH pH 8.4, 2.5 mM EDTA, 5 mM MgCl₂) for further use.

For thylakoid preparation, leaves from 4-week-old plants were harvested and homogenized in ice-cold T1 buffer (0.4 M sorbitol, 0.1 M Tricine/KOH pH 7.8, 0.5% milk powder) in the presence of protease inhibitors (200 µM PMSF, 1 mM benzamidine, 5 mM aminocaproic acid). The homogenate was filtered through two layers of Miracloth and centrifuged at 4 °C, 1500 g for 5 min. The pellet was resuspended in T2 buffer (20 mM HEPES/KOH pH 7.5, 10 mM EDTA pH 8.0), and thylakoids were collected by centrifugation at 10000 g for 5 min and subsequent resuspended in TMK buffer (10 mM Tris-HCl pH6.8, 10 mM MgCl₂, 20 mM KCl) for further use.

2.9. SDS-PAGE and Western blot analyses

Thylakoids equivalent to 4-5 µg of chlorophyll were solubilized in SDS loading buffer (50 mM Tris/HCl pH 6.8, 2% w/v SDS, 12% v/v glycerol, 50 mM DTT, 0.01% bromophenol blue) at 65 °C for 10 min and subsequently loaded and separated by SDS-PAGE (15% acrylamide (AA)) as described by Schagger and von Jagow (1987).

Proteins of denaturing SDS were transferred to PVDF membranes (Millipore, Eschborn, Germany) using a semi-dry blotter (Biorad) according to manufactor's instruction (Millipore) with some modifications. In detail, the semi-dry blotter was placed on a level bench top and

one sheet of wet filter paper from anode buffer I (0.3 M Tris, 10% methanol, pH 10.4) was placed. Two sheets of filter paper from anode buffer II (25 mM Tris, 10% methanol, pH 10.4) were placed on top of the first sheet, followed by placement of prepared PVDF membrane (activated in 100% methanol and transferred to anode buffer II, equilibrium for 5 min). Gel was pre-incubated in cathode buffer (25 mM Tris, 40 mM glycine, 10% methanol, pH 9.4) for 5 min and then placed on top of the membrane, covered by three sheets of filter papers from cathode buffer. In each step, air bubbles were removed by carefully rolling a glass stick over the surface of the layer to ensure an even transfer. Blot was carried out with current density of 1 mA cm^{-2} for 1 h. Membrane was stained with Ponceau-S red (0.5% Ponceau-S red, 1% acetic acid) as a control directly for an equal protein transfer. In short, the membrane was put in Ponceau-S red for 1 min and destained with 100% methanol to the desired contrast. For protein detection, the membrane was incubated with specific primary antibodies at RT for 2 h, followed by washing with TBST (10 mM Tris/HCl, pH 8.0, 150 mM NaCl, 0.1% Tween-20 v/v) for three times (10 min each). The washed membranes were incubated with secondary antibodies conjugated with horseradish peroxidase (HRP). Secondary antibody detection was performed by enhanced chemiluminescence (ECL kit, Amersham Biosciences).

2.10. Blue-native (BN) and second dimension (2-D) PAGE

For native PAGE analysis, thylakoids were prepared as described above and protein amounts were adjusted according to the chlorophyll concentration (Porra, 2002). Thylakoids equivalent to 100 μg of chlorophyll were washed twice with 200 μl TMK buffer, and then incubated in 750 mM ϵ -aminocaproic acid (ACA), 50 mM Bis-Tris/HCl pH 7.0, 5 mM EDTA pH 7.0, 50 mM NaCl with 1.6% (w/v) digitonin at 4 $^{\circ}\text{C}$ for 1 h on a wheel, or for 20 min with 1% (w/v) n-dodecyl- β -D-maltoside (β -DM) on ice. Solubilized protein complexes were obtained after centrifugation, 16000 g at 4 $^{\circ}\text{C}$ for 1 h (digitonin) or for 20 min (β -DM). The supernatant was supplemented with 5% (w/v) Coomassie Brilliant Blue in 750 mM ACA, and loaded onto polyacrylamide (PA) gels (5-12% AA). One-dimensional BN-PAGE was carried out as described by Schagger and von Jagow (1991). Stripes or BN-gels were used for 2-D PAGE analysis. In detail, stripes were incubated in solubilization buffer (100 mM DTT, 2% SDS, 66

mM Na₂CO₃) for 1 h at RT before loaded on the second dimension. The 2-D PAGE was carried out with a 15% AA denaturing SDS-PAGE.

2.11. Protein quantification

Protein amounts of different genotypes were quantified as follows: Linear gradient amounts of wild type protein (e.g. thylakoids equal to 4, 3, 2, and 1 µg of chlorophyll) and replicates of the proteins to be quantified were loaded in the same gel. SDS-PAGE and Western blot analysis were performed as described in section 2.9. Intensities of protein signals were analyzed using the software BioID.

2.12. Co-Immunoprecipitation (CoIP) assay

Isolated thylakoids equivalent to 100 µg of chlorophyll were resuspended in 120 µl Co-IP buffer (50 mM HEPES/KOH pH 8.0, 330 mM sorbitol, 150 mM NaCl, 1 mM PMSF). 30 µl of 5% digitonin was added and solubilization was carried out on a wheel at 4 °C for 1 h. Solubilized thylakoid membranes were collected as supernatant after centrifugation at 16000 g for 1 h at 4 °C. The soluble fraction was diluted 1:5 with Co-IP buffer and incubated on a wheel at 4 °C for 2 h after 1-20 µl of specific primary antibodies were added to allow for the antigen-antibody reaction to take place. Subsequently, pre-washed proteinA-agarose beads (five times with Co-IP buffer) were added and incubated on a wheel at 4 °C for another 2 h to capture antibody-bound proteins. Afterwards, the agarose beads were collected by centrifugation at 1000 g for 2 min and washed three times with the Co-IP buffer containing 1% digitonin and twice with Co-IP buffer. Captured proteins were eluted from the beads by incubation with SDS loading buffer at 65 °C for 10 min. Finally, samples were subjected to SDS-PAGE and Western blot analysis.

2.13. Immunogold labeling

For protein localization visualized by immunogold labeling, intact chloroplasts were isolated and resuspended in RB buffer as described before (see section 2.8). Chloroplast aliquots equivalent to 50 µg of chlorophyll were frozen and thawed to remove the chloroplast envelopes,

and then resuspended in 200 μ l Immuno-buffer (50 mM HEPES/KOH pH 8.0, 330 mM sorbitol, 0.50 mM BSA). Incubation with 40 μ l of primary antibodies was allowed overnight and unbound antibodies were washed twice using 400 μ l Immuno-buffer. Samples were collected at 200 g for 2.5 min and resuspended in 200 μ l Immuno-buffer, followed by addition of 20 μ l Anti-Rabbit IgG-Gold antibody (SIGMA). Incubation was on wheel at 4 $^{\circ}$ C for 1 h and samples were washed again with 400 μ l Immuno-buffer for five times to remove unbound secondary antibody. The samples were fixed as follows: First, the materials were incubated in fixation buffer (75 mM cacodylate, 2 mM $MgCl_2$, pH 7.0) containing 2.5% glutardialdehyde for 1 h and subsequently washed four times with fixation buffer (5 min, 15 min, 30min, and 60 min, respectively). The washed materials were incubated in fixation buffer containing 1% OsO_4 for 1 h and washed with fixation buffer for 15 min, followed by three additional washings with distilled water (5 min, 30 min, and 60 min, respectively). Second, dehydration steps were performed by incubation of the materials in water solutions with increased acetone concentration (10%, 20%, 40%, 60%, 80%, 100% acetone, each solution for 15 min). Afterwards, the materials were dried and subject to SEM and images were obtained by Gerhard Wanner (AG Wanner).

2.14. Scanning electron microscopy (SEM) and transmission electron microscopy (TEM) analyses

For scanning electron microscopy, envelope-free chloroplasts were scanned at 1 kV with a Zeiss AURIGA[®] high-resolution field-emission scanning electron microscope. For detection of immunogold labeling, the energy-selective in-lens (EsB) detector was used to obtain the back-scattered electron images.

For transmission electron microscopy, the sixth or seventh true leaf of 4 to 5 week-old plants were cut to slides and fixed as follows: First, the materials were incubated in fixation buffer containing 2.5% glutardialdehyde overnight and subsequently washed four times with fixation buffer (5 min, 15 min, 30min, and 60 min, respectively). The washed materials were incubated in fixation buffer containing 1% OsO_4 for 2 h and washed with fixation buffer for 15 min, followed by three additional washings with distilled water (15 min, 30min, and 60

min, respectively). Second, dehydration steps were performed by incubation of the materials in water solutions with increased acetone concentration (10% acetone for 2 h, 20% acetone for 30 min, 40% acetone for 15 min, 60% acetone for 30 min, 80% acetone for 15 min, 100% acetone overnight). Embedding was performed by incubation of the materials in resin/acetone mixture stepwise (1:1 for 4 h, 2:1 for 4 h and at last in 100% resin overnight). After complete polymerization, the materials were cut into slides with a microtome. Images were taken by Gerhard Wanner (AG Wanner) with an EM 912 electron microscope (Zeiss) installed with an integrated OMEGA energy filter operated in the zero-loss mode.

Table 2.1 T-DNA insertion lines in this work. Project names, AGI accessions, T-DNA accessions and the corresponding ecotypes are listed. The lines generated in the course of this work are underlined.

Name	AGI accession number	T-DNA insertion line	Ecotype background
<i>curt1a-1</i>	At4g01150	SGT4784	<i>Ler</i>
<i>curt1a-2</i>	At4g01150	GT_5_19630	<i>Ler</i>
<i>curt1b</i>	At2g46820	RATM15-2546-1_H	No-0
<i>curt1c</i>	At1g52220	SALK_052057	Col-0
<i>curt1d</i>	At4g38100	SAIL_1240_C05	Col-0
<i>curt1abcd</i>	At4g01150	<i>curt1a-1</i>	Col-0, <i>Ler</i> , No-0
	At2g46820	<i>curt1b</i>	
	At1g52220	<i>curt1c</i>	
	At4g38100	<i>curt1d</i>	
<i>oeCRUT1A</i>	At4g01150	GT_5_19630	<i>Ler</i>
<i>stn8</i>	At5g01920	SALK_060869	Col-0
<i>stn7 8</i>	At1g68830, At5g01920	SALK_073254	Col-0
<i>tap38</i>	At4g27800	SALK_025713	Col-0
<i>pbcp</i>	At2g30710	SALK_127920	Col-0
<i>pgr5</i>	At2g05620	EMS	Col-5
<i>trol</i>	At4g01050	SAIL_027_B04	Col-0
<i>oeCURT1A stn8</i>			Col-0, <i>Ler</i>
<i>curt1abc tap38</i>			Col-0, <i>Ler</i> , No-0
<i>curt1abcd pgr5</i>			Col-0, <i>Ler</i> , No-0, Col-5
<i>Bcurt1abcd</i>		<i>curt1abcd</i> backcross	Col-0

Table 2.2 List of primers used for characterizing T-DNA insertion lines. Gene-specific primers are grouped with respective background. T-DNA specific primers are listed separately. Ds3-1 and Ds3-2 are for DS-lines; LB1 is for SAIL-lines; LBB1 is for SALK-lines.

Gene	Name	Sequences 5' to 3'
<i>CURTIA</i>	154s	AACACCACTGAGTTGGATTTC
	410as	GACGAGGTCTCTTCTGAAGAA
	995as	AACATACAGAGAGAAAGCTGG
<i>CURTIB</i>	222s	ACTCCAAGATCGTCTCTACG
	521as	GGGGTTCTGCTGGAATGATT
<i>CURTIC</i>	20s	CAACTTTGCCTTCGCCATTGT
	817as	CTGGCCAAGTATATCCGCTA
<i>CURTID</i>	10s	TGCACCAGGTCTACCACAAT
	1125as	CACTCACTATCAGACCCAAG
<i>STN8</i>	promF	GAAAGGGAGAGCTTCAAAGAGATA
	exon1R	CAATCAGAGTGTCGAGGCCAA
<i>TAP38</i>	tap-s	GCATTGCAAGCTGGATCGTTG
	tap-as	TCATCAACACCCTTCTTTAAC
<i>oeCURTIA</i>	411s	TTCTTCAGAAGAGACCTCGTC
	916as	CTCAGCCAATTCCTTTCTGC
general	Ds3-1	GGTCCCCTCCGATTTCTGACT
	Ds3-2	CCGGATCGTATCGGTTTTTCG
	LB1	GCCTTTTCAGAAATGGATAAATAGCCTT GCTTCC
	LBB1	GCGTGGACCGCTTGCTGCAACT

Table 2.3 Primers used for the construction of the different complementation lines. AttB sequences for gateway cloning are underlined and altered nucleotides for amino acid exchange are indicated in lowercase characters.

Gene	Name	Sequences 5' to 3'	
<i>CURT1A</i>	Gate F	<u>GGGGACAAGTTTGTACAAAAAAGCAG</u> <u>GCTTCACCATGGCGATATCAGTAGCA</u>	
	Gate R	<u>GGGGACCACTTTGTACAAGAAAGC</u> <u>TGGGTGCTATTCGCTTCCTGCGAT</u>	
	S64A F	gcgTCAGAAGAGACCTCG	
	S64A R	CGAGGTCTCTTCTGA _{cg}	
	S65A F	TCT _{gcg} GAAGAGACCTCG	
	S65A R	CGAGGTCTCTTC _{cg} AGA	
	T68A F	TCTTCAGAAGAG _{gcg} TCG	
	T68A R	CG _{Acgc} CTCTTCTGAAGA	
	TripleA F	gctgcaGAAGAG _{gcc} TCGTCC	
	TripleA R	GGACG _{aggc} CTCTT _{ctgc} gc	
	TripleD F	gatgacGAAGAG _{gac} TCGTCC	
	TripleD R	gtcCTCTTC _{gtcatc} AGCTCT	
	<i>CURT1B</i>	Gate F	<u>GGGGACAAGTTTGTACAAAAAAGCAG</u> <u>GCTTCACCATGGCTTCTCTTTCAGTC</u>
		Gate R	<u>GGGGACCACTTTGTACAAGAAAGC</u> <u>TGGGTGTCAGCTGCTCCCTAATAT</u>
T65A F		AGAGCT _{gcg} ACTGAAGTT	
T65A R		AACTTCAGT _{cg} AGCTCT	
T66A F		AGAGCTACT _{gcg} GAAGTT	
T66A R		AACTTC _{cg} AGTAGCTCT	
DoubleA F		AGAGCT _{gctgct} GAAGTT	
DoubleA R		AACTTC _{agcagc} AGCTCT	
DoubledD F		AGAGCT _{gatgat} GAAGTTGGT	
DoubledD R		AACTTC _{atcatc} AGCTCTCGT	

Materials and Methods

<i>CURT1C</i>	GateF	<u>GGGGACAAGTTTGTACAAAAAAGCAGG</u> <u>CTTCACCATGGCTTCAATTTCTGCAAC</u>
	GateR	<u>GGGGACCACTTTGTACAAGAAAGC</u> <u>TGGGTGTCACTGGCCAAGTATATC</u>
<i>CURT1D</i>	GateF	<u>GGGGACAAGTTTGTACAAAAAAGCAG</u> <u>GCTTCACCATGGAGCTCTGCACCAGG</u>
	GateR	<u>GGGGACCACTTTGTACAAGAAAGC</u> <u>TGGGTGTCACTCACTATCAGACCC</u>
<i>synCURT1</i>	GateF	<u>GGGGACAAGTTTGTACAAAAAAGCAG</u> <u>GCTTCACCATGGCTTCCTCTATGCTC</u>
	GateR	<u>GGGGACCACTTTGTACAAGAAAGC</u> <u>TGGGTGCTAACCGCCAAAATTG</u>
	Fusion F	AAGAGTTAACATGGGCCGTA
	Fusion R	TACGGCCCATGTAACTCTT

Table 2.4 Complementation lines and lines including positional amino acid exchanges are categorized into three groups based on the mutant background. Project names, exchange positions and altered amino acids are listed in the table. Native or phosphorylation-site exchange (PSE) variants are described. Ser, Serine; Thr, threonine; Ala, alanine; Asp, aspartic acid.

Background	Name	Exchange position	Amino acids
<i>curt1a-1</i>	Native	Native	-
	S64A	64	Ser to Ala
	S65A	65	Ser to Ala
	T68A	68	Thr to Ala
	STT-AAA	64, 65, 68	All to Ala
	STT-DDD	64, 65, 68	All to Asp
<i>curt1b</i>	Native	Native	-
	T65A	65	Thr to Ala
	T66A	66	Thr to Ala
	TT-AA	65, 66	Both to Ala
	TT-DD	65, 66	Both to Asp
<i>curt1abc</i>	<i>35S:synCURT1 curt1abc</i>	Native	
	<i>35S:CURT1A curt1abc</i>	Native	
	<i>35S:CURT1B curt1abc</i>	Native	
	<i>35S:CURT1C curt1abc</i>	Native	
	<i>35S:CURT1D curt1abc</i>	Native	

3. Results

3.1. Characterization of *oeCURT1A* and *curt1abcd*

3.1.1. CURT1A is mainly localized in the thylakoid margin in *oeCURT1A* line

To check the localization of CURT1A in *oeCURT1A* line, immunogold labeling experiments were performed. During this experiment, a protein equally distributed over the thylakoid membrane (PETA) was used as a control. As shown in Fig. 3.1A, a SEM image revealed a surface view of characteristic envelope-free chloroplast of *oeCURT1A*—containing grana stacking (flat areas) and grana margins (bending membrane regions), and CURT1A displayed a localization predominantly in the margin area. This property was further supported by quantification of the gold signal distribution, where the gold signal densities approximately in margin were 4-fold higher than those in other area of thylakoid (Fig. 3.1B), indicating a higher accumulation occurred in the margins. These results demonstrated that even when CURT1A is overexpressed, it is still mainly localized in the margins, consistent with the previous observation on CURT1A distribution in WT plants (Armbruster *et al.*, accepted).

3.1.2. Growth of *oeCURT1A* and *curt1abcd* plants is retarded under various light conditions

As described previously (Armbruster *et al.*, accepted), grana stacks in *oeCURT1A* showed smaller diameter (0.37 μm versus 0.41~0.47 μm in WT) and consisted of more horizontal membrane layers (0.17 μm versus 0.11 μm in WT), however, *curt1abcd* displayed longer (1.66 μm) stacking with fewer layers (0.06 μm). To assess the influence of the altered thylakoid ultrastructure on plant growth, leaf areas of *oeCURT1A* and *curt1abcd* mutant plants under different light conditions were monitored every week as an indicator of growth. As shown in Fig. 3.2A-E, both *oeCURT1A* and *curt1abcd* exhibited a strong tendency for a smaller leaf area under all tested light conditions, while the leaf color was not altered compared to WT. The overall growth of *oeCURT1A* was more significantly affected in comparison to *curt1abcd*, especially under HL conditions. In Fig. 3.2F, the resulting retarded growth of *oeCURT1A*

under HL compared to WT is shown for 3-5 weeks old plants.

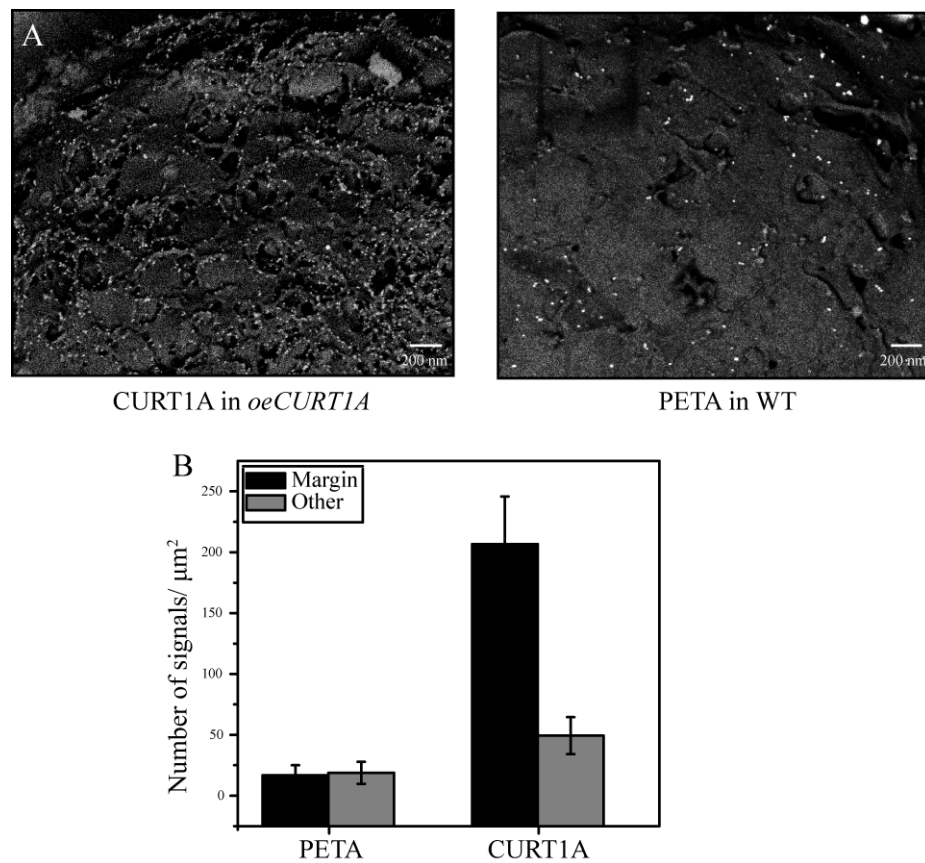


Fig. 3.1 Localization of CURT1A in *oeCURT1A* thylakoids by immunogold labeling. (A) Gold signals deriving from envelope-free chloroplasts, that represent the CURT1A protein distribution, were detected by scanning electron microscopy (SEM). Scale bars corresponding to 200 nm. (B) Comparison of CURT1A distribution between margins and other areas of thylakoid. PETA, which evenly localizes to the thylakoid, was used as a control. At least 8-10 SEM images were used to determine the distribution ration. Standard deviations were indicated by error bars.

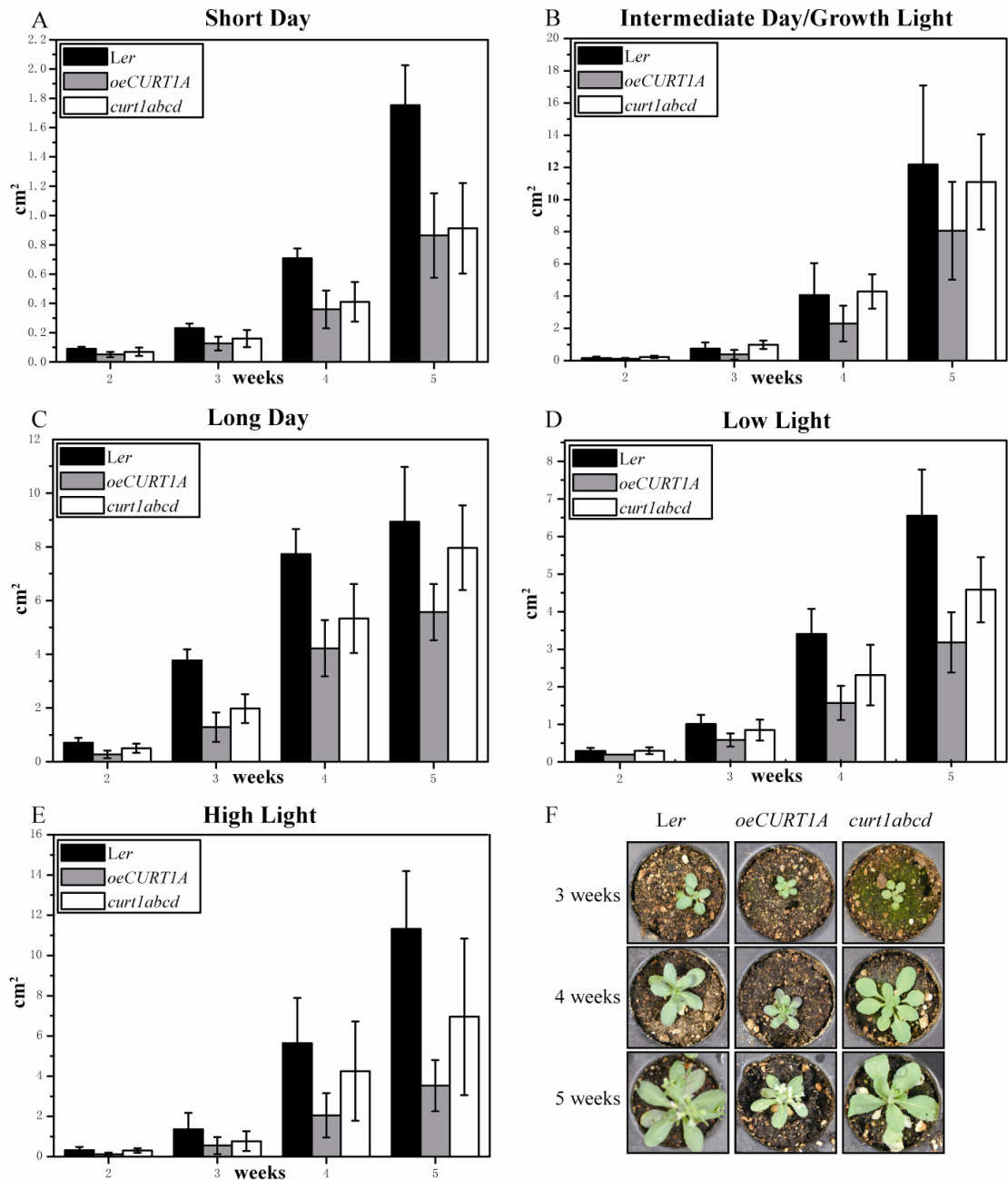


Fig. 3.2 Growth kinetics of *Ler*, *oeCURT1A*, and *curt1abcd* mutant plants under various light conditions. (A-E) Determination of leaf areas of *Ler*, *oeCURT1A*, and *curt1abcd* plants after 2-5 weeks of short day, intermediate day, long day, low light, and high light conditions. In each experiment, leaf areas of more than 10 plants were measured for each genotype. Standard deviations are indicated by error bars; (F) Pictures of *Ler*, *oeCURT1A*, and *curt1abcd* plants grown under HL conditions for 3, 4, and 5 weeks.

3.1.3. Differential CURT1A accumulation exerts pleiotropic effects on photosynthesis

To determine potential causes for the reduction in growth, photosynthesis efficiency of *oeCURT1A* and *curt1abcd* was examined under short day, intermediate day, and long day, as

well as LL, GL, and HL conditions. As shown in Table 3.1A and 3.1B, all three lines grown under GL conditions with different light cycles (long, short, and intermediate day), displayed no significant differences in the F_v/F_m and NPQ, indicating a functional PSII and regular non-photochemical quenching. However, in comparison to WT (*Ler*), Y(II) values of *oeCURT1A* and *curt1abcd* were decreased (Intermediate day: *oeCURT1A*, 0.66 ± 0.02 , *curt1abcd*, 0.54 ± 0.02 versus WT, 0.71 ± 0.01 ; Long day: *oeCURT1A*, 0.71 ± 0.01 , *curt1abcd*, 0.67 ± 0.01 versus WT, 0.75 ± 0.01 ; Short day: *oeCURT1A*, 0.65 ± 0.03 , *curt1abcd*, 0.58 ± 0.06 versus WT, 0.73 ± 0.02) whereas 1-qL values were increased (Intermediate day: *oeCURT1A*, 0.43 ± 0.04 , *curt1abcd*, 0.72 ± 0.02 versus WT, 0.33 ± 0.03 ; Long day: *oeCURT1A*, 0.35 ± 0.02 , *curt1abcd*, 0.51 ± 0.06 versus WT, 0.23 ± 0.06 ; Short day: *oeCURT1A*, 0.34 ± 0.09 , *curt1abcd*, 0.63 ± 0.06 versus WT, 0.28 ± 0.03). These observations implied a reduced quantum yield and higher excitation pressure in *oeCURT1A* and *curt1abcd*. As shown in Table 3.1C, no significant differences of these four parameters were observed in *oeCURT1A* under LL conditions compared to WT. Under the same conditions, *curt1abcd* showed similar F_v/F_m and NPQ values, but lower Y(II) (*curt1abcd*, 0.58 ± 0.06 versus WT, 0.73 ± 0.02) and much higher 1-qL values (*curt1abcd*, 0.63 ± 0.06 versus WT, 0.28 ± 0.03), like under GL conditions. Under HL conditions, the above mentioned parameters of *oeCURT1A* were similar to those of WT, nevertheless, *curt1abcd* mutants displayed decreased F_v/F_m (*curt1abcd*, 0.46 ± 0.13 versus WT, 0.80 ± 0.01) and Y(II) values (*curt1abcd*, 0.29 ± 0.12 versus WT, 0.75 ± 0.02), but increased NPQ (*curt1abcd*, 0.17 ± 0.09 versus WT, 0.07 ± 0.04) and 1-qL values (*curt1abcd*, 0.34 ± 0.22 versus WT, 0.09 ± 0.07). It is worth noting that high-light acclimated WT plants usually showed decreased NPQ values (WT grown under HL conditions, 0.07 ± 0.04) compared to WT grown under GL conditions, 0.38 ± 0.03), however, the NPQ values of *curt1abcd* mutants were similar under all tested conditions.

Taken together, the *oeCURT1A* plants showed moderately lower Y(II) and higher 1-qL values under GL, but no difference under LL and HL conditions. The *curt1abcd* line instead showed a more obvious reduction in Y(II) and a significant increased 1-qL under all tested conditions. Besides Y(II) and 1-qL values, *curt1abcd* grown under high light also showed reduced F_v/F_m and the tendency of increased NPQ compared to *Ler*. Our data suggest that the CURT1 proteins exert pleiotropic effects of on photosynthesis.

Results

Table 3.1A PAM parameters of *Ler*, *oeCURTIA*, and *curt1abcd* plants under growth light (12 h light/12 h dark cycle). Plants were kept under controlled climate chamber for 4 weeks under growth light before being subjected to PAM measurement.

	F_v/F_m	Y(II)	NPQ	1-qL	qT
<i>Ler</i>	0.84 ± 0.01	0.71 ± 0.01	0.38 ± 0.03	0.33 ± 0.03	0.10 ± 0.02
<i>oeCURTIA</i>	0.82 ± 0.01	0.66 ± 0.02	0.32 ± 0.04	0.43 ± 0.04	0.13 ± 0.04
<i>curt1abcd</i>	0.84 ± 0.01	0.54 ± 0.02	0.24 ± 0.01	0.72 ± 0.02	0.04 ± 0.01

Table 3.1B PAM parameters of *Ler*, *oeCURTIA*, and *curt1abcd* under long day (16 h light/8 h dark cycle) and short day (8 h/16 h dark light cycle). 3-week-old plants were measured for long day and 6-week-old plants for short day.

Long day					
	F_v/F_m	Y(II)	NPQ	1-qL	
<i>Ler</i>	0.83 ± 0.01	0.75 ± 0.01	0.23 ± 0.05	0.23 ± 0.06	
<i>oeCURTIA</i>	0.82 ± 0.01	0.71 ± 0.01	0.23 ± 0.05	0.35 ± 0.02	
<i>curt1abcd</i>	0.84 ± 0.01	0.67 ± 0.01	0.16 ± 0.04	0.51 ± 0.06	
Short day					
	F_v/F_m	Y(II)	NPQ	1-qL	
<i>Ler</i>	0.83 ± 0.01	0.73 ± 0.02	0.24 ± 0.04	0.28 ± 0.03	
<i>oeCURTIA</i>	0.78 ± 0.02	0.65 ± 0.03	0.25 ± 0.06	0.34 ± 0.09	
<i>curt1abcd</i>	0.82 ± 0.02	0.58 ± 0.06	0.17 ± 0.06	0.63 ± 0.06	

Table 3.1C PAM parameters of *Ler*, *oeCURTIA*, and *curt1abcd* under high light (900 $\mu\text{mol photons m}^{-2} \text{s}^{-1}$, 12 h light/12 h dark cycle) and low light (30 $\mu\text{mol photons m}^{-2} \text{s}^{-1}$, 12 h light/12 h dark cycle). 5-week-old plants were measured for both conditions.

High light					
	F_v/F_m	Y(II)	NPQ	1-qL	
<i>Ler</i>	0.80 ± 0.01	0.75 ± 0.02	0.07 ± 0.04	0.09 ± 0.07	
<i>oeCURTIA</i>	0.78 ± 0.01	0.76 ± 0.01	0.05 ± 0.05	0.02 ± 0.02	
<i>curt1abcd</i>	0.46 ± 0.13	0.29 ± 0.12	0.17 ± 0.09	0.34 ± 0.22	
Low light					
	F_v/F_m	Y(II)	NPQ	1-qL	
<i>Ler</i>	0.83 ± 0.00	0.68 ± 0.03	0.25 ± 0.12	0.39 ± 0.02	
<i>oeCURTIA</i>	0.80 ± 0.02	0.65 ± 0.05	0.26 ± 0.04	0.31 ± 0.16	
<i>curt1abcd</i>	0.79 ± 0.01	0.49 ± 0.03	0.17 ± 0.05	0.68 ± 0.05	

3.1.4. Overexpression of CURT1A has no effect on major thylakoid complex assembly and migration behavior

The altered photosynthetic parameters and growth kinetics of *oeCURT1A* under GL conditions (see section 3.1.3) might result from changes in the composition of major thylakoid complexes. To this end, thylakoids of WT (*Ler*), *oeCURT1A*, and *curt1abcd* after different light exposure were analyzed by BN-PAGE. In Fig. 3.3A left panel, the *oeCURT1A* exhibited equal complex distribution patterns under all three light conditions compared to *Ler*, which indicates the correct complex assembly or migration behavior. This conclusion was further confirmed by the Western blot analysis of LHCB1, PSAB, and PETB distribution patterns. In addition, CURT1A was also detected and its distribution patterns were the same for both phenotypes (Fig. 3.3B). The *curt1abcd* line, which has been shown no defects in major thylakoid complex assembly (Armbruster *et al.*, accepted), was included as a control. Taken together, these observations suggested the assembly and migration behavior of the major thylakoid complexes, as well as CURT1 complexes, was not affected in the *oeCURT1A* line.

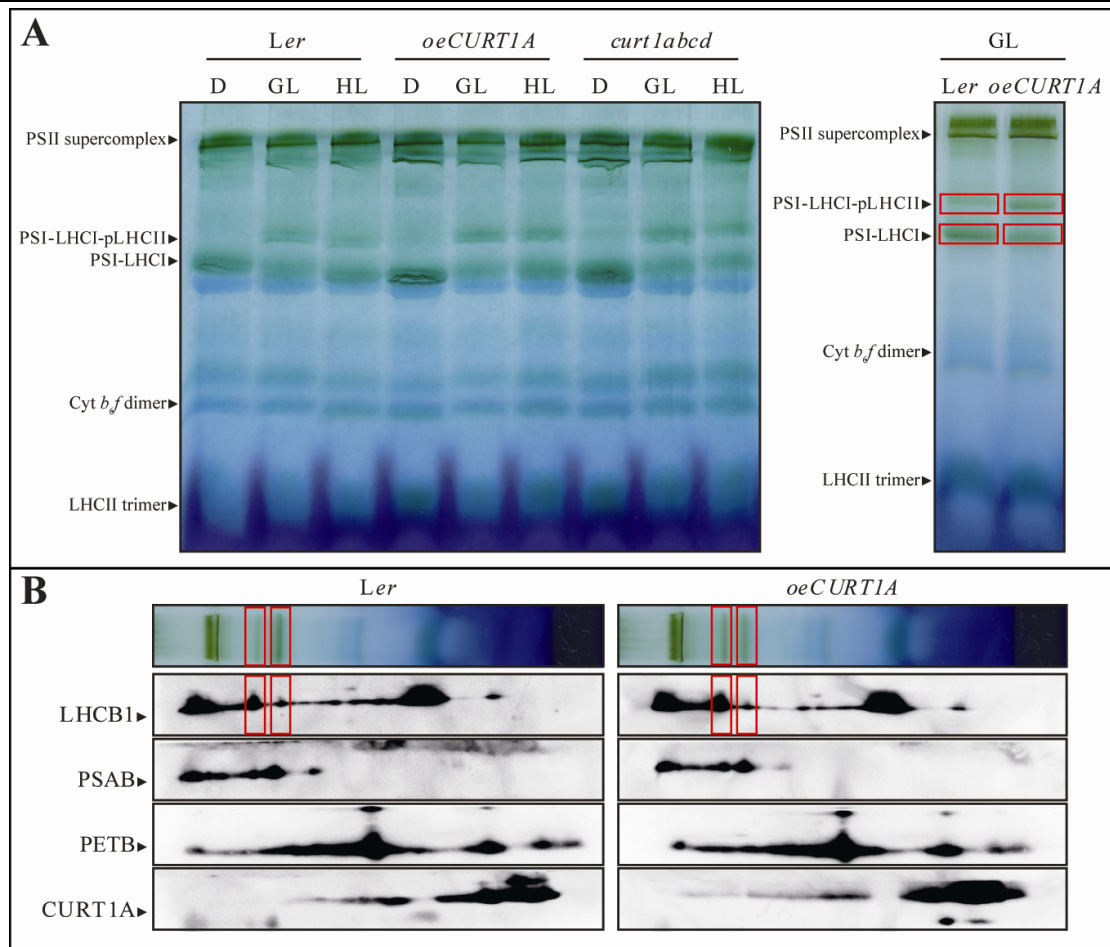


Fig. 3.3 CURT1 family members are not subunits of the known major thylakoid complexes (PSI, PSII, the cytochrome *b₆/f* complex or ATP synthase) according to BN- and 2-D PAGE analyses. Thylakoids of *Ler*, *oeCURT1A*, and *curt1abcd* equal to 50 μ g of chlorophyll were loaded. No significant changes among these three phenotypes, either in pigment complex compositions (BN) or complex distributions (2-D PAGE), could be observed. (A) Left panel: BN patterns of digitonin treated *Ler*, *oeCURT1A*, and *curt1abcd* thylakoids after dark, GL, and HL exposure; Right panel: BN patterns of digitonin treated *Ler* and *oeCURT1A* after GL exposure. (B) 2-D PAGE of *Ler* and *oeCURT1A* thylakoids under GL exposure. To obtain comparable signal intensities, the exposure time during ECL detection of CURT1A in *oeCURT1A* were significantly decreased. D, dark; GL, growth light; HL, high light.

3.1.5. The *oeCURT1A* line shows a more pronounced state 2 under GL conditions

It is interesting to note that in *oeCURT1A* the stoichiometry between PSI-LHCI-pLHCII and PSI-LHCI was significantly altered under GL conditions (Fig. 3.3A, right panel) compared to WT (*Ler*). Since these two complexes are indicators for state transitions (PSI-LHCI-pLHCII for state 2 and PSI-LHCI for state 1), their altered stoichiometry drove us to analyze state transitions by PAM-fluorimetry. The comparison of average qT values between *oeCURT1A*

and WT (*oeCURT1A*, 0.13 ± 0.04 versus WT, 0.10 ± 0.02), indicated a more pronounced extent in state transitions within *oeCURT1A*. The quadruple mutant *curt1abcd* as a control, behaved in accordance with previously reported values (0.04 ± 0.01) (Armbruster *et al.*, accepted). Our data indicated that in contrast to the *curt1abcd* mutant, *oeCURT1A* plants exhibited a larger extent of state transitions and formed more PSI-LHCI-pLHCII complexes under GL conditions.

3.1.6. The overall CURT1 levels remain stable under dark, GL, and HL conditions

The observed alternations in growth of *oeCURT1A* under GL conditions could possibly result from differences in CURT1 stability induced by light. To test this hypothesis, the accumulation of CURT1 members was examined after dark, GL, and HL treatment. CURT1A, B, and C remained stably expressed under all tested conditions in *Ler*. Similarly, in *oeCURT1A* no differences were observed under different conditions with respect to the protein levels of CURT1A, B, and C. CURT1D was not detected in both lines due to its low abundance, as observed before (Armbruster *et al.*, accepted). Therefore, we concluded that it is not the CURT1 stability that accounts for growth phenotype differences.

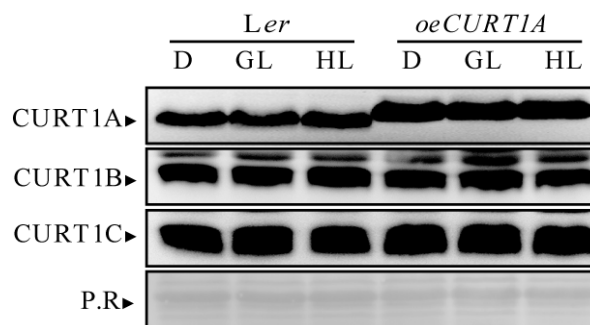


Fig. 3.4 Amounts of CURT1 family members remain stable regardless of the light conditions. To assess the light-dependence of CURT1 protein accumulations, CURT1A, CURT1B, CURT1C, and CURT1D levels were examined under dark, GL, and HL in *Ler* and *oeCURT1A*. Ponceau-S red staining was used as a loading control. D, dark; GL, growth light; HL, high light.

3.1.7. D1 turnover is not affected in *oeCURT1A*, but slightly affected in *curt1abcd*, under short HL conditions

Recently, D1 turnover efficiency was suggested to be affected by grana stacking modulation

(Fristedt *et al.*, 2009b). The growth phenotypes of *oeCURTIA* and *curt1abcd* might be due to the defects in D1 turnover. To elucidate the D1 turnover rates in *oeCURTIA* and *curt1abcd*, F_v/F_m was monitored as a measure of PSII integrity. F_v/F_m values were recorded during 3 h of HL exposure and 3 h of recovery in the dark. In order to repress the D1 repair cycle, lincomycin was added to inhibit the *de novo* synthesis of plastid encoded proteins. Fig. 3.5A (water) and 3.5B (lincomycin) depicted the results of the D1 turnover assay of leaves exposed to 900 $\mu\text{mol photons m}^{-2} \text{s}^{-1}$, the same HL conditions used for the growth measurement (section 3.1.2). As shown in Fig. 3.5A, the F_v/F_m values of *Ler* showed a steady decline (0.74 to 0.44) during HL exposure after 3 h and recovered to 0.53 after dark incubation. The *oeCURTIA* and *curt1abcd* plants showed a similar performance: The F_v/F_m values of *oeCURTIA* decreased from 0.70 to 0.43, and recovered to 0.49. Likewise, The F_v/F_m values of *curt1abcd* dropped from 0.71 to 0.40, and were restored to 0.45 after the dark recovery phase. When *de novo* D1 translation was blocked by addition of lincomycin (Fig. 3.5B), the F_v/F_m curves showed a significantly different progression. The F_v/F_m values in *Ler* decreased sharply (0.73 to 0.14) and only slightly recovered (0.17). The F_v/F_m values of *oeCURTIA* displayed a similar behavior, the significant reduction (0.70 to 0.16) and minor recovery (0.17). For *curt1abcd*, the F_v/F_m values reduced to a similar level during the HL illumination (0.73 to 0.11), but further decreased after the recovery phase (0.09). The identical performance of *Ler* and *oeCURTIA* under 900 $\mu\text{mol photons m}^{-2} \text{s}^{-1}$ might be due to insufficient stress from this light intensity, so intense high light (IHL) conditions (1300 $\mu\text{mol photons m}^{-2} \text{s}^{-1}$) were applied (Fig. 3.5C water, Fig. 3.5D lincomycin). The F_v/F_m values of *oeCURTIA* and *curt1abcd* showed no significant differences compared to *Ler* in water-treated leaves. The F_v/F_m values of *Ler* reduced from 0.78 to 0.49 after IHL exposure and recovered to 0.54 after dark incubation (Fig. 3.5C). Similarly, the values of *oeCURTIA* dropped from 0.76 to 0.52 and were raised to 0.55, and values of *curt1abcd* reduced from 0.78 to 0.46 and were restored to 0.52 after the recovery phase (Fig. 3.5C). When lincomycin was applied, the F_v/F_m values of *Ler* and *oeCURTIA* exhibited no significant differences. The values of *Ler* decreased from 0.78 to 0.07 after exposure then recovered to 0.15. The *oeCURTIA* displayed the comparable values (reduce from 0.79 to 0.11, recovered to 0.16) (Fig. 3.5D). In contrast, the F_v/F_m values of *curt1abcd* severely reduced after HL exposure (0.78 to 0.01) and after the dark recovery phase recovered to 0.09, which

remained significantly lower compared to *Ler*. Based on these results, we propose that photoinhibition in water-incubated leaves was not significantly affected in the *oeCURT1A* and *curt1abcd* lines under short HL treatments. In the presence of lincomycin, the *curt1abcd* mutant showed a slower dark recovery of the F_v/F_m values compared to the other two genotypes, which could result from a retarded D1 turnover process.

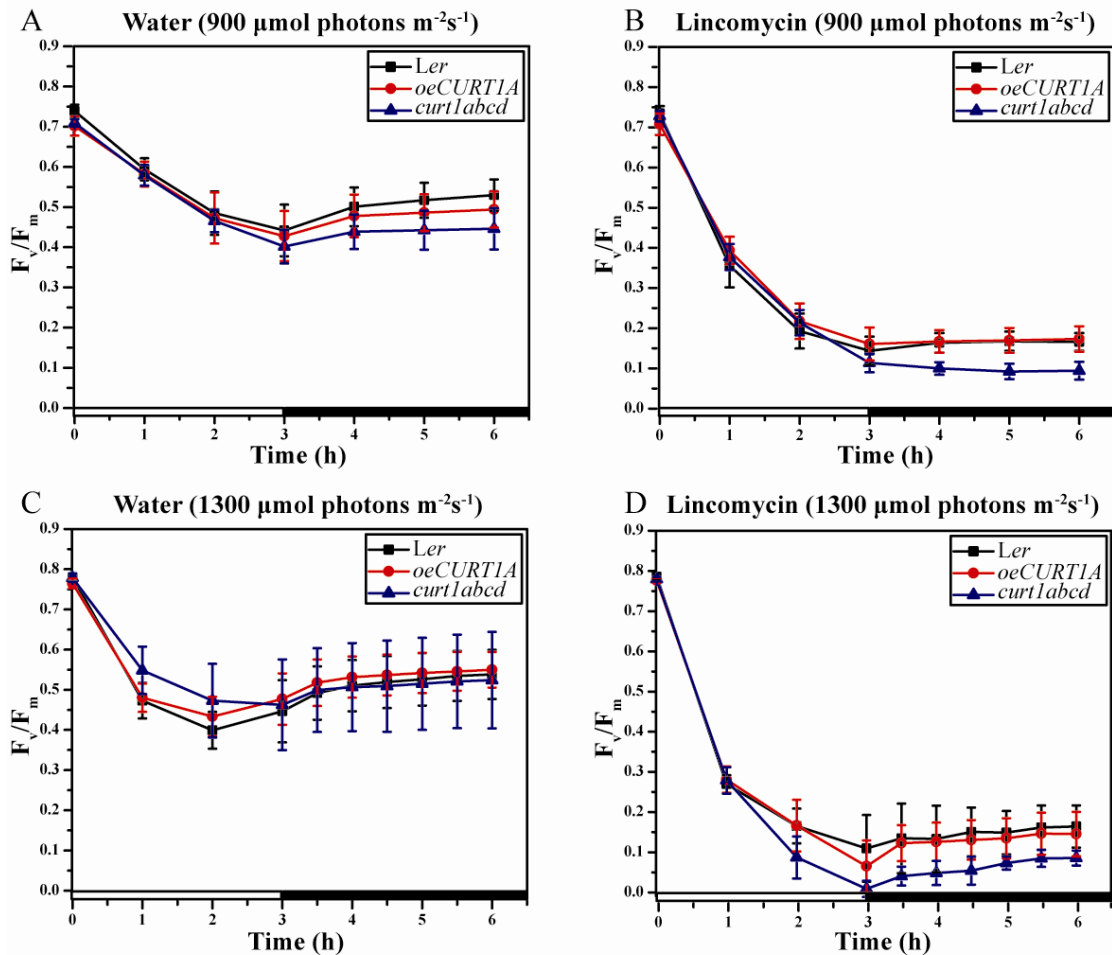


Fig. 3.5 Photoinhibition and recovery analysis in WT (*Ler*), *oeCURT1A*, and *curt1abcd*. PSII integrity was monitored via the F_v/F_m value under different HL intensities and lincomycin treatments. (A+B) HL (900 $\mu\text{mol photons m}^{-2}\text{s}^{-1}$), was applied to detached leaves for 3 h to induce photoinhibition. Leaves were allowed to recover in the dark for 3 h after treatment. 1 μM lincomycin (B) was applied to inhibit D1 *de novo* synthesis in comparison to water treatment (A). In (A+B), F_v/F_m was measured every 1 h. (C+D) IHL (1300 $\mu\text{mol photons m}^{-2}\text{s}^{-1}$) was applied to induce photoinhibition for 3 h, followed by 3 h dark relaxation. In comparison to (A+B), the F_v/F_m value was assessed every 1 h during light exposure and every 30 min during recovery stage. Panel C, water treatment; Panel D, lincomycin treatment. For each time point, at least five leaves were measured. Mean values and standard deviations are indicated by error bars. HL, high light; IHL, intense high light.

3.2. Grana stacking is affected by (I) the amount of CURT1 and (II) thylakoid phosphorylation

Previous observations have suggested that the CURT1 protein family probably functions to induce membrane curvature, and thus involved in grana formation in a dosage-dependent manner (Armbruster *et al.*, accepted). On the other hand, thylakoid phosphorylation was also shown to affect the degree of grana stacking based on the investigation of the protein kinase (PK)/phosphatase (PP) mutants such as, *stn7 8* and *pbcp* (Fristedt *et al.*, 2009b; Samol *et al.*, 2012). Data in section 3.2 provided some insights into interference of CURT1-dosage and thylakoid phosphorylation regarding grana stacking.

3.2.1. CURT1A levels are decreased in *stn7* and *stn7 8*

To further clarify the effects of differential thylakoid phosphorylation on grana formation and assess whether the grana stacking phenotypes of lines with altered thylakoid phosphorylation are caused by different expression levels of CURT1, we investigated accumulation of CURT1A in five PK and PP mutant lines, *tap38*, *pbcp*, *stn7*, *stn8*, and *stn7 8*. CURT1A levels of different lines were detected and quantified based on their signal intensities (Fig. 3.6A). As shown in Fig. 3.6B, compared to WT plants, CURT1A levels in *stn8*, *tap38* or *pbcp* did not exhibit significant differences, although differential grana stacking was found in *stn8* and *pbcp* plants (Fristedt *et al.*, 2009b; Samol *et al.*, 2012), indicating that differences in grana stacking of *stn8* and *pbcp* result from altered PSII core protein phosphorylation, rather than changes in CURT1 accumulation. The expression of CURT1A in *stn7* was moderately decreased (CURT1A percentage, $78 \pm 8\%$ of WT) while *stn7 8* mutant displayed the lowest expression of CURT1A ($68 \pm 7\%$ of WT).

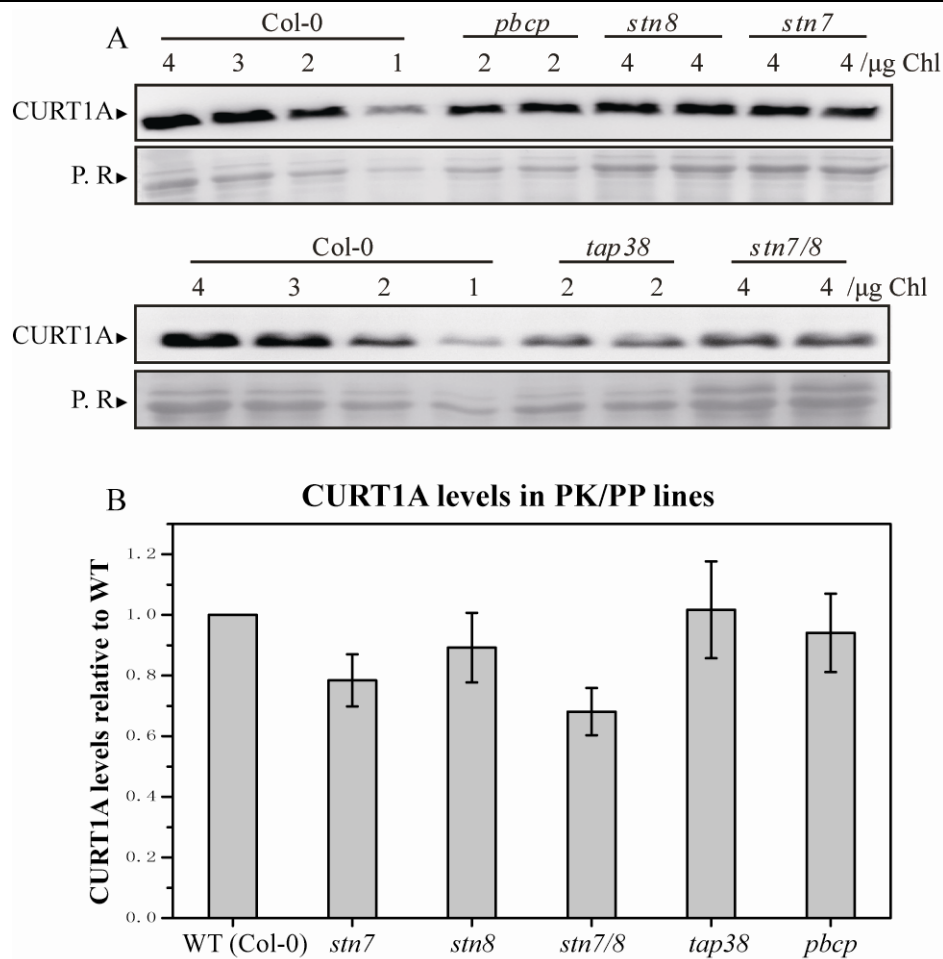


Fig. 3.6 CURT1A levels in thylakoid-protein kinase (PK) and phosphatase (PP) mutants, including *stn7*, *stn8*, *stn7 8*, *tap38*, and *pbcp*. (A) Col-0 thylakoids were loaded in a dilution series (4, 3, 2, and 1 μg of chlorophyll) while PK/PP mutant thylakoids were loaded two replicates corresponding to 2 or 4 μg of chlorophyll. Ponceau-S red staining of LHCII proteins on PVDF membrane was shown below as a loading control. (B) Accumulation levels of CURT1A in these PK/PP mutants relative to Col-0. The BioID software was used to quantify signal intensities in (A). Standard deviations are indicated by error bars.

3.2.2. Overall thylakoid phosphorylation is not altered in *oeCURT1A*

On the other hand, we also explored the effect of protein phosphorylation on grana stacking in *oeCURT1A* plants. To this purpose, the thylakoid phosphorylation levels in 4-week-old plants were analyzed. For WT (*Ler*), after dark-incubation phosphorylation of LHCII (pLHCII) was hardly observed and D1 was moderately phosphorylated (pD1). However, pLHCII level was significantly increased under GL conditions while pD1 level was obviously enhanced under HL conditions (Fig. 3.7A, left panel). The *oeCURT1A* line showed similarly phosphorylation

patterns to WT, with increased pLHCII levels under GL conditions and elevated pD1 levels under HL exposure (Fig. 3.7A, right panel). As shown in Fig. 3.7B, pD1 ratios of *oeCURTIA* under all tested conditions were comparable to those of WT. For pLHCII, no significant difference was observed between *oeCURTIA* and WT plants under GL conditions. While the pLHCII ratio of *oeCURTIA* was increased in the dark and about 2-fold higher than that of WT (*oeCURTIA* $23 \pm 6\%$ versus WT $11 \pm 5\%$), thus led to reduced pLHCII percentage under HL conditions (*oeCURTIA* $33 \pm 5\%$ versus WT $42 \pm 2\%$). The *oeCURTIA* plants exhibited altered grana stacking, but no significant changes in PSII core protein phosphorylation, suggesting that the CURT1 dosage affect grana stacking independent of thylakoid phosphorylation.

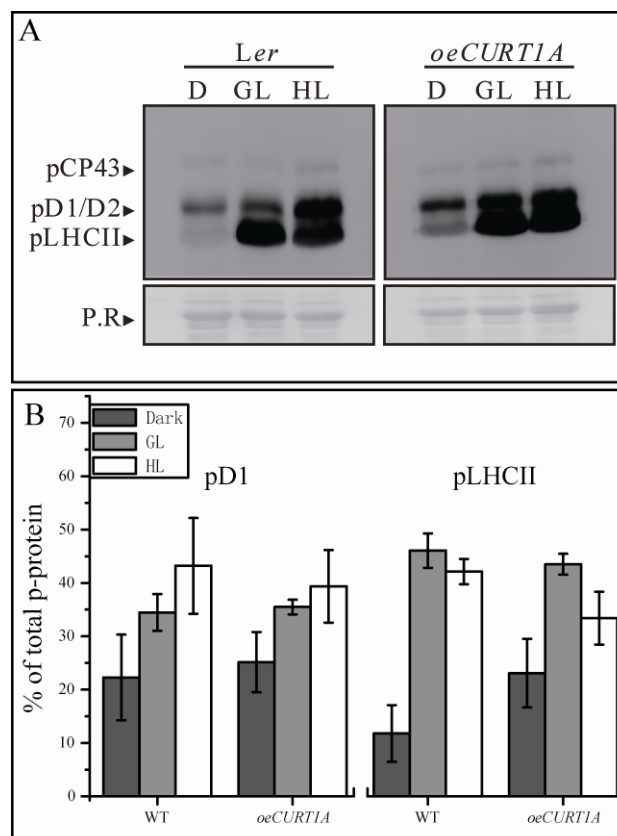


Fig. 3.7 Thylakoid phosphorylation patterns of WT (*Ler*) and *oeCURTIA* under dark, GL and HL conditions. (A) A p-Thr antibody was used for detection of thylakoid phosphorylation in *Ler* and *oeCURTIA* under dark, GL, and HL conditions. Thylakoid corresponding to 5 μ g of chlorophyll were loaded. Ponceau-S red staining of LHCII proteins was shown as a loading control. (B) The ratio of phosphorylated D1 (pD1) or LHCII (pLHCII) under different conditions was plotted according to (A). The whole signal intensity of pD1 or pLHCII of one genotype under all light conditions was set as 100%. Western blots were repeated in triplicates and the BioID software was used for quantification. Standard deviations are indicated by error bars. GL, growth light; HL, high light.

3.2.3. The *curt1abc tap38* mutant shows grana stacking similar to the *curt1abc* mutant

Previously, *curt1abc* mutant was found to form grana stacking with increased diameter but reduced height, whereas grana of *tap38* mutant showed decreased diameter but enhanced stacking (Armbruster *et al.*, accepted). Therefore, to determine whether CURT1 amount overrides the stacking effects of thylakoid phosphorylation, a new quadruple mutant *curt1abc tap38* was generated. As shown in Fig. 3.8, grana stacking of *curt1abc tap38* (right panel) displayed a long and flat structure, which was similar to that of *curt1abc* (left panel), implying that CURT1 dosage shows more dominant effects than thylakoid phosphorylation.

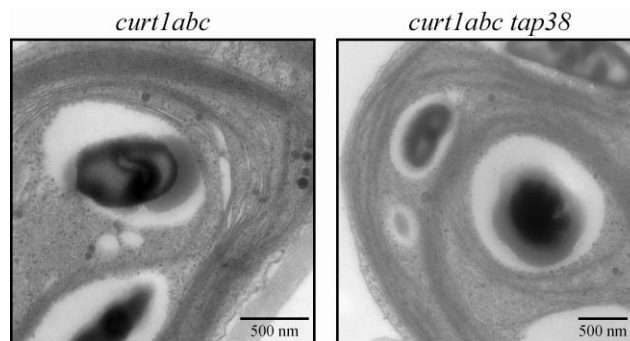


Fig. 3.8 TEM analysis of thylakoid ultrastructures of *curt1abc* and *curt1abc tap38*. Leaves were from 5-week-old plants and fixed after 2 h onset of light (intermediate day, growth light) and subject to TEM. Left image: Thylakoid ultrastructure of *curt1abc* mutant; Right image: Thylakoid ultrastructure of *curt1abc tap38* mutant. Scale bars corresponding to 500 nm.

3.3. CURT1A represents the major constituent in formation of grana stacking

3.3.1. Solely CURT1A amounts are increased in the *oeCURT1A* line

As previously described, all four CURT1 proteins A, B, C, and D are present in a single complex with different stoichiometry in WT plants (Armbruster *et al.*, accepted). Since *oeCURT1A* line is known to produce grana of reduced diameter but increased stacking height, we wanted to further clarify whether the stoichiometry is still maintained in the *oeCURT1A* line and therefore crucial for CURT1 complex composition and its function. To this end, the abundance of CURT1A, B, and C levels in *oeCURT1A* plants were determined by

quantification of the respective Western blot signals (Fig. 3.9A). In Fig. 3.9B, the quantification data of the individual CURT1 members are presented. The *oeCURT1A* was generated on the basis of the *curt1a-1* mutant, which was shown to express decreased amounts of CURT1B and CURT1C (Armbruster *et al.*, accepted). In *oeCURT1A*, CURT1A levels were increased (CURT1A percentage, $224 \pm 30\%$ of WT), while expression of CURT1B ($81 \pm 9\%$ of WT) and CURT1C ($75 \pm 4\%$ of WT) remained reduced, similar to the *curt1a* mutant. We did not observe any CURT1D signal probably due to its low abundance. Taken together, our data indicated that high expression levels of CURT1A were sufficient to affect grana stacking while other CURT1 components not required to be simultaneously up-regulated.

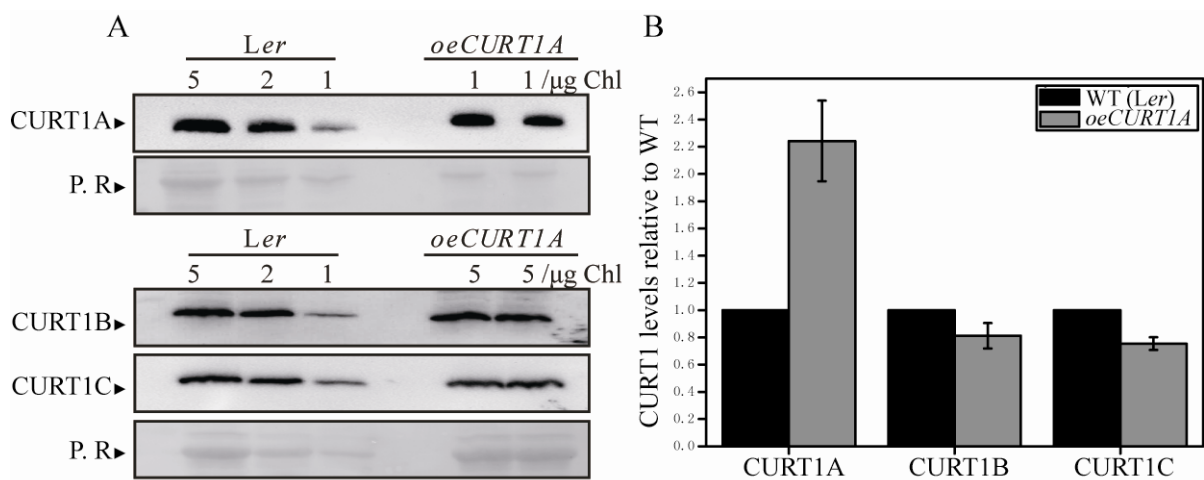


Fig. 3.9 Quantification of CURT1 levels in *oeCURT1A*. (A) WT (*Ler*) thylakoids corresponding to 5, 2, and 1 μg of chlorophyll and *oeCURT1A* thylakoids equal to either 5 or 1 μg of chlorophyll were loaded. CURT1A, B, and C were detected by corresponding antibodies. Ponceau-S red staining of LHCII proteins was used as a loading control. (B) The ratios of CURT1A, B and C proteins in *oeCURT1A* compared to *Ler* were plotted according to (A). The Western blots were repeated in triplicates and the BioID software was used for quantification analysis. Standard deviations are indicated by error bars.

3.3.2. CURT1A can induce grana formation in the *curt1abc* line

The *oeCURT1A* line was generated in the *curt1a* mutant background, in which CURT1B, C, and D are still present, even though at decreased levels. To determine the ability of single CURT1 member to cause grana formation, CURT1 proteins were ectopically expressed in the *curt1abc* mutant. Complementation of *curt1abc* by individual CURT1 family member was performed and the respective T2 plants were selected by Western blot analysis employing

CURT1-specific antibodies (Fig. 3.10A). We failed to obtain complementing lines with significant CURT1B or CURT1D expression. However, for CURT1A and CURT1C, partial complementation regarding WT protein levels was achieved. To investigate a potential functional complementation, *curt1abc* mutants ectopically expressing CURT1A (*35S:CURT1A curt1abc*) were analyzed by TEM regarding thylakoid grana formation. As shown in Fig. 3.10B, *35S:CURT1A curt1abc* displayed clear grana stacking formation and differentiation of grana and stroma lamellae in comparison to the *curt1abc* line.

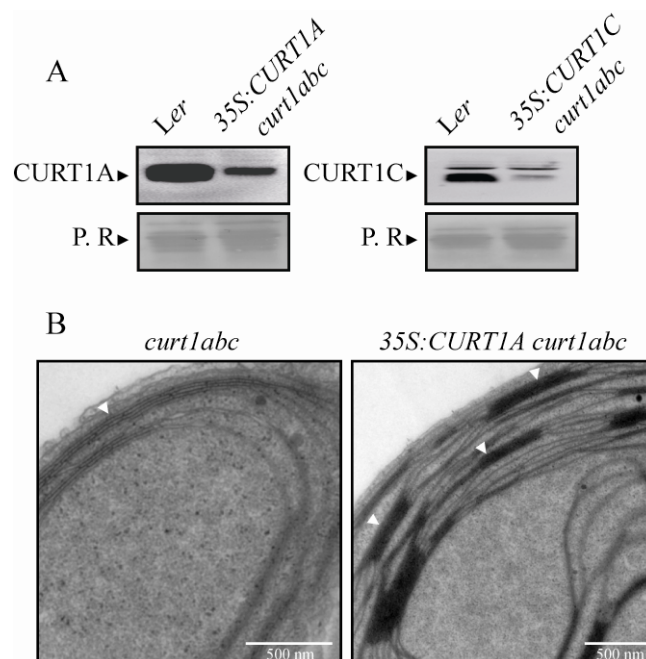


Fig. 3.10 Effect of *curt1abc* complementation by single CURT1 member. (A) CURT1A and CURT1C accumulation in *35S:CURT1A curt1abc* and *35S:CURT1C curt1abc* mutant lines. Coding sequences of CURT1A and CURT1C, under the control of a 35S promoter, were transformed into *curt1abc* plants. The accumulation levels of CURT1A (left panel) and CURT1C (right panel) of selected T2 plants were compared with WT (*Ler*) by Western blot. Thylakoids corresponding to 4 μ g of chlorophyll were loaded. Ponceau-S red staining of LHCII was used as a loading control. (B) TEM analysis of *curt1abc* and complementing line *35S:CURT1A curt1abc*. TEM images were obtained from 5-week-old plants to check for restored grana formation. Grana stacking of *35S:CURT1A curt1abc* is indicated by white arrows. Scale bars corresponding to 500 nm.

3.3.3. CURT1A containing complexes are disassembled under HL exposure

Under HL exposure, grana showed a decreased diameter and reduced distance between adjacent grana, in which thylakoid phosphorylation is suggested as the key player (Herbstova

et al., 2012). To investigate the CURT1 dosage effect on the thylakoid structural dynamics under HL conditions, the stability of different CURT1 proteins was examined. As shown in section 3.1.6, the amounts of CURT1 proteins remained stable under different light conditions, including HL. However, it was not ruled out whether CURT1 proteins undergo conformational changes upon exposure to different light conditions, which in turn might affect complex assembly or stability.

As shown in Fig. 3.11A left panel, under GL and HL conditions, the *oeCURT1A* line exhibited similar complex distribution patterns compared to *Ler* under all tested light conditions. In Fig. 3.11A (right panel), CURT1A signals were detected in high molecular weight region after Western blot of BN stripes and the overall signal intensity of *oeCURT1A* is much stronger than *Ler*. As CURT1 proteins co-migrate in specific complex (Armbruster *et al.*, accepted) and CURT1A represents the major constituent of these complexes, CURT1A patterns were examined in 2-D PAGE following BN-PAGE. After dark incubation and GL exposure, clear CURT1A signals could be detected in high molecular weight regions both in the *Ler* and *oeCURT1A* lines (Fig. 3.11B), while these high molecular weight CURT1A signals were not detectable after HL exposure. One could note that the overall CURT1A signal intensity of *oeCURT1A* remains stronger than that of *Ler* in 2-D PAGE. These observations suggest that, CURT1A shifted to low molecular weight regions, which might be due to the disassembly of the oligomeric CURT1 protein complexes.

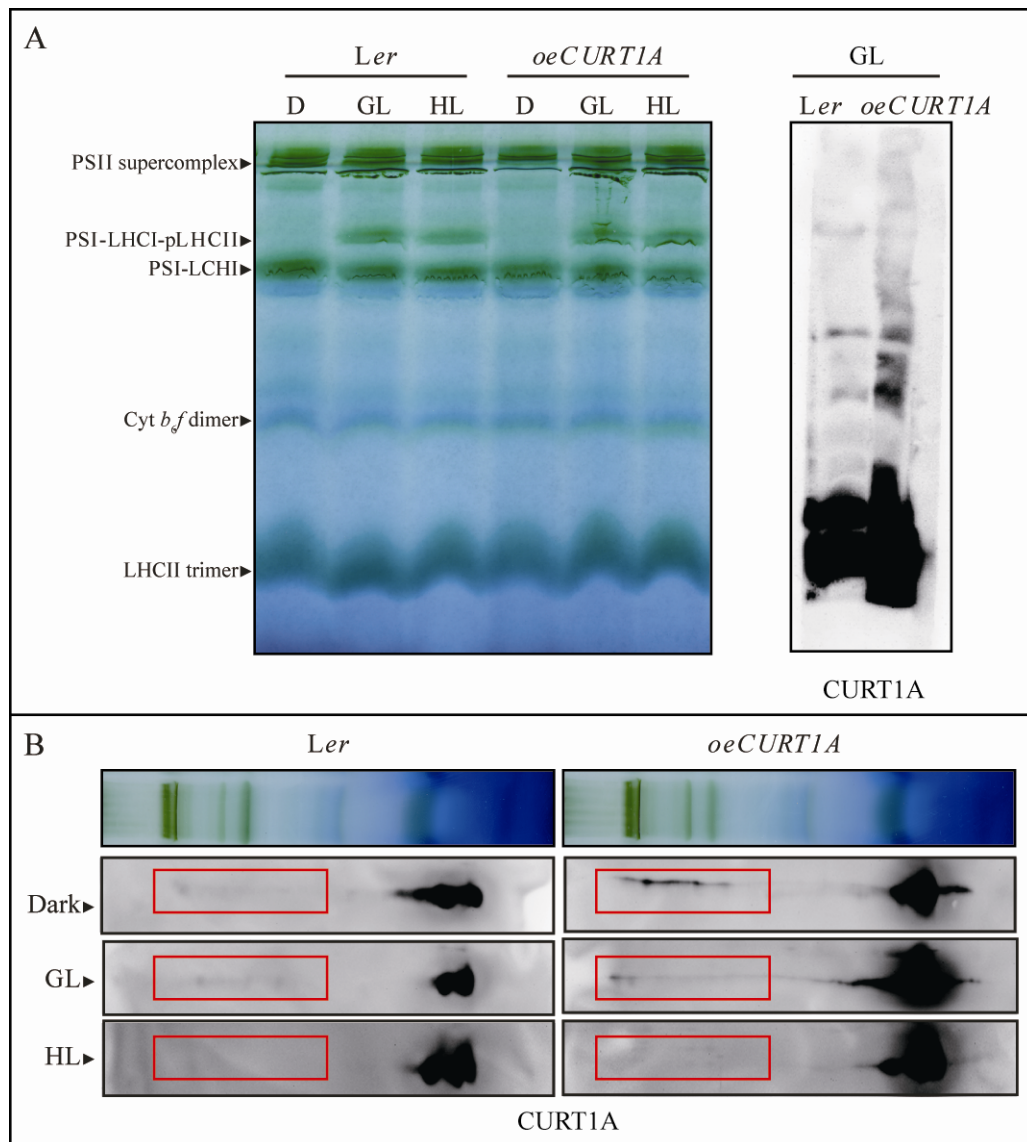


Fig. 3.11 High molecular weight CURT1A complexes disassemble under HL conditions. (A) BN-PAGE was performed with digitonin solubilized thylakoids corresponding to 100 μ g of chlorophyll. Prior to thylakoid isolation, *Ler* and *oeCURT1A* plants were incubated in the dark overnight, then under GL for 2 h and further under HL conditions for 2 h. BN stripes from GL samples were directly blotted after incubation for 1 h in solubilization buffer and CURT1A was detected by specific antibodies. (B) Comparison of CURT1A complex pattern under dark, GL and HL conditions. BN stripes from (A) were used for 2-D PAGE. All six stripes presented in the panel were blotted onto one membrane to allow comparison. Signals corresponding to high molecular weight regions were highlighted by red rectangles. D, dark; GL, growth light; HL, high light.

3.4. Effects of CURT1 phosphorylation: generation of phospho-site exchange (PSE) complementation lines

Previous data (Fristedt *et al.*, 2009b; Armbruster *et al.*, accepted) and analyses described in

this work (see section 2.3) indicate a connection between CURT1 dosage and thylakoid phosphorylation with respect to grana stacking. Furthermore, phospho-proteomic screening by Reiland *et al.* (2009) suggests that several amino acids of CURT1A and CURT1B experience reversible phosphorylation. The PhosPhAt database (Durek *et al.*, 2010) indicates three amino acids (serines at positions 64, 65, and threonine at position 68) of CURT1A and two amino acids (threonines at positions 65 and 66) of CURT1B to be phosphorylated. Based on these findings we hypothesize that the reversible phosphorylation of CURT1 proteins is the link between the two regulatory processes of grana stacking, CURT1 dosage and thylakoid phosphorylation.

To clarify the impact of CURT1 phosphorylation on grana stacking, the amino acids involved in reversible phosphorylation were exchanged with alanines or aspartic acids (mimicking hypo- or hyperphosphorylation). The *curt1a* mutant plants were complemented with *CURT1A* constructs containing the endogenous sequence or single or triple amino acid substitutions. Accordingly, different *CURT1B* constructs with or without amino acid substitutions were transformed into *curt1b* mutant plants. The accumulation of CURT1A or CURT1B variants in selected T2 plants was analyzed by Western blot analysis. The expression of *CURT1A* in the S65A, T68A, and SST-DDD lines is comparable to that of WT (Fig. 3.12A), while in the lines expressing native, S64A, and SST-AAA CURT1A, the detected accumulation levels were lower. This suggests that the lack of overexpression is not due to the modulation of these variants. In *curt1b* mutant lines, the complementation with TT-DD and native CURT1B showed higher protein levels than the other three complemented lines (TT-AA, T65A, and T66A), although all the lines expressed at a much lower level than the WT (Fig. 3.12B). None of the analyzed lines exhibited an overexpression of CURT1A or CURT1B proteins, which might be due to a limited pool size during the screening process. For future analyses, we harvested the seeds of lines showing a relatively high protein expression level (i.e. CURT1A: NATIVE-1, S64A-5, S64A-7, T68A-1, T68A-2, S65A-2, S65A-3, SST-AAA-1, SST-DDD-2; CURT1B: TT-AA-3, T65A-2, NATIVE-3, TT-DD-3, TT-DD-5, S65A-3) (Fig. 3.12).

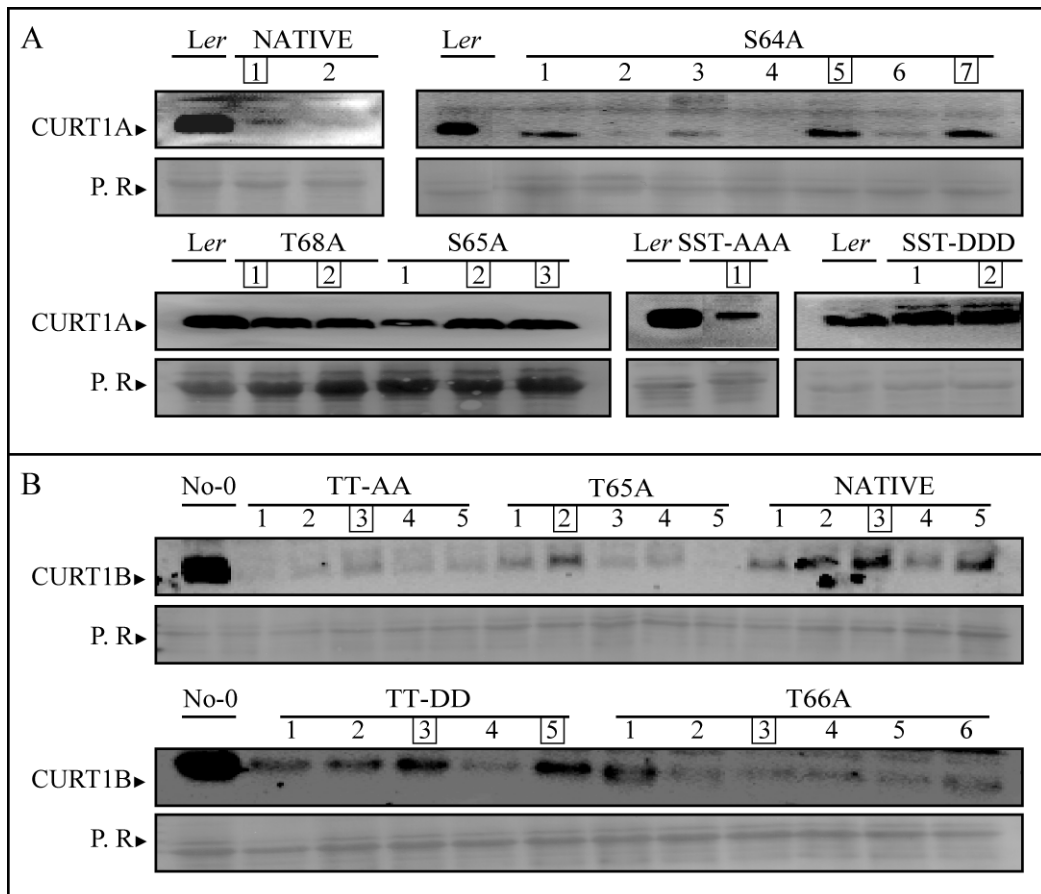


Fig. 3.12 Complementation of *curt1a* and *curt1b* mutant plants with corresponding phospho-site exchange (PSE) variants. (A) CURT1A accumulation levels in PSE complementation lines. The different amino acid exchanges were indicated. Native: no amino acid exchange; S64A: serine at position 64 exchanged with alanine; S65A: serine at position 65 exchanged with alanine; T68A: threonine at position 68 exchanged with alanine; SST-AAA: serines at positions 64 and 65 and threonine at position 68 exchanged with alanines; SST-DDD: serines at positions 64 and 65 and threonine at position 68 exchanged with aspartic acids. The numbers indicate individual T2 plants. (B) CURT1B accumulation levels in PSE complementation lines. Native: no amino acid exchange; T65A: threonine at position 65 exchanged with alanine; T66A: threonine at position 66 exchanged with alanine; TT-AA: threonines at positions 65 and 66 were exchanged with alanines; TT-DD: threonines at positions 65 and 66 were exchanged with aspartic acids. The numbers indicate individual T2 plants. (A+B) All constructs were driven by a 35S promoter. Thylakoids equal to 4 μ g of chlorophyll were loaded. Ponceau-S red staining of LHCII proteins was used as a loading control. Thylakoids of *Ler* and No-0, the corresponding WT genetic backgrounds to *curt1a* and *curt1b* mutant lines were loaded for comparison. The lines selected for harvesting seeds are highlighted by black rectangles.

3.5. Identification of putative interacting proteins of CURT1

3.5.1. CURT1 oligomerization is STN8-independent under different light conditions

As shown in Fig. 3.6, CURT1 protein levels were not significantly changed in *stn8* mutant plants. However, it is possible that STN8 phosphorylates CURT1 proteins, resulting in an indirect effect on grana stacking in a CURT1 dependent manner. To investigate this possibility, we used the migration effects upon HL exposure which has been described in section 3.3.3, to characterize WT (Col-0), *stn8*, and *oeSTN8* lines. As depicted in Fig. 3.13A, no CURT1B complexes were observed in the high molecular weight region of the WT or *stn8* samples, either under GL or HL conditions. For *oeSTN8*, CURT1B complexes in the high molecular weight region were detected under GL conditions, but almost completely disappeared under HL exposure as highlighted by rectangles in Fig. 3.13A. Similar results were observed for the migration behavior of CURT1A (Fig. 3.13B). In *stn8* samples, no CURT1A signals were detected in the high molecular weight region independent of the light condition, whereas CURT1A signals were present in the high molecular weight region under GL conditions in WT and *oeSTN8* lines and disappeared after HL exposure (highlighted by rectangles in Fig. 3.13B). We did not detect any CURT1A or CURT1B in the high molecular weight region of *stn8*, probably caused by the decreased levels of CURT1 proteins in *stn8* (CURT1A percentage, $89 \pm 11\%$ of WT). Therefore, impaired grana stacking of *stn8* is possibly caused by the lack of CURT1 oligomers. However, findings of migration behavior of CURT1A and CURT1B in *oeSTN8* plants suggested that STN8 is not closely involved in CURT1 oligomerization under the tested light conditions. Additionally, in contrast to previous observations (Armbruster *et al.*, accepted), no CURT1B signals were detectable in high molecular weight complexes of WT samples under GL conditions, which might be caused by harsh solubilization conditions prior to BN-PAGE.

Results

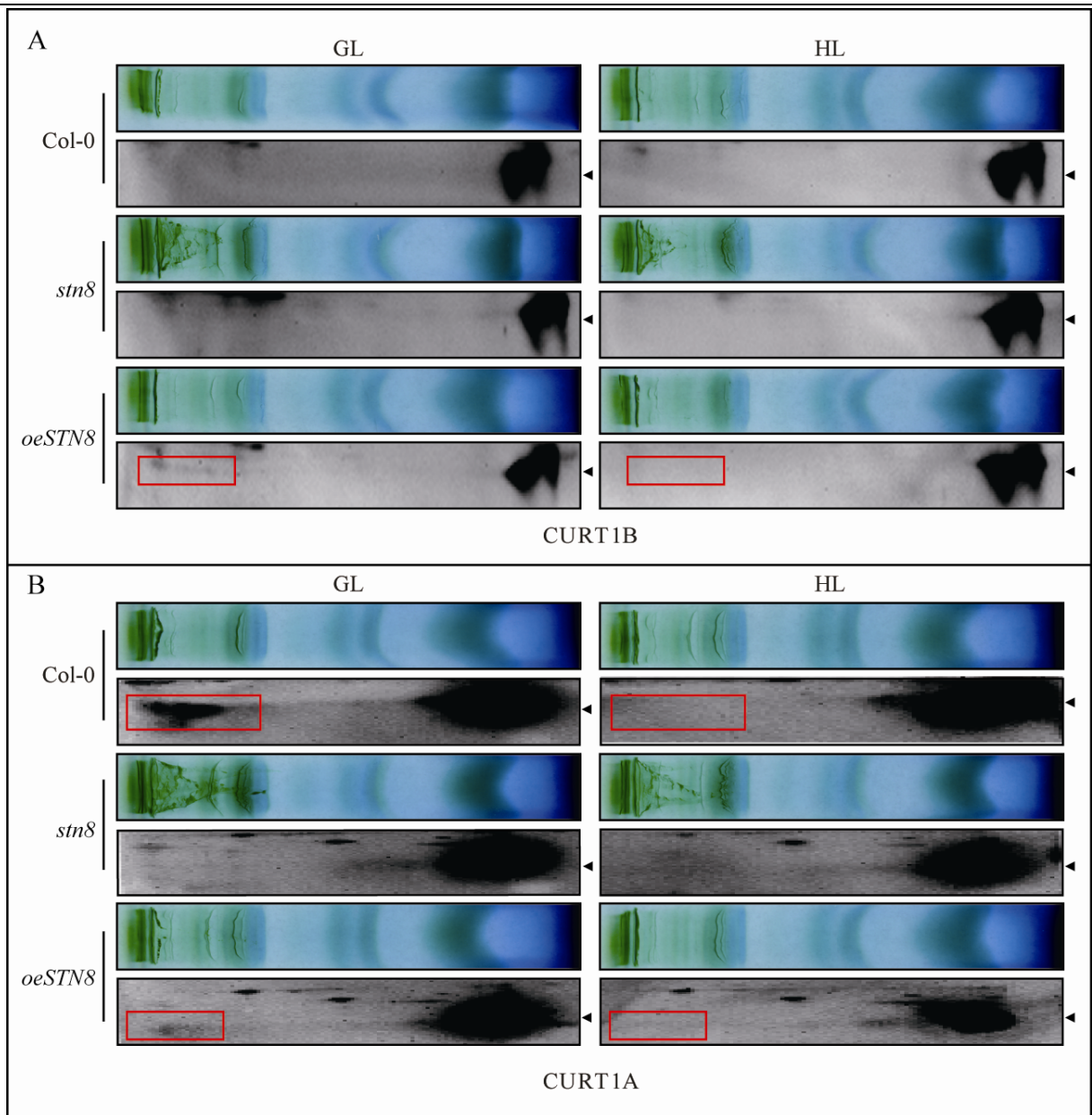


Fig. 3.13 CURT1B and CURT1A oligomerization behavior in Col-0, *stn8*, and *oeSTN8* under GL and HL conditions. (A) CURT1B distribution patterns in Col-0, *stn8*, and *oeSTN8*. In BN-PAGE 1.6% digitonin was used for solubilization. Specific CURT1B signals are indicated by arrows. In *oeSTN8*, CURT1B signals in the high molecular weight region are highlighted by red rectangles. (B) CURT1A distribution patterns in Col-0, *stn8*, and *oeSTN8*. Specific CURT1A signals are indicated by arrows. For Col-0 and *oeSTN8*, specific CURT1A signals in the high molecular weight region are indicated by red rectangles. All six stripes in the same panel were blotted onto one membrane for a direct signal comparison.

3.5.2. Thylakoid rhodanese-like protein (TROL) is not a stable interaction partner of CURT1 complexes

Our CoIP results indicate a direct interaction between CURT1 and TROL proteins (data not

shown), which has been found essential for tethering FNR (ferredoxin:NADP⁺ oxidoreductase) and sustaining LEF in plants (Juric *et al.*, 2009). To further discern the interaction between TROL and CURT1, the expression level of CURT1 was first examined in the *trol* mutant line to clarify whether TROL is required for accumulation of CURT1 proteins. As shown in Fig. 3.14A, CURT1A levels were not significantly different between WT (Col-0) and *trol* mutant lines. BN- and 2-D PAGE revealed similar distribution patterns of the major thylakoid complexes (Fig. 3.14B) and CURT1 oligomers (Fig. 3.14C) between WT and *trol* mutant lines. These data indicate that TROL does not play a role in forming and maintaining stable CURT1 complexes.

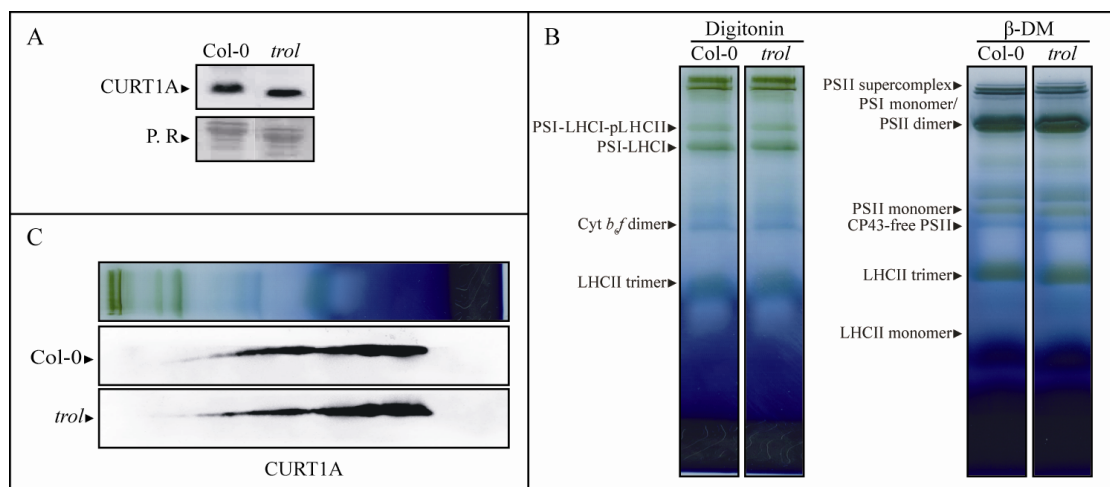


Fig. 3.14 TROL is not a stable interaction partner of CURT1 complexes. (A) CURT1A protein levels in Col-0 and *trol* plants. Thylakoids of Col-0 and *trol* corresponding to 4 μ g of chlorophyll were loaded. Ponceau-S red staining of LHCII proteins was shown as a loading control. (B) BN-PAGE of Col-0 and *trol* thylakoids after solubilization with digitonin (left panel) or β -DM (right panel). (C) CURT1A distribution patterns of Col-0 and *trol* thylakoids solubilized with digitonin.

3.6. The CURT1 from *Synechocystis* (synCURT1) fails to induce grana formation in *A. thaliana curt1abc* line

The observations that the expression of *Arabidopsis* CURT1A in *Synechocystis* led to an altered thylakoid structure and reduced endogenous CURT1 levels (Armbruster *et al.*, accepted), prompted us to investigate whether CURT1 from *Synechocystis* (synCURT1) affects grana stacking in land plants. The cTP sequence of the small subunit of RuBisCO was

fused to the 5' end of *synCURT1* sequence for the correct chloroplast localization. The vector containing *cTP-synCURT1* sequence was introduced to *curt1abc* mutant plants by transformation. The transgenic line *35S:synCURT1-5 curt1abc* accumulating the highest protein level was subjected to TEM analysis (Fig. 3.15A). The *35S:synCURT1-5 curt1abc* line exhibited a similar ultrastructure compared to the *curt1abc* mutant, suggesting that *synCURT1* is not sufficient to induce grana stacking in plant.

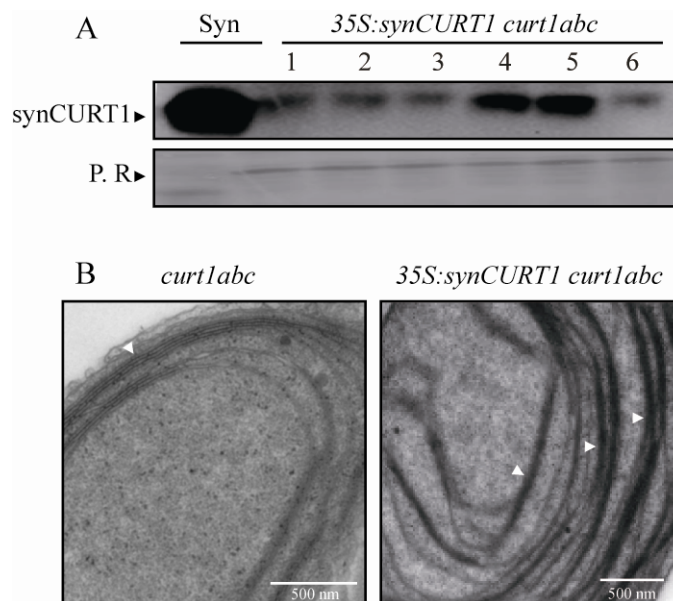


Fig. 3.15 TEM analysis of *curt1abc* mutants complemented with the CURT1 of *Synechocystis* (*synCURT1*). (A) *synCURT1* accumulation in *curt1abc* mutant line. *synCURT1* expression was driven by a 35S promoter. The *synCURT1* levels of 6 selected T2 plants were detected with a *synCURT1* specific antibody. Thylakoids of *Synechocystis* (Syn, as positive control) and *Arabidopsis* (samples 1-6) corresponding to 4 μ g of chlorophyll were loaded. Ponceau-S red staining of LHCII proteins was used as a loading control. (B) TEM analysis of *curt1abc* complemented with *synCURT1*. Leaves of 5-week-old plants were fixed after 2 h onset of light (intermediate day, growth light) and subjected to TEM analysis. Grana are indicated by white arrows. Scale bars corresponding to 500 nm.

4. Discussion

4.1. Is grana stacking essential for photosynthesis?

Ever since the resolution of the thylakoid ultrastructure, it is under debate whether grana stacking is essential for photosynthesis (Allen and Forsberg, 2001; Anderson *et al.*, 1988; Mullineaux, 2005). To address this question, one option is to characterize the photosynthetic performance of plants with altered grana stacking. Recently the *gdc1* (grana-deficient chloroplast1) mutant was discovered, which lacked grana stacking and might be used for photosynthetic characterization. However, the additional developmental defects of *gdc1*, i.e. seedling lethality with pale green cotyledons and true leaves, were incompatible with physiological analysis (Cui *et al.*, 2011). Even more recently, the CURT1 protein family was discovered to act in inducing grana formation by insertion into the thylakoid membrane and formation of oligomers. The membrane curvature was dependent on CURT1 protein amounts, as CURT1 overexpression and quadruple mutant lines (*oeCURT1A* and *curt1abcd*) showed opposite alteration in thylakoid ultrastructure. However, both lines exhibited only a moderate deficiency in photosynthesis and growth, thus representing an excellent system to explore the relationship between grana stacking and photosynthetic efficiency (Armbruster *et al.*, accepted).

The leaf areas of WT, *oeCURT1A*, and *curt1abcd* plants grown under different light conditions were recorded every week to determine their growth rate. Under all tested light conditions, the *oeCURT1A* plants developed smaller leaf areas compared to WT with this tendency being more significant under HL conditions. The *curt1abcd* plants also showed reduced leaf areas under these conditions, however to a lesser extent (Fig. 3.2). To dissect whether the slow growth rate is linked to a reduced photosynthetic efficiency, photosynthetic parameters under these light conditions were monitored. Under GL conditions, independent of the light cycle length (short, intermediate, or long day), the *oeCURT1A* plants exhibited a decreased Y(II) and increased 1-qL values relative to WT. This was also true for *curt1abcd* mutant plants where those tendencies were even more pronounced, indicating a reduced quantum yield and higher excitation pressure in *oeCURT1A* and *curt1abcd* (Table 3.1a and b). Under LL and HL

conditions, the discrepancy between *oeCURTIA* and WT was negligible, while *curt1abcd* mutants maintained lower Y(II) and higher 1-qL values under these light conditions. Furthermore, under HL conditions *curt1abcd* mutants even showed reduced F_v/F_m and increased NPQ values (Table 3.1c). To understand what leads to the alteration in photosynthetic efficiency, several possible mechanisms were examined and discussed, such as assembly of major thylakoid protein complexes, D1 turnover kinetics, and electron flow. (i) Assembly of major thylakoid protein complexes. As defects in the major photosynthetic protein complexes, i.e. PSI, PSII, and Cyt *b₆f*, usually lead to significant deficiencies in photosynthesis, the distribution patterns of those thylakoid protein complexes were investigated by BN and 2-D PAGE under different light conditions (Fig. 3.3). The *oeCURTIA* and *curt1abcd* plants exhibited similar photosynthetic complex distribution patterns under all tested conditions as the WT. These observations suggest that altered photosynthetic parameters of *oeCURTIA* and *curt1abcd* plants do not result from defects in the accumulation and assembly of the major thylakoid protein complexes, a conclusion which was drawn by characterization of the *curt1* mutants (Armbruster *et al.*, accepted). Although no differences were observed in their distribution patterns, *oeCURTIA* plants showed more PSI-LHCI-pLHCII complexes than WT under GL conditions (Fig. 3.3A right panel). This implies a clear adaptation tendency towards state 2 in *oeCURTIA* plants, which is consistent with state transitions (qT) measurements performed in these lines (*oeCURTIA*, 0.13 ± 0.04 versus WT 0.10 ± 0.02). According to these results, we speculate that the smaller grana diameter facilitates migration of pLHCII. Correspondingly, *curt1abcd* plants with increased grana diameter showed retarded state transitions (*curt1abcd*, 0.04 ± 0.01). (ii) D1 turnover kinetics. D1 turnover is a key process, that replaces photodamaged PSII subunit D1 during photoinhibition (Baena-Gonzalez *et al.*, 1999; Rintamaki *et al.*, 1996), and its rate has been suggested to closely correlated with grana stacking (Fristedt *et al.*, 2009b; Tikkanen *et al.*, 2008). The moderately reduced F_v/F_m value of *curt1abcd* under HL conditions prompted us to explore the D1 turnover kinetics under photoinhibitory conditions (Table 3.1c, Fig. 3.5). To this end, water or lincomycin treated leaves were exposed to HL ($900 \mu\text{mol photons m}^{-2} \text{s}^{-1}$) or IHL (intense high light, $1300 \mu\text{mol photons m}^{-2} \text{s}^{-1}$) conditions to induce photoinhibition, and were then allowed to recover by dark incubation. Water treated leaves of these three lines showed no significant differences under

both light conditions, while after lincomycin treatment, *curt1abcd* leaves exhibited a slower recovery in the dark, which speaks in favor of a retarded D1 turnover process in the *curt1abcd* mutant. Despite only a slight recovery deficiency in lincomycin treated leaves, these findings suggest that the lower F_v/F_m value of *curt1abcd* grown under HL conditions is caused by a delayed D1 turnover. (iii) Electron flow. In the *curt1abcd* mutant, linear transfer flow (LEF) is perturbed in the electron transfer steps between the plastoquinone pool and PSI, and also cyclic transfer flow (CEF) was moderately decreased (Armbruster *et al.*, accepted), which explains for the reduced Y(II) and increased 1-qL values observed in the *oeCURTIA* and *curt1abcd* mutant plants under the different light regimes.

It is interesting to note that *oeCURTIA* and *curt1abcd* plants possess opposite altered thylakoid ultrastructures but both exhibit a reduced photosynthetic efficiency. This suggests a certain optimum regarding grana stacking dependent on the light conditions and the need for plasticity in grana structure. In *oeCURTIA* and *curt1abcd*, this lack in the ability to modulate the grana ultrastructure seems to negatively affect photosynthetic performance. While no differences of these photosynthetic parameters were observed between *oeCURTIA* and WT plants under LL and HL conditions, we propose the following plausible reasons. Under LL conditions, WT showed altered photosynthetic efficiency due to light limitation, while *oeCURTIA* plants seemed not to be significantly affected, thus eliminating the differences. While under HL conditions, the similar photosynthetic behavior can be interpreted as *oeCURTIA* has already simulated grana organization being suitable for HL exposure, and therefore showed comparable photosynthetic parameters to WT plants (Anderson, 1999; Anderson *et al.*, 1988). The better photosynthetic performance of *oeCURTIA* compared to *curt1abcd* mutant plants under all tested light conditions, suggests that the presence of CURT1 proteins *per se* and hence the ability to form grana, is required to adjust photosynthesis by regulating grana plasticity.

It was unexpected to observe a better photosynthetic performance but more retarded growth phenotype of *oeCURTIA* compared to *curt1abcd*. Especially under HL exposure, *oeCURTIA* possessed a severely reduced leaf area compared to that of *curt1abcd* (Fig. 3.2, Table 3.1). This might be explained by the smaller leaf area of *oeCURTIA* being the result of an active acclimation process rather than photoinhibition. This could be to avoid light exposure, because the grana ultrastructure is already in a maximal 'HL adapted state'. Taken together, we propose

that grana formation is not an essential feature for photosynthesis and growth; however photosynthesis and growth benefit from several regulatory process being optimized by grana formation like, electron flow, D1 turnover, state transitions, or yet unknown processes (Albertsson and Andreasson, 2004; Kaftan *et al.*, 2002).

So far, it was described that the altered grana stacking due to lack of CURT1 complexes leads to pleiotropic effects on photosynthesis (Armbruster *et al.*, accepted). Here, the photosynthetic performance and growth of *oeCURT1A* and *curt1abcd* under five different light conditions further support this statement (Fig. 3.2). For thoroughly elucidating the links between grana stacking and photosynthesis, more conditions and mutant lines are required for analysis. The following experiments could be thought of or improved, such as growth measurement, LEF and CEF measurement, D1 turnover kinetics. (i) Growth measurement. It is worth evaluating the behavior of *oeCURT1A* and *curt1abcd* plants under fluctuating light conditions. This experiments would clarify the ability of CURT1 proteins to flexibly modulate the grana structure, and whether a loss of this ability (e.g. in the case of *curt1abcd* mutant) leads to a more significant reduction in photosynthetic efficiency (Pesaresi *et al.*, 2010; Tikkanen *et al.*, 2010). In addition, it would be interesting to study growth behavior of *curt1abcd* backcrossed line (*Bcurt1abcd*), which represents the *curt1abcd* into the Col-0 ecotype background (Fig. 5.2). *Bcurt1abcd* plants will allow for a direct growth comparison between the *curt1abcd* mutation and WT, and are currently grown in field trails. (ii) LEF and CEF measurements. In *curt1abcd* plants, it has been observed that LEF is perturbed in electron transfer between the plastoquinone pool and PSI, and CEF is decreased to a similar level as in *crr2*, a mutant line defective in NDH-dependent CEF (Hashimoto *et al.*, 2003; Armbruster *et al.*, accepted). To dissect the deficiencies in electron flow and to determine which CEF pathway is affected in the *curt1abcd* mutant, the *curt1abcd pgr5* line was generated for further investigation (Fig. 5.3). (iii) D1 turnover kinetics. The D1 turnover rate in *curt1abcd* mutant leaves was altered in the presence of lincomycin while no significant difference was detected in water treated leaves when compared to WT (Fig. 3.5). However, we did observe reduced F_v/F_m values of *curt1abcd* plants grown under HL conditions compared to WT, suggesting that a retarded PSII repair cycle acts in *curt1abcd*. The observed inconsistencies can be explained by short- and long-term HL

treatments being not truly comparable. Therefore, a long-term monitoring of D1 turnover is worth to be considered, e.g. using intact plants instead of detached leaves for long-term F_v/F_m measurements. On the other hand, more harsh light conditions, for instance VHL (very high light, $1800 \mu\text{mol photons m}^{-2} \text{s}^{-1}$) in short-term assays could be applied to analyze D1 turnover in *oeCURT1A* and *curt1abcd* plants (Wunder *et al.*, 2013).

4.2. How is grana formation induced by CURT1 proteins?

So far, many proteins were described to induce membrane curvature. These proteins usually possess an ENTH (epsin N-terminal homology) domain or a BAR (Bin-amphiphysin-Rvs) domain, both containing an N-terminal helix crucial for their insertion into the lipid bilayer (De Camilli *et al.*, 2002; Farsad and De Camilli, 2003; Ford *et al.*, 2002; Kay *et al.*, 1999; Zimmerberg and Kozlov, 2006). However, in chloroplasts no such proteins were known to be located in the thylakoid membrane. Some years ago, LHCII trimers were suggested to be necessary for grana stacking, although this statement remains controversial (Allen and Forsberg, 2001; Andersson *et al.*, 2003). A recent study on *gdc1* mutant plants suggests that the absence of the GDC1 protein leads to reduced LHCII trimer levels, which subsequently affects grana formation (Cui *et al.*, 2011). However, more recently *curt1* mutant plants were found to display significantly altered grana ultrastructure without being affected in LHCII trimer accumulation (Armbruster *et al.*, accepted), which speaks in favor of a different mechanism. CURT1 proteins consist of about 100 amino acids and are smaller than a typical ENTH (~150 amino acids) or BAR domain (~200 amino acids). However, they include an amphipathic helix at their N-terminus that is thought to be critical for insertion into membranes. We propose that insertion of CURT1 proteins into the thylakoid membrane and their oligomerization leads to membrane curvature based on the following observations: (i) CURT1A proteins are embedded in the thylakoid membrane with N- and C-termini being exposed to the stroma. (ii) CURT1 proteins form oligomers. (iii) CURT1 proteins are enriched in the strong membrane bending area—the grana margins. (iv) Thylakoid architecture of *Synechocystis* is altered by ectopic expression of *Arabidopsis* CURT1A. and (v) Liposomes are tubulated by CURT1A insertion (Armbruster *et al.*, accepted) (Fig. 4.1 A).

It is known that the CURT1 protein family in *Arabidopsis* contains four members, but their individual contribution to grana formation remains unclear. Due to its high abundance, as well as its direct liposome binding and bending ability, CURT1A is suggested to be the major component of the CURT1 complex acting in grana formation (Armbruster *et al.*, accepted). In this work, we confirmed that the CURT1A protein is sufficient to generate thylakoid curvature by two independent approaches. First, in *oeCURT1A* plants only CURT1A protein levels were increased to about 2-fold of the WT level, while CURT1B and C levels remained at about ~80% and ~75% of the WT level, which are comparable to the *curt1a* mutant background in which CURT1 overexpression was performed (Fig. 3.9). These findings indicate that overexpression of CURT1A protein, but not simultaneous overexpression of CURT1B and C, is sufficient to induce higher grana stacking with reduced grana diameter. Second, CURT1A expression in *curt1abc* plants (*35S:CURT1A curt1abc*) induced grana formation, even though the CURT1A expression levels were much lower than in the WT. These observations suggest that CURT1A, if not solely, then together with low amounts of CURT1D, can induce grana formation without the need for CURT1B or C.

The question still remains where and how CURT1 proteins initiate membrane curvature, or alternatively, sense the 'grana margin forming' sites. Adam and colleagues (2011) demonstrated that thylakoid grana formation in plants undergoes four stages: prothylakoid with peripherally associated lamellae; lamellae expansion upon light illumination; ontogenesis of multiple and parallel oriented lamellae; grana with overlapping lamellae, which are altogether accomplished within one or several days. In this study, the analysis of CURT1 protein expression during different developmental stages showed that all four CURT1 members already reached high expression levels in young seedlings, which is a hint for CURT1 participating in grana formation at a very early stage (Fig. 5.4). So far, little is known about the grana formation process, i.e. initiation sites, interacting proteins. However, two factors are suggested to be involved in this process. One is the existence of proteins that can sense membrane curvature, which usually interact with membranes dependent on an amphipathic helix (AH) motif. The other is the ability of membranes to attract proteins dependent on their charge density (Borch Jensen *et al.*, 2011). In our case, CURT1 proteins containing amphipathic helix are most likely able to sense membrane curvature. On the other hand, thylakoid phosphorylation might play the

role in modulating surface charge of the thylakoid membrane (Akoyunoglou and Argyroudi-Akoyunoglou, 1974; Fristedt *et al.*, 2009b).

CURT1A was characterized as a major constituent that can induce grana stacking without the assistance of CURT1B and C in this study, but it is also interesting to check the complementary effect of the other CURT1 members. To this end, the *curt1abc* mutant was complemented with CURT1B, C and D. Further studies of these lines will help to dissect the CURT1 complex composition and functionality. To illustrate whether evolutionarily conserved CURT1 proteins are redundant in function, CURT1 from *Synechocystis* (synCURT1) was ectopically expressed in *curt1abc* mutant plants (*35S:synCURT1 curt1abc*). Unlike the expression of *Arabidopsis* CURT1A in *Synechocystis* resulting in thylakoid deformation, grana ultrastructure of the *35S:synCURT1 curt1abc* line resembled that of *curt1abc* (Fig. 3.15). There are several possibilities why synCURT1 failed to induce grana formation in *Arabidopsis*. Firstly, synCURT1 proteins might not be correctly localized or assembled in *Arabidopsis*, as grana formation requires a specific localization of CURT1 proteins to the margins and oligomerization to take place. Therefore the correct localization of synCURT1 and the potential patterns of oligomer need to be confirmed by immunogold labeling, BN- and 2-D PAGE. Second, grana stacking does not occur in cyanobacteria, so the synCURT1 protein might regulate thylakoid ultrastructure in a different way than to induce grana stacking. The third possibility is that average lumen size of cyanobacteria seems smaller than that of plants (cyanobacteria, 5-7 nm versus plants, 16-19 nm), so synCURT1 proteins in plants would lead to a stronger degree of membrane bending that is not suitable for OEC complex (5-7 nm) to accommodate (De Las Rivas *et al.*, 2007; Kirchhoff *et al.*, 2011; Liberton *et al.*, 2006; Nield and Barber, 2006; van de Meene *et al.*, 2006).

During the curvature mechanism, we speculate that two types of protein interactions are required. One occurs among CURT1 members being essential for CURT1 oligomerization. And the other involves CURT1 proteins and other binding partners, possibly proteins or lipids that help to stabilize membrane curvature. To better understand the first type of interactions, truncated CURT1 variants lacking either N- or C-terminal domains could be designed and used to complement the respective mutant plants. Then the distribution patterns of CURT1

oligomers and grana formation could be examined in order to investigate which protein domains are necessary for protein interaction and grana formation. In another approach, one could check the distribution patterns of CURT1 oligomers in the *35S:CURT1A curt1abc* line, to determine whether CURT1A reconstituted grana formation in the absence of CURT1B and C with a different oligomerization strategy (Fig. 3.10). With respect to the second type of interaction, various approaches were undertaken to identify potential interactors of CURT1 proteins. For example, the TROL protein, which is localized majorly to the stroma lamellae and provides docking site for FNR (Juric *et al.*, 2009), was pulled down by CoIP experiment using CURT1B specific antibodies (data not shown). This suggested that TROL could be a direct interaction partner of CURT1 proteins in stabilizing thylakoid curvature. However, TROL was excluded as a stable interaction partner because the *trol* mutant showed a similar CURT1A levels and complex distribution patterns compared to WT (Fig. 3.14). It might be possible that an interaction between TROL and CURT1 proteins is very weak, so conditions for solubilization could be optimized in future experiments. Besides the TROL protein, STN8 was suggested to be the putative kinase that phosphorylates CURT1B proteins (Reiland *et al.*, 2011). For this reason, the phosphorylation status of CURT1B should be examined in WT, *stn8* and *oeSTN8* lines. CURT1B was successfully pulled down during CoIP experiments, but no CURT1B phosphorylation (pCURT1B) could be detected using p-Thr antibodies. This might be due to low abundance of pCURT1B (data not shown). Besides potential interacting proteins, insertion of CURT1 proteins into membranes might also depend on an interplay with lipids. We applied CoIP experiments to identify interacting lipids; however, the amounts of captured lipids were below detectable levels (data not shown). Alternatively, the *in vitro* liposome system that was recently established to elucidate the function of CURT1A (Armbruster *et al.*, accepted), seems to be an excellent platform for exploring the lipid preference of CURT1 proteins as the lipid composition can be controlled precisely.

4.3. How are grana structural dynamics regulated?

CURT1 proteins seem to affect grana stacking at a basic level, whereas thylakoid phosphorylation seems to function on a more regulatory level. This conclusion could be drawn

from the following observations: (i) CURT1 proteins and thylakoid phosphorylation affect grana stacking at different levels, which was shown by PK/PP mutants exhibiting altered grana stacking without significant changes of CURT1A protein levels. On the other hand, *oeCURT1A* plants showed significantly altered grana stacking without major changes in thylakoid phosphorylation (Fig. 3.6 and Fig. 3.7). (ii) Grana stacking is more severely altered in *curt1* mutant plants than in PK/PP mutant plants. TEM images showed that grana of *curt1a* and *curt1abcd* lines had an increased diameter but reduced height compared to *stn7 8* plants (*curt1abcd*, diameter $1.66 \pm 0.41 \mu\text{m}$, height $0.06 \pm 0.02 \mu\text{m}$ versus *stn7 8*, diameter $0.87 \pm 0.19 \mu\text{m}$, height $0.09 \pm 0.03 \mu\text{m}$). Similarly, grana of *oeCURT1A* plants are smaller in diameters and higher than these of *tap38* plants (*oeCURT1A*, diameter $0.37 \pm 0.06 \mu\text{m}$, height $0.17 \pm 0.05 \mu\text{m}$ versus *tap38*, diameter $0.46 \pm 0.08 \mu\text{m}$, height $0.15 \pm 0.06 \mu\text{m}$) (Armbruster *et al.*, accepted). (iii) Effects of CURT1 protein on grana stacking override those of thylakoid phosphorylation. For example, *curt1abcd* mutant plants showed thylakoid hyperphosphorylation, which was thought to result in grana diameter reduction and increased height (Fristedt *et al.*, 2009b). However, this effect was overridden by a lack of CURT1 proteins and as a consequence, *curt1abcd* plants displayed extended grana stacking with fewer layers (Armbruster *et al.*, accepted). Another hint for CURT1 playing a dominant role is that grana stacking in the *curt1abc tap38* mutant is very similar to that of *curt1abc* (Fig. 3.8).

It is widely supported that thylakoid phosphorylation regulates the thylakoid ultrastructure (Fristedt *et al.*, 2009b; Goral *et al.*, 2010; Herbstova *et al.*, 2012); however, it remains unclear how CURT1 proteins exert their effect on grana dynamics. In this work, we could show that protein levels of CURT1A, B, and C accumulated stably under dark, GL, and HL conditions (Fig. 3.4), but as shown for CURT1A, disassembled to monomer or low molecular weight complexes under HL conditions (Fig. 3.11). Based on these observations, we speculate that under HL conditions CURT1 protein complexes disassemble, which might lead to modulation and destabilization of the grana margin area. This in turn might create the required plasticity of the grana to facilitate photosynthesis, e.g. by the expansion of lumen upon light illumination to facilitate plastocyanin diffusion (Fig. 4.1B) (Kirchhoff *et al.*, 2011). The mechanism underlying the HL disassembly of CURT1 complexes is yet elusive, but one could speculate that again thylakoid phosphorylation might play a regulatory role regarding its close correlation with

grana formation and light transitions, as well as the demonstrated phosphorylation of the CURT1 proteins (Baginsky and Gruijssem, 2009; Reiland *et al.*, 2011; Reiland *et al.*, 2009). The STN8 kinase might play a role in this mechanism since it is a light-regulated kinase that possibly targets CURT1B (Bonardi *et al.*, 2005; Reiland *et al.*, 2011), and most importantly, its loss also leads to altered grana stacking (Fristedt *et al.*, 2009a). To address this hypothesis, CURT1B migration of thylakoids from WT, *stn8*, and *oeSTN8* plants was examined by BN- and 2-D PAGE under GL and HL conditions (Fig. 3.13). However, no significant changes in CURT1 HL disassembly could be observed. This led us to conclude that either STN8 is not the kinase that regulates CURT1 phosphorylation under HL conditions, or that CURT1 phosphorylation is not essential for its disassembly.

We focused on a potential role of the STN8 kinase in CURT1 complex disassembly in this study (Fig. 3.13). However, in the future the following experiments could be performed. First, we will assess the CURT1 complex disassembly under HL conditions in other different PK/PP mutants, e.g. *stn7 8*, *tap38*, *pbcp*, and other 14 chloroplast PK mutant lines. On the other hand, one could perform immunogold labeling experiments with these PK/PP mutants exposed to different light conditions. The PK/PP mutant lines exhibiting altered behavior of CURT1 complex disassembly or localization of CURT1 proteins could be the candidate to regulate CURT1 protein (de)phosphorylation. Second, we would investigate the CURT1 complex formation in phosphor-site exchange (PSE) lines. In the PSE variants, when serine or threonine residues are substituted by alanine, a state of permanent dephosphorylation is simulated, whereas the substitution by aspartic acid mimicks a state of permanent phosphorylation, in respect to both the additional negative charge and spatial hindrance. The PSE variants thus are uncoupled from natively occurring phosphorylation events at these residues and these lines will be helpful to reveal the effects of CURT1 phosphorylation during HL disassembly behavior and CURT1 complex formation. So in case CURT1 disassembly is related to phosphorylation events, an altered response of the corresponding PSE proteins could give hints on the underlying mechanism. Furthermore, comparison of the HL disassembly in different lines with single and multiple amino acid substitutions could provide clues on whether the process is regulated by a phosphorylation cascade.

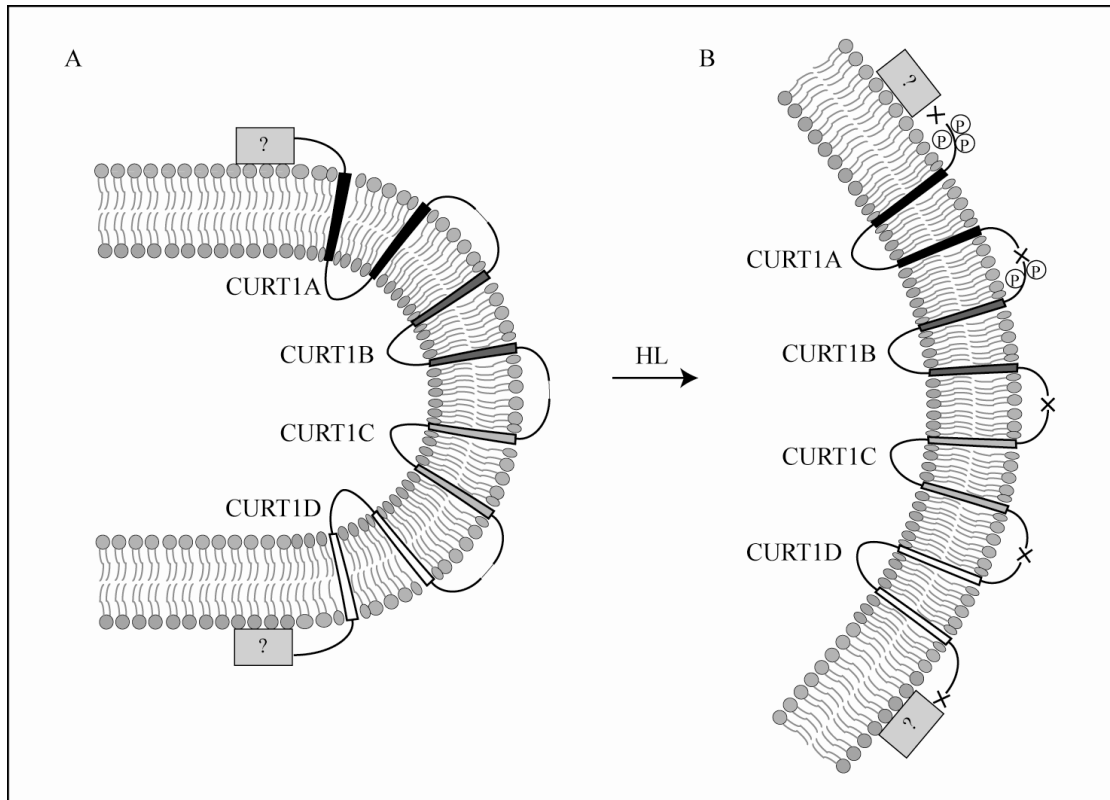


Fig. 4.1 Schematic model of CURT1 proteins promoting and regulating grana stacking under HL conditions.

(A) Membrane curvature is generated by insertion and oligomerization of CURT1 proteins. Membrane curvature is maintained by yet unknown interacting partners (rectangles with question marks) (B) Disassembly of CURT1 proteins release the tension of thylakoid membrane under HL conditions, allowing a more flexible membrane for regulation to optimize photosynthesis. Possible phosphorylation sites of CURT1A and B under the same conditions are indicated by P . CURT1A-D amounts from high to low levels are indicated by decreased color intensities. Dark (CURT1A), grey (CURT1B), light grey (CURT1C), and white (CURT1D).

5. Appendix

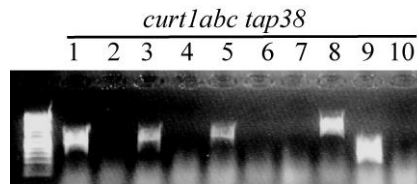


Fig. 5.1 PCR confirmation for *curt1abc tap38* line. The loci of *CURTIA-D* and *TAP38* were screened by T-DNA or gene-specific specific primers. The involved primers were: Lane 1. *TAP38* (tap-as and LB1); Lane 2. *TAP38* (tap-s and tap-as); Lane 3. *CURTIA* (410as and Ds3-1); Lane 4. *CURTIA* (145s and 995as); Lane 5. *CURTIB* (222s and Ds3-2); Lane 6. *CURTIB* (222s and 521as); Lane 7. *CURTID* (1125as and LB1); Lane 8. *CURTID* (10s and 1125as); Lane 9. *CURTIC* (20s and LBB1); Lane 10. *CURTIC* (20s and 817as). The primer sequences and combinations were described in Table 2.2.

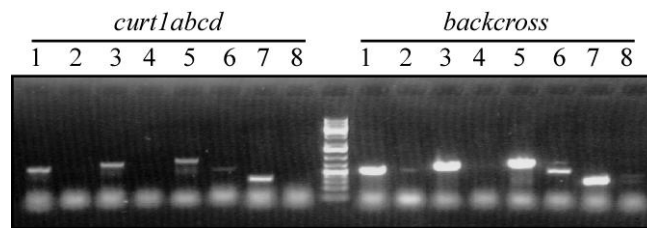


Fig. 5.2 PCR confirmation for *curt1abcd backcross* line. The loci of *CURTIA-D* were screened by T-DNA or gene-specific specific primers with *curt1abcd* as a positive control. The involved primers were corresponding to: Lane 1. *CURTIA* (410as and Ds3-1); Lane 2. *CURTIA* (145s and 995as); Lane 3. *CURTIB* (222s and Ds3-2); Lane 4. *CURTIB* (222s and 521as); Lane 5. *CURTID* (1125as and LB1); Lane 6. *CURTID* (10s and 1125as); Lane 7. *CURTIC* (20s and LBB1); Lane 8. *CURTIC* (20s and 817as). The primer sequences and combinations were described in Table 2.2.

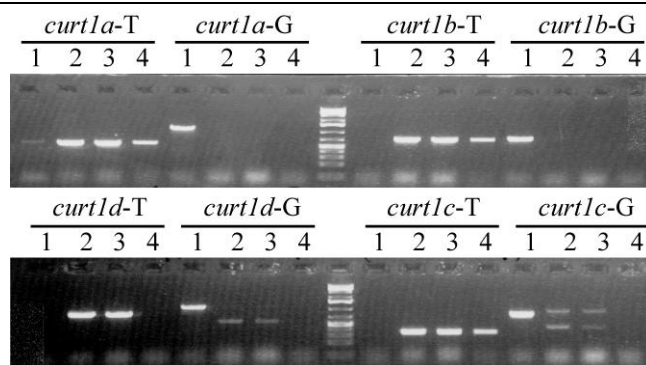


Fig. 5.3 PCR confirmation for *curt1abcd pgr5* line. *PGR5* locus was confirmed homozygous by measurement of transient NPQ. The loci of *CURTIA-D* were screened by T-DNA or gene-specific specific primers as described in Table 2.2 (suffix with T or G), respectively. Corresponding lines: 1. WT; 2. *curt1abcd pgr5-1*; 3. *curt1abcd pgr5-2*; 4. *curt1abcd*.

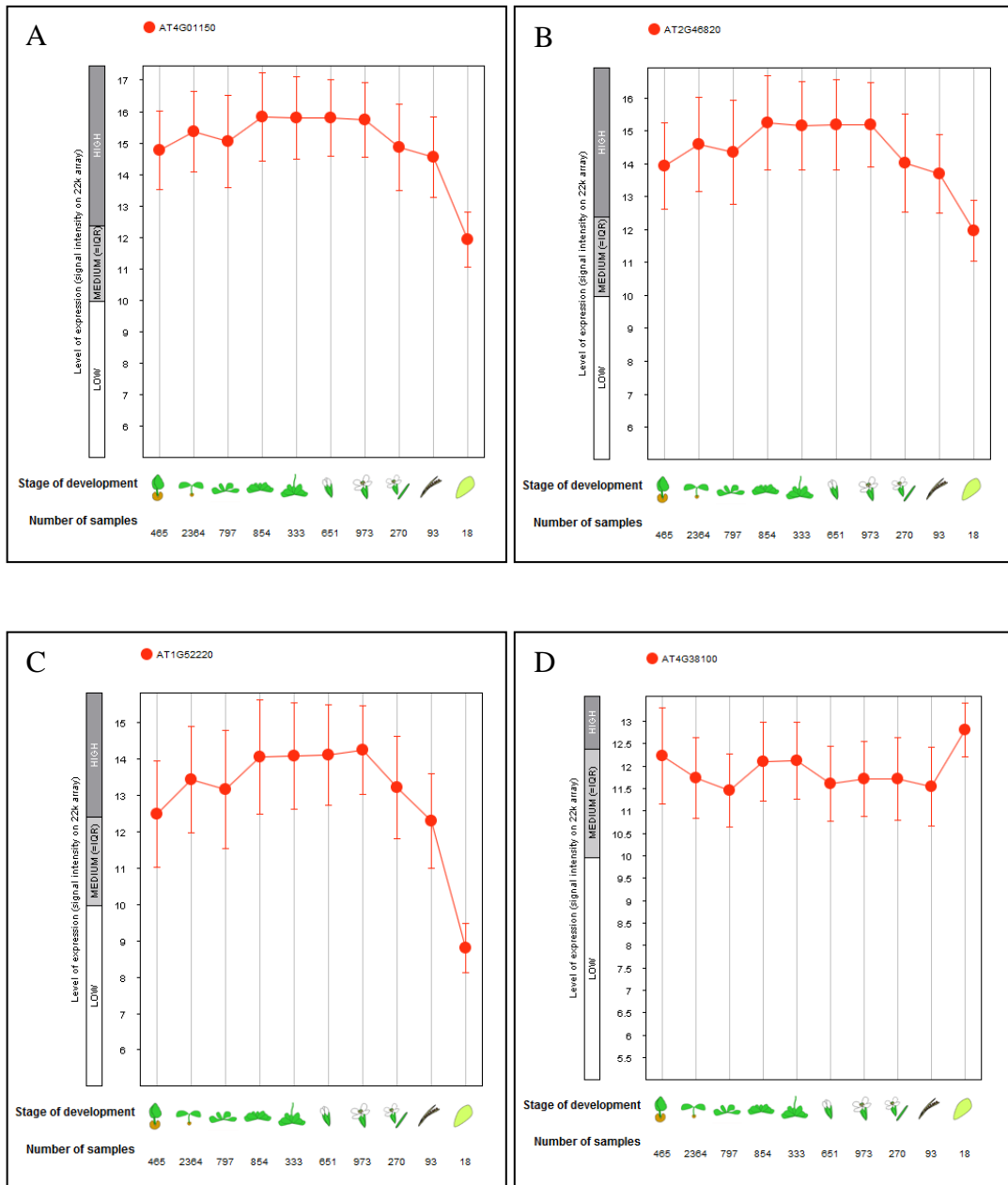


Fig. 5.4 Analysis of CURT1 protein expression at different developmental stages. The corresponding stages of development are: germinated seeds, seedling, young rosette, developed rosette, bolting, young flower, developed flower, flowers and siliques, mature siliques, and senescence. (A) CURT1A expression levels, (B) CURT1B expression levels, (C) CURT1C expression levels, (D) CURT1D expression levels.

6. References

A

Abramoff, M.D., Magelhaes, P.J., and Ram, S.J. (2004). Image processing with ImageJ. *Biophotonics International* **11**, 36-42.

Adam, Z., Charuvi, D., Tsabari, O., Knopf, R.R., and Reich, Z. (2011). Biogenesis of thylakoid networks in angiosperms: knowns and unknowns. *Plant Mol Biol* **76**, 221-234.

Akoyunoglou, G., and Argyroudi-Akoyunoglou, J. (1974). Reconstitution of grana thylakoids in spinach chloroplasts. *FEBS Lett* **42**, 135-140.

Albertsson, P.A., and Andreasson, E. (2004). The constant proportion of grana and stroma lamellae in plant chloroplasts. *Physiol Plant* **121**, 334-342.

Allen, J. (2002). Photosynthesis of ATP-electrons, proton pumps, rotors, and poise. *Cell* **110**, 273-276.

Allen, J.F., and Forsberg, J. (2001). Molecular recognition in thylakoid structure and function. *Trends Plant Sci* **6**, 317-326.

Anderson, J.M. (1999). Insights into the consequences of grana stacking of thylakoid membranes in vascular plants: a personal perspective. *Aust J Plant Physiol* **26**, 625-639.

Anderson, J.M., Chow, W.S., and Goodchild, D.J. (1988). Thylakoid membrane organization in sun shade acclimation. *Aust J Plant Physiol* **15**, 11-26.

Anderson, J.M., Chow, W.S., and De Las Rivas, J. (2008). Dynamic flexibility in the structure and function of photosystem II in higher plant thylakoid membranes: the grana enigma. *Photosynth Res* **98**, 575-587.

Anderson, J.M., Horton, P., Kim, E.H., and Chow, W.S. (2012). Towards elucidation of dynamic structural changes of plant thylakoid architecture. *Philos Trans R Soc Lond B Biol Sci* **367**, 3515-3524.

Andersson, J., Wentworth, M., Walters, R.G., Howard, C.A., Ruban, A.V., Horton, P., and Jansson, S. (2003). Absence of the Lhcb1 and Lhcb2 proteins of the light-harvesting complex of photosystem II—effects on photosynthesis, grana stacking and fitness. *Plant J* **35**, 350-361.

Aronsson, H., and Jarvis, P. (2002). A simple method for isolating import-competent *Arabidopsis* chloroplasts. *FEBS Lett* **529**, 215-220.

Asada, K. (1999). The water-water cycle in chloroplasts: scavenging of active oxygens and

dissipation of excess photons. *Annu Rev Plant Physiol Plant Mol Biol* **50**, 601-639.

B

Baena-Gonzalez, E., Barbato, R., and Aro, E.M. (1999). Role of phosphorylation in the repair cycle and oligomeric structure of photosystem II. *Planta* **208**, 196-204.

Baginsky, S., and Gruissem, W. (2009). The chloroplast kinase network: new insights from large-scale phosphoproteome profiling. *Mol Plant* **2**, 1141-1153.

Baginsky, S., Tiller, K., Pfannschmidt, T., and Link, G. (1999). PTK, the chloroplast RNA polymerase-associated protein kinase from mustard (*Sinapis alba*), mediates redox control of plastid in vitro transcription. *Plant Mol Biol* **39**, 1013-1023.

Baker, N.R. (2008). Chlorophyll fluorescence: a probe of photosynthesis in vivo. *Annu Rev Plant Biol* **59**, 89-113.

Baniulis, D., Yamashita, E., Zhang, H., Hasan, S.S., and Cramer, W.A. (2008). Structure-function of the cytochrome *b₆f* complex. *Photochem Photobiol* **84**, 1349-1358.

Bayer, R.G., Stael, S., Rocha, A.G., Mair, A., Vothknecht, U.C., and Teige, M. (2012). Chloroplast-localized protein kinases: a step forward towards a complete inventory. *J Exp Bot* **63**, 1713-1723.

Bellaïf, S., Barneche, F., Peltier, G., and Rochaix, J.D. (2005). State transitions and light adaptation require chloroplast thylakoid protein kinase STN7. *Nature* **433**, 892-895.

Biehl, A., Richly, E., Noutsos, C., Salamini, F., and Leister, D. (2005). Analysis of 101 nuclear transcriptomes reveals 23 distinct regulons and their relationship to metabolism, chromosomal gene distribution and co-ordination of nuclear and plastid gene expression. *Gene* **344**, 33-41.

Bonardi, V., Pesaresi, P., Becker, T., Schleiff, E., Wagner, R., Pfannschmidt, T., Jahns, P., and Leister, D. (2005). Photosystem II core phosphorylation and photosynthetic acclimation require two different protein kinases. *Nature* **437**, 1179-1182.

Borch Jensen, M., Bhatia, V.K., Jao, C.C., Rasmussen, J.E., Pedersen, S.L., Jensen, K.J., Langen, R., and Stamou, D. (2011). Membrane curvature sensing by amphipathic helices: a single liposome study using α -synuclein and annexin B12. *J Biol Chem* **286**, 42603-42614.

Bricker, T.M., Roose, J.L., Fagerlund, R.D., Frankel, L.K., and Eaton-Rye, J.J. (2012). The extrinsic proteins of photosystem II. *Biochim Biophys Acta* **1817**, 121-142.

C

Chen, M.S., Obar, R.A., Schroeder, C.C., Austin, T.W., Poodry, C.A., Wadsworth, S.C., and Vallee, R.B. (1991). Multiple forms of dynamin are encoded by *shibire*, a *Drosophila* gene involved in endocytosis. *Nature* **351**, 583-586.

Chow, W.S. (1984). The extent to which the spatial separation between photosystems I and II associated with granal formation limits noncyclic electron flow in isolated lettuce chloroplasts. *Arch Biochem Biophys* **232**, 162-171.

Chow, W.S., Ford, R.C., and Barber, J. (1981). Possible effects of the detachment of stromal lamellae from granal stacks on salt-induced changes in spillover. A study by sonication of chloroplasts. *Biochim Biophys Acta* **635**, 317-326.

Chow, W.S., Kim, E.H., Horton, P., and Anderson, J.M. (2005). Granal stacking of thylakoid membranes in higher plant chloroplasts: the physicochemical forces at work and the functional consequences that ensue. *Photochem Photobiol Sci* **4**, 1081-1090.

Clough, S.J., and Bent, A.F. (1998). Floral dip: a simplified method for *Agrobacterium*-mediated transformation of *Arabidopsis thaliana*. *Plant J* **16**, 735-743.

Cohen, P. (2000). The regulation of protein function by multisite phosphorylation—a 25 year update. *Trends Biochem Sci* **25**, 596-601.

Cui, Y.L., Jia, Q.S., Yin, Q.Q., Lin, G.N., Kong, M.M., and Yang, Z.N. (2011). The GDC1 gene encodes a novel ankyrin domain-containing protein that is essential for grana formation in *Arabidopsis*. *Plant Physiol* **155**, 130-141.

D

DalCorso, G., Pesaresi, P., Masiero, S., Aseeva, E., Schunemann, D., Finazzi, G., Joliot, P., Barbato, R., and Leister, D. (2008). A complex containing PGRL1 and PGR5 is involved in the switch between linear and cyclic electron flow in *Arabidopsis*. *Cell* **132**, 273-285.

De Camilli, P., Chen, H., Hyman, J., Panepucci, E., Bateman, A., and Brunger, A.T. (2002). The ENTH domain. *FEBS Lett* **513**, 11-18.

De Las Rivas, J., Heredia, P., and Roman, A. (2007). Oxygen-evolving extrinsic proteins (PsbO,P,Q,R): bioinformatic and functional analysis. *Biochim Biophys Acta* **1767**, 575-582.

Dekker, J.P., and Boekema, E.J. (2005). Supramolecular organization of thylakoid membrane proteins in green plants. *Biochim Biophys Acta* **1706**, 12-39.

Dietzel, L., and Pfannschmidt, T. (2008). Photosynthetic acclimation to light gradients in

plant stands comes out of shade. *Plant Signal Behav* **3**, 1116-1118.

Dorne, A.J., Joyard, J., and Douce, R. (1990). Do thylakoids really contain phosphatidylcholine. *Proc Natl Acad Sci U S A* **87**, 71-74.

Durek, P., Schmidt, R., Heazlewood, J.L., Jones, A., MacLean, D., Nagel, A., Kersten, B., and Schulze, W.X. (2010). PhosPhAt: the *Arabidopsis thaliana* phosphorylation site database. An update. *Nucleic Acids Res* **38**, D828-834.

E

Evert, R.F., and Eichhorn, S.E. (2013). *Biology of Plants* 8th Edition.

F

Farsad, K., and De Camilli, P. (2003). Mechanisms of membrane deformation. *Curr Opin Cell Biol* **15**, 372-381.

Fey, V., Wagner, R., Brautigam, K., and Pfannschmidt, T. (2005). Photosynthetic redox control of nuclear gene expression. *J Exp Bot* **56**, 1491-1498.

Finazzi, G. (2005). The central role of the green alga *Chlamydomonas reinhardtii* in revealing the mechanism of state transitions. *J Exp Bot* **56**, 383-388.

Ford, M.G., Mills, I.G., Peter, B.J., Vallis, Y., Praefcke, G.J., Evans, P.R., and McMahon, H.T. (2002). Curvature of clathrin-coated pits driven by epsin. *Nature* **419**, 361-366.

Fristedt, R., and Vener, A.V. (2011). High light induced disassembly of photosystem II supercomplexes in *Arabidopsis* requires STN7-dependent phosphorylation of CP29. *PloS one* **6**, e24565.

Fristedt, R., Willig, A., Granath, P., Crevecoeur, M., Rochaix, J.D., and Vener, A.V. (2009a). Phosphorylation of photosystem II controls functional macroscopic folding of photosynthetic membranes in *Arabidopsis*. *Plant Cell* **21**, 3950-3964.

Fristedt, R., Carlberg, I., Zygadlo, A., Piippo, M., Nurmi, M., Aro, E.M., Scheller, H.V., and Vener, A.V. (2009b). Intrinsically unstructured phosphoprotein TSP9 regulates light harvesting in *Arabidopsis thaliana*. *Biochemistry* **48**, 499-509.

Fujita, Y. (1997). A study on the dynamic features of photosystem stoichiometry: accomplishments and problems for future studies. *Photosynth Res* **53**, 83-93.

G

Goral, T.K., Johnson, M.P., Brain, A.P., Kirchhoff, H., Ruban, A.V., and Mullineaux, C.W. (2010). Visualizing the mobility and distribution of chlorophyll proteins in higher plant thylakoid membranes: effects of photoinhibition and protein phosphorylation. *Plant J* **62**, 948-959.

Gounaris, K., and Barber, J. (1983). Monogalactosyldiacylglycerol - the most abundant polar lipid in nature. *Trends Biochem Sci* **8**, 378-381.

H

Hashimoto, M., Endo, T., Peltier, G., Tasaka, M., and Shikanai, T. (2003). A nucleus-encoded factor, CRR2, is essential for the expression of chloroplast *ndhB* in *Arabidopsis*. *Plant J* **36**, 541-549.

Herbstova, M., Tietz, S., Kinzel, C., Turkina, M.V., and Kirchhoff, H. (2012). Architectural switch in plant photosynthetic membranes induced by light stress. *Proc Natl Acad Sci U S A* **109**, 20130-20135.

Hertle, A.P., Blunder, T., Wunder, T., Pesaresi, P., Pribil, M., Armbruster, U., and Leister, D. (2013). PGRL1 is the elusive ferredoxin-plastoquinone reductase in photosynthetic cyclic electron flow. *Mol Cell* **49**, 511-523.

Holt, N.E., Zigmantas, D., Valkunas, L., Li, X.P., Niyogi, K.K., and Fleming, G.R. (2005). Carotenoid cation formation and the regulation of photosynthetic light harvesting. *Science* **307**, 433-436.

Horton, P., and Ruban, A. (2005). Molecular design of the photosystem II light-harvesting antenna: photosynthesis and photoprotection. *J Exp Bot* **56**, 365-373.

I

Ingelsson, B., and Vener, A.V. (2012). Phosphoproteomics of *Arabidopsis* chloroplasts reveals involvement of the STN7 kinase in phosphorylation of nucleoid protein pTAC16. *FEBS Lett* **586**, 1265-1271.

J

Jensen, P.E., Bassi, R., Boekema, E.J., Dekker, J.P., Jansson, S., Leister, D., Robinson, C., and Scheller, H.V. (2007). Structure, function and regulation of plant photosystem I. *Biochim Biophys Acta* **1767**, 335-352.

Johnson, G.N. (2005). Cyclic electron transport in C3 plants: fact or artefact? *J Exp Bot* **56**, 407-416.

Johnson, M.P., Goral, T.K., Duffy, C.D., Brain, A.P., Mullineaux, C.W., and Ruban, A.V. (2011). Photoprotective energy dissipation involves the reorganization of photosystem II light-harvesting complexes in the grana membranes of spinach chloroplasts. *Plant Cell* **23**, 1468-1479.

Joliot, P., and Joliot, A. (2002). Cyclic electron transfer in plant leaf. *Proc Natl Acad Sci U S A* **99**, 10209-10214.

Juric, S., Hazler-Pilepic, K., Tomasic, A., Lepadus, H., Jelacic, B., Puthiyaveetil, S., Bionda, T., Vojta, L., Allen, J.F., Schleiff, E., and Fulgosi, H. (2009). Tethering of ferredoxin:NADP⁺ oxidoreductase to thylakoid membranes is mediated by novel chloroplast protein TROL. *Plant J* **60**, 783-794.

K

Kaftan, D., Brumfeld, V., Nevo, R., Scherz, A., and Reich, Z. (2002). From chloroplasts to photosystems: in situ scanning force microscopy on intact thylakoid membranes. *EMBO J* **21**, 6146-6153.

Kanervo, E., Suorsa, M., and Aro, E.M. (2005). Functional flexibility and acclimation of the thylakoid membrane. *Photochem Photobiol Sci* **4**, 1072-1080.

Kay, B.K., Yamabhai, M., Wendland, B., and Emr, S.D. (1999). Identification of a novel domain shared by putative components of the endocytic and cytoskeletal machinery. *Protein Sci* **8**, 435-438.

Kirchhoff, H., Hall, C., Wood, M., Herbstova, M., Tsabari, O., Nevo, R., Charuvi, D., Shimoni, E., and Reich, Z. (2011). Dynamic control of protein diffusion within the granal thylakoid lumen. *Proc Natl Acad Sci U S A* **108**, 20248-20253.

Koncz, C., Mayerhofer, R., Koncz-Kalman, Z., Nawrath, C., Reiss, B., Redei, G.P., and Schell, J. (1990). Isolation of a gene encoding a novel chloroplast protein by T-DNA tagging in *Arabidopsis thaliana*. *EMBO J* **9**, 1337-1346.

Kramer, D.M., Avenson, T.J., and Edwards, G.E. (2004). Dynamic flexibility in the light reactions of photosynthesis governed by both electron and proton transfer reactions. *Trends Plant Sci* **9**, 349-357.

Krause, G.H., and Weis, E. (1991). Chlorophyll fluorescence and photosynthesis - the basics. *Annu Rev Plant Physiol Plant Mol Biol* **42**, 313-349.

Kulheim, C., Agren, J., and Jansson, S. (2002). Rapid regulation of light harvesting and plant fitness in the field. *Science* **297**, 91-93.

Kurisu, G., Zhang, H., Smith, J.L., and Cramer, W.A. (2003). Structure of the cytochrome *b₆f* complex of oxygenic photosynthesis: tuning the cavity. *Science* **302**, 1009-1014.

Kutschera, U., and Niklas, K.J. (2005). Endosymbiosis, cell evolution, and speciation. *Theory Biosci* **124**, 1-24.

L

Li, X.P., Bjorkman, O., Shih, C., Grossman, A.R., Rosenquist, M., Jansson, S., and Niyogi, K.K. (2000). A pigment-binding protein essential for regulation of photosynthetic light harvesting. *Nature* **403**, 391-395.

Li, Z., Wakao, S., Fischer, B.B., and Niyogi, K.K. (2009). Sensing and responding to excess light. *Annu Rev Plant Biol* **60**, 239-260.

Liberton, M., Howard Berg, R., Heuser, J., Roth, R., and Pakrasi, B.H. (2006). Ultrastructure of the membrane systems in the unicellular cyanobacterium *Synechocystis* sp. strain PCC 6803. *Protoplasma* **227**, 129-138.

Liu, Y.G., Mitsukawa, N., Oosumi, T., and Whittier, R.F. (1995). Efficient isolation and mapping of *Arabidopsis thaliana* T-DNA insert junctions by thermal asymmetric interlaced PCR. *Plant J* **8**, 457-463.

Lodish, H., Berk, A., Kaiser, C.A., Krieger, M., Bretscher, A., Ploegh, H., Amon, A., and Scott, M.P. (2013). *Molecular Cell Biology Seventh Edition*.

Long, S.P., Humphries, S., and Falkowski, P.G. (1994). Photoinhibition of photosynthesis in nature. *Annu Rev Plant Physiol Plant Mol Biol* **45**, 633-662.

M

Martin, D.M., Miranda-Saavedra, D., and Barton, G.J. (2009). Kinomer v. 1.0: a database of systematically classified eukaryotic protein kinases. *Nucleic Acids Res* **37**, D244-250.

Masuda, M., Takeda, S., Sone, M., Ohki, T., Mori, H., Kamioka, Y., and Mochizuki, N. (2006). Endophilin BAR domain drives membrane curvature by two newly identified structure-based mechanisms. *EMBO J* **25**, 2889-2897.

Mehler, A.H. (1951). Studies on reactions of illuminated chloroplasts: I. mechanism of the reduction of oxygen and other hill reagents. *Arch Biochem Biophys* **33**, 65-77.

Melis, A. (1991). Dynamics of photosynthetic membrane-composition and function. *Biochim Biophys Acta* **1058**, 87-106.

Melis, A. (1999). Photosystem-II damage and repair cycle in chloroplasts: what modulates the rate of photodamage ? *Trends Plant Sci* **4**, 130-135.

Miyake, C. (2010). Alternative electron flows (water-water cycle and cyclic electron flow around PSI) in photosynthesis: molecular mechanisms and physiological functions. *Plant Cell Physiol* **51**, 1951-1963.

Muller, P., Li, X.P., and Niyogi, K.K. (2001). Non-photochemical quenching. A response to excess light energy. *Plant Physiol* **125**, 1558-1566.

Mullineaux, C.W. (2005). Function and evolution of grana. *Trends Plant Sci* **10**, 521-525.

Munekage, Y., Hojo, M., Meurer, J., Endo, T., Tasaka, M., and Shikanai, T. (2002). PGR5 is involved in cyclic electron flow around photosystem I and is essential for photoprotection in *Arabidopsis*. *Cell* **110**, 361-371.

Munekage, Y., Hashimoto, M., Miyake, C., Tomizawa, K., Endo, T., Tasaka, M., and Shikanai, T. (2004). Cyclic electron flow around photosystem I is essential for photosynthesis. *Nature* **429**, 579-582.

Mustardy, L., and Garab, G. (2003). Granum revisited. A three-dimensional model—where things fall into place. *Trends Plant Sci* **8**, 117-122.

N

Nield, J., and Barber, J. (2006). Refinement of the structural model for the photosystem II supercomplex of higher plants. *Biochim Biophys Acta* **1757**, 353-361.

Nixon, P.J., Michoux, F., Yu, J., Boehm, M., and Komenda, J. (2010). Recent advances in understanding the assembly and repair of photosystem II. *Ann Bot* **106**, 1-16.

O

Opalinski, L., Veenhuis, M., and van der Klei, I.J. (2011). Peroxisomes: membrane events accompanying peroxisome proliferation. *Int J Biochem Cell Biol* **43**, 847-851.

P

Pesaresi, P., Pribil, M., Wunder, T., and Leister, D. (2011). Dynamics of reversible protein phosphorylation in thylakoids of flowering plants: the roles of STN7, STN8 and TAP38. *Biochim Biophys Acta* **1807**, 887-896.

- Pesaresi, P., Hertle, A., Pribi, M., Schneider, A., Kleine, T., and Leister, D.** (2010). Optimizing photosynthesis under fluctuating light: the role of the *Arabidopsis* STN7 kinase. *Plant Signal Behav* **5**, 21-25.
- Pfannschmidt, T., Schutze, K., Brost, M., and Oelmüller, R.** (2001). A novel mechanism of nuclear photosynthesis gene regulation by redox signals from the chloroplast during photosystem stoichiometry adjustment. *J Biol Chem* **276**, 36125-36130.
- Porra, R.J.** (2002). The chequered history of the development and use of simultaneous equations for the accurate determination of chlorophylls a and b. *Photosynth Res* **73**, 149-156.
- Pribil, M., Pesaresi, P., Hertle, A., Barbato, R., and Leister, D.** (2010). Role of plastid protein phosphatase TAP38 in LHCII dephosphorylation and thylakoid electron flow. *PLoS Biol* **8**, e1000288.
- Puthiyaveetil, S., Ibrahim, I.M., and Allen, J.F.** (2013). Evolutionary rewiring: a modified prokaryotic gene-regulatory pathway in chloroplasts. *Philos Trans R Soc Lond B Biol Sci* **368**, 20120260.
- Puthiyaveetil, S., Ibrahim, I.M., Jelacic, B., Tomasic, A., Fulgosi, H., and Allen, J.F.** (2010). Transcriptional control of photosynthesis genes: the evolutionarily conserved regulatory mechanism in plastid genome function. *Genome Biol Evol* **2**, 888-896.
- Puthiyaveetil, S., Kavanagh, T.A., Cain, P., Sullivan, J.A., Newell, C.A., Gray, J.C., Robinson, C., van der Giezen, M., Rogers, M.B., and Allen, J.F.** (2008). The ancestral symbiont sensor kinase CSK links photosynthesis with gene expression in chloroplasts. *Proc Natl Acad Sci U S A* **105**, 10061-10066.

R

- Reiland, S., Messerli, G., Baerenfaller, K., Gerrits, B., Endler, A., Grossmann, J., Gruissem, W., and Baginsky, S.** (2009). Large-scale *Arabidopsis* phosphoproteome profiling reveals novel chloroplast kinase substrates and phosphorylation networks. *Plant Physiol* **150**, 889-903.
- Reiland, S., Finazzi, G., Endler, A., Willig, A., Baerenfaller, K., Grossmann, J., Gerrits, B., Rutishauser, D., Gruissem, W., Rochaix, J.D., and Baginsky, S.** (2011). Comparative phosphoproteome profiling reveals a function of the STN8 kinase in fine-tuning of cyclic electron flow (CEF). *Proc Natl Acad Sci U S A* **108**, 12955-12960.
- Rintamäki, E., Kettunen, R., and Aro, E.M.** (1996). Differential D1 dephosphorylation in functional and photodamaged photosystem II centers. Dephosphorylation is a prerequisite for degradation of damaged D1. *J Biol Chem* **271**, 14870-14875.

Rochaix, J.D. (2011). Regulation of photosynthetic electron transport. *Biochim Biophys Acta* **1807**, 375-383.

Rochaix, J.D., Lemeille, S., Shapiguzov, A., Samol, I., Fucile, G., Willig, A., and Goldschmidt-Clermont, M. (2012). Protein kinases and phosphatases involved in the acclimation of the photosynthetic apparatus to a changing light environment. *Philos Trans R Soc Lond B Biol Sci* **367**, 3466-3474.

S

Samol, I., Shapiguzov, A., Ingelsson, B., Fucile, G., Crevecoeur, M., Vener, A.V., Rochaix, J.D., and Goldschmidt-Clermont, M. (2012). Identification of a photosystem II phosphatase involved in light acclimation in *Arabidopsis*. *Plant Cell* **24**, 2596-2609.

Schagger, H., and von Jagow, G. (1987). Tricine-sodium dodecyl sulfate-polyacrylamide gel electrophoresis for the separation of proteins in the range from 1 to 100 kDa. *Anal Biochem* **166**, 368-379.

Schagger, H., and von Jagow, G. (1991). Blue native electrophoresis for isolation of membrane protein complexes in enzymatically active form. *Anal Biochem* **199**, 223-231.

Schonberg, A., and Baginsky, S. (2012). Signal integration by chloroplast phosphorylation networks: an update. *Front Plant Sci* **3**, 256.

Shapiguzov, A., Ingelsson, B., Samol, I., Andres, C., Kessler, F., Rochaix, J.D., Vener, A.V., and Goldschmidt-Clermont, M. (2010). The PPH1 phosphatase is specifically involved in LHCII dephosphorylation and state transitions in *Arabidopsis*. *Proc Natl Acad Sci U S A* **107**, 4782-4787.

Shi, L.X., and Schroder, W.P. (2004). The low molecular mass subunits of the photosynthetic supracomplex, photosystem II. *Biochim Biophys Acta* **1608**, 75-96.

Shikanai, T., Endo, T., Hashimoto, T., Yamada, Y., Asada, K., and Yokota, A. (1998). Directed disruption of the tobacco *ndhB* gene impairs cyclic electron flow around photosystem I. *Proc Natl Acad Sci U S A* **95**, 9705-9709.

Shimizu, M., Kato, H., Ogawa, T., Kurachi, A., Nakagawa, Y., and Kobayashi, H. (2010). Sigma factor phosphorylation in the photosynthetic control of photosystem stoichiometry. *Proc Natl Acad Sci U S A* **107**, 10760-10764.

Singer, S.J., and Nicolson, G.L. (1972). The fluid mosaic model of the structure of cell membranes. *Science* **175**, 720-731.

Standfuss, J., Terwisscha van Scheltinga, A.C., Lamborghini, M., and Kuhlbrandt, W.

(2005). Mechanisms of photoprotection and nonphotochemical quenching in pea light-harvesting complex at 2.5 Å resolution. *EMBO J* **24**, 919-928.

Stock, A.M., Robinson, V.L., and Goudreau, P.N. (2000). Two-component signal transduction. *Annu Rev Biochem* **69**, 183-215.

Sugiyama, N., Nakagami, H., Mochida, K., Daudi, A., Tomita, M., Shirasu, K., and Ishihama, Y. (2008). Large-scale phosphorylation mapping reveals the extent of tyrosine phosphorylation in *Arabidopsis*. *Mol Syst Biol* **4**, 193.

Sweitzer, S.M., and Hinshaw, J.E. (1998). Dynamin undergoes a GTP-dependent conformational change causing vesiculation. *Cell* **93**, 1021-1029.

T

Taiz, L., and Zeiger, E. (2010). *Plant Physiology Fifth Edition*.

Tikkanen, M., Nurmi, M., Kangasjarvi, S., and Aro, E.M. (2008). Core protein phosphorylation facilitates the repair of photodamaged photosystem II at high light. *Biochim Biophys Acta* **1777**, 1432-1437.

Tikkanen, M., Grieco, M., Kangasjarvi, S., and Aro, E.M. (2010). Thylakoid protein phosphorylation in higher plant chloroplasts optimizes electron transfer under fluctuating light. *Plant Physiol* **152**, 723-735.

Tikkanen, M., Piippo, M., Suorsa, M., Sirpio, S., Mulo, P., Vainonen, J., Vener, A.V., Allahverdiyeva, Y., and Aro, E.M. (2006). State transitions revisited—a buffering system for dynamic low light acclimation of *Arabidopsis*. *Plant Mol Biol* **62**, 779-793.

Trissl, H.W., and Wilhelm, C. (1993). Why do thylakoid membranes from higher-plants form grana stacks. *Trends Biochem Sci* **18**, 415-419.

V

Vainonen, J.P., Hansson, M., and Vener, A.V. (2005). STN8 protein kinase in *Arabidopsis thaliana* is specific in phosphorylation of photosystem II core proteins. *J Biol Chem* **280**, 33679-33686.

Vainonen, J.P., Sakuragi, Y., Stael, S., Tikkanen, M., Allahverdiyeva, Y., Paakkarinen, V., Aro, E., Suorsa, M., Scheller, H.V., Vener, A.V., and Aro, E.M. (2008). Light regulation of CaS, a novel phosphoprotein in the thylakoid membrane of *Arabidopsis thaliana*. *FEBS J* **275**, 1767-1777.

van de Meene, A.M., Hohmann-Marriott, M.F., Vermaas, W.F., and Roberson, R.W.

(2006). The three-dimensional structure of the cyanobacterium *Synechocystis* sp. PCC 6803. *Arch Microbiol* **184**, 259-270.

van der Blik, A.M., and Meyerowitz, E.M. (1991). Dynamin-like protein encoded by the *Drosophila* shibire gene associated with vesicular traffic. *Nature* **351**, 411-414.

Varotto, C., Pesaresi, P., Meurer, J., Oelmuller, R., Steiner-Lange, S., Salamini, F., and Leister, D. (2000). Disruption of the *Arabidopsis* photosystem I gene PsaE1 affects photosynthesis and impairs growth. *Plant J* **22**, 115-124.

W

Wollman, F.A. (2001). State transitions reveal the dynamics and flexibility of the photosynthetic apparatus. *EMBO J* **20**, 3623-3630.

Wunder, T., Liu, Q., Aseeva, E., Bonardi, V., Leister, D., and Pribil, M. (2013). Control of STN7 transcript abundance and transient STN7 dimerisation are involved in the regulation of STN7 activity. *Planta* **237**, 541-558.

Z

Zimmerberg, J., and Kozlov, M.M. (2006). How proteins produce cellular membrane curvature. *Nat Rev Mol Cell Bio* **7**, 9-19.

Acknowledgements

First of all, I would like to thank Prof. Dr. Dario Leister for giving me the opportunity to work in his research group and especially for his trust during my PhD period.

I would like to thank PD Dr. Cordelia Bolle for acting as the “Zweitgutachter”.

I want to thank Dr. Mathias Pribil for 4 years’ supervision. I appreciated his novel ideas, helpful discussions and endless motivations, which always inspired me to persist.

I would like to thank Dr. Ute Armbruster for introducing me into the nice project. To Prof. Dr. Gerhard Wanner and Silvia Dobler for conducting the microscope analysis.

To Mathias Labs, Qiuping Liu, Stefania Viola, Luca Tadini, Evgenia Vamvaka, Salar Torabi for reading and correcting my thesis.

To my current and previous colleagues in this lab like Angie, Henning, Tobi, Alex, who are always willing to help with experimental problems or difficulties in my daily life.

I would like to thank all soccer players of the “Abst über” team, who gave me the best memory of football.

To CSC program for the financial support.

Most of all, I want to give my thanks to my parents and my fiancé, Yingjie, for their constant support and encouragement. Thank you!

Curriculum vitae

Personal data

Name: WENTENG XU

Date of birth: 1984.06.14

Place of birth: Linyi, Shandong, P.R China

Nationality: Chinese

Educations

November 2009-present

Ludwig-Maximilians-Universität München

Department Biology I, Botany

CSC-LMU program, Ph.D candidate

Supervisor Prof. Dr. Dario Leister & Dr. Mathias Pribil

September 2006-July 2009

Shandong University

College of life science: Molecular Biology

Master-doctorate program

Supervisor: Prof. Dr. Jinxing Wang;

September 2002-July 2006

Shandong University

College of life science: Biotechnology;

Bachelor of Science

Language

Chinese, mother tongue

English, fluent

German, basic

Publications

Armbruster, U., Labs, M., Pribil, M., Viola, S., **Xu, W. T.**, Scharfenberg, M., Hertle, A. P., Rojahn, U. R., Jensen, P. E., Rappaport, F. R., Joliot, P., Dörmann, P., Wanner, G., and Leister, D. *Plant Cell*, accepted.

Sun, C., **Xu, W. T.**, Zhang, H. W., Dong, L. P., Zhang, T., Zhao, X. F., and Wang, J. X. (2011) *Fish Shellfish Immunol* 30, 295-303

Xu, W. T., Wang, X. W., Zhang, X. W., Zhao, X. F., Yu, X. Q., and Wang, J. X. (2010) *Amino Acids* 39, 1227-1239

Sun, C., Du, X. J., **Xu, W. T.**, Zhang, H. W., Zhao, X. F., and Wang, J. X. (2010) *Fish Shellfish Immunol* 28, 517-524

Zhang, X. W., **Xu, W. T.**, Wang, X. W., Mu, Y., Zhao, X. F., Yu, X. Q., and Wang, J. X. (2009) *Mol Immunol* 46, 1626-1637

Wang, X. W., Zhang, X. W., **Xu, W. T.**, Zhao, X. F., and Wang, J. X. (2009) *Dev Comp Immunol* 33, 1039-1047

Wang, X. W., **Xu, W. T.**, Zhang, X. W., Zhao, X. F., Yu, X. Q., and Wang, J. X. (2009) *Fish Shellfish Immunol* 27, 556-562

publication related to this thesis

Declaration / Eidesstattliche Versicherung

Hiermit versichere ich, dass ich die vorliegende Arbeit selbständig und nur unter Verwendung der angegebenen Hilfsmittel und Quellen angefertigt habe. Der Autor hat zuvor nicht versucht, anderweitig eine Dissertation einzureichen oder sich einer Doktorprüfung zu unterziehen. Die Dissertation wurde keiner weiteren Prüfungskommission weder in Teilen noch als Ganzes vorgelegt.

München, 3. Juli 2013

.....

Wenteng Xu